



Multiple mantle plume components involved in the petrogenesis of subduction-related lavas from the northern termination of the Tonga Arc and northern Lau Basin: Evidence from the geochemistry of arc and backarc submarine volcanics

Trevor J. Falloon

ARC Centre of Excellence in Ore Deposits and Centre for Marine Sciences, UTAS, Private Bag 79, Hobart, Tasmania 7001, Australia (trevor.falloon@utas.edu.au)

Leonid V. Danyushevsky and Tony J. Crawford

ARC Centre of Excellence in Ore Deposits and School of Earth Sciences, UTAS, Private Bag 79, Hobart, Tasmania 7001, Australia (l.dan@utas.edu.au; tony.crawford@utas.edu.au)

Roland Maas and Jon D. Woodhead

School of Earth Sciences, University of Melbourne, Parkville, Victoria 3010, Australia (maasr@unimelb.edu.au; jdwood@unimelb.edu.au)

Stephen M. Eggins

Research School of Earth Sciences, Australian National University, Canberra, ACT 0200, Australia (stephen.eggins@anu.edu.au)

Sherman H. Bloomer and Dawn J. Wright

Department of Geosciences, Oregon State University, Corvallis, Oregon 97331-5506, USA (sherman.bloomer@oregonstate.edu; dawn@dusk.geo.orst.edu)

Sergei K. Zlobin

Vernadsky Institute of Geochemistry and Analytical Chemistry, Russian Academy of Sciences, 19 Kosygin Street, 119991, Moscow, Russia

Andrew R. Stacey

ARC Centre of Excellence in Ore Deposits and School of Earth Sciences, UTAS, Private Bag 79, Hobart, Tasmania 7001, Australia (arstacey@utas.edu.au)

[1] We report new geochemical data for boninites and backarc basin-type basalts recovered from the northern termination of the Tonga trench and Lau Basin. Boninitic pillow lavas, ranging from high-Mg compositions to andesites and dacites, have been erupted within large submarine volcanic edifices (calderas and volcanoes) associated with active rifting of both the northern end of the Tofua volcanic arc and in a backarc position relative to the arc volcanoes on the northern Tonga Ridge. The mantle sources in the area are a complex mixture of (1) the “normal” Tongan mantle wedge source that has “Pacific”-type isotopic signature with (2) the plume-related components (EMI, EMII, and HIMU) and (3) an “Indian”-type source upwelling beneath the backarc spreading. Some of these sources, such as the “normal” mantle wedge and variably depleted residual plume mantle, are fluxed by subduction components from the slab,

which produces boninites, tholeiites, and mixtures thereof. Other mantle sources, such as “Indian”-type backarc mantle and also some of the plume mantle, produce melts due to adiabatic decompression. These melts are variably mixed with each other and with the slab-fluid fluxed subduction-related melts to form the observed spectrum of magma compositions.

Components: 26,336 words, 21 figures, 18 tables.

Keywords: boninites; Tonga; Lau Basin; trench-transform intersection; subduction-related magma genesis.

Index Terms: 3001 Marine Geology and Geophysics: Back-arc basin processes; 3039 Marine Geology and Geophysics: Oceanic transform and fracture zone processes; 3613 Mineralogy and Petrology: Subduction zone processes (1031, 3060, 8170, 8413); 3075 Marine Geology and Geophysics: Submarine tectonics and volcanism; 3619 Mineralogy and Petrology: Magma genesis and partial melting (1037).

Received 27 February 2007; **Revised** 5 June 2007; **Accepted** 12 June 2007; **Published** 7 September 2007.

Falloon, T. J., L. V. Danyushevsky, T. J. Crawford, R. Maas, J. D. Woodhead, S. M. Eggins, S. H. Bloomer, D. J. Wright, S. K. Zlobin, and A. R. Stacey (2007), Multiple mantle plume components involved in the petrogenesis of subduction-related lavas from the northern termination of the Tonga Arc and northern Lau Basin: Evidence from the geochemistry of arc and backarc submarine volcanics, *Geochem. Geophys. Geosyst.*, 8, Q09003, doi:10.1029/2007GC001619.

1. Introduction

[2] Boninites are an important “end-member” supra-subduction zone magmatic suite as they have the highest H₂O contents and require the most refractory of mantle wedge sources. They are characterized by relatively high SiO₂, H₂O and low TiO₂ contents compared to tholeiitic suites (>52 wt% SiO₂, MgO > 8 wt% and TiO₂ < 0.5 wt% [Crawford *et al.*, 1989; Le Maitre *et al.*, 1989; Le Bas, 2000]). They lack plagioclase in rocks more mafic than andesite, and contain very magnesian olivine phenocrysts (up to Fo₉₄, [Crawford *et al.*, 1989]). Two broad types of boninite magmas are recognized, the high-Ca and low-Ca boninite series [Crawford *et al.*, 1989]. Both types of boninite are a rare but important component of many supra-subduction-related ophiolites and forearcs [Bloomer *et al.*, 1995; Rogers *et al.* 1989; Falloon *et al.*, 1997]. As boninite petrogenesis requires a unique combination of high temperatures at shallow depths in the mantle wedge [Crawford *et al.*, 1989], the presence of boninites has important implications for tectonic setting and/or initiation of subduction zones [Bloomer *et al.*, 1995; Crawford *et al.*, 1989]. High-Ca series boninites from the northern termination of the Tonga Ridge are of particular interest, as they have been well studied in terms of their petrology, geochemistry and mineralogy and so far are the only known occurrence of boninites from an active arc setting [Sharaskin *et al.*, 1983; Falloon and Green, 1986; Danyushevsky and Sobolev, 1987; Falloon *et al.*, 1987, 1989; Falloon and Crawford, 1991; Danyushevsky *et al.*, 1992, 1995; Sobolev and

Danyushevsky, 1994]. Thus a complete understanding of the tectonic setting and petrogenesis of these Tongan boninites and associated volcanics has the potential to provide important insights into the origin of boninites found in non-active older settings and subduction zone processes in general.

[3] A particularly interesting aspect of Tongan boninite petrogenesis is the requirement of temperatures as high as ~1480°C at depths of ~45 km in the mantle wedge [Sobolev and Danyushevsky, 1994; Falloon and Danyushevsky, 2000]. In order to account for these high temperatures, Danyushevsky *et al.* [1995] proposed a model involving the melting of Samoan plume mantle. In the model of Danyushevsky *et al.* [1995] refractory Samoan plume mantle (component D1 in their model), which has moved across the “slab edge” formed by the transform fault–trench intersection above the subducting Pacific plate, undergoes melting due to contact with H₂O-rich fluids derived from dehydration processes in subducted Pacific oceanic crust (component E1 in their model). The model of Danyushevsky *et al.* [1995] also includes a separate low-degree plume-derived silicate melt fraction as a distinct component in the petrogenesis of some boninites (their component E2). In the model of Danyushevsky *et al.* [1995] the geochemistry of the boninites was successfully modeled in general terms by mixing between the components D1, E1 and E2. However, more recent work on north Tonga volcanics has provided strong evidence that more than one mantle plume component is involved in their petrogenesis [Regelous *et al.*,

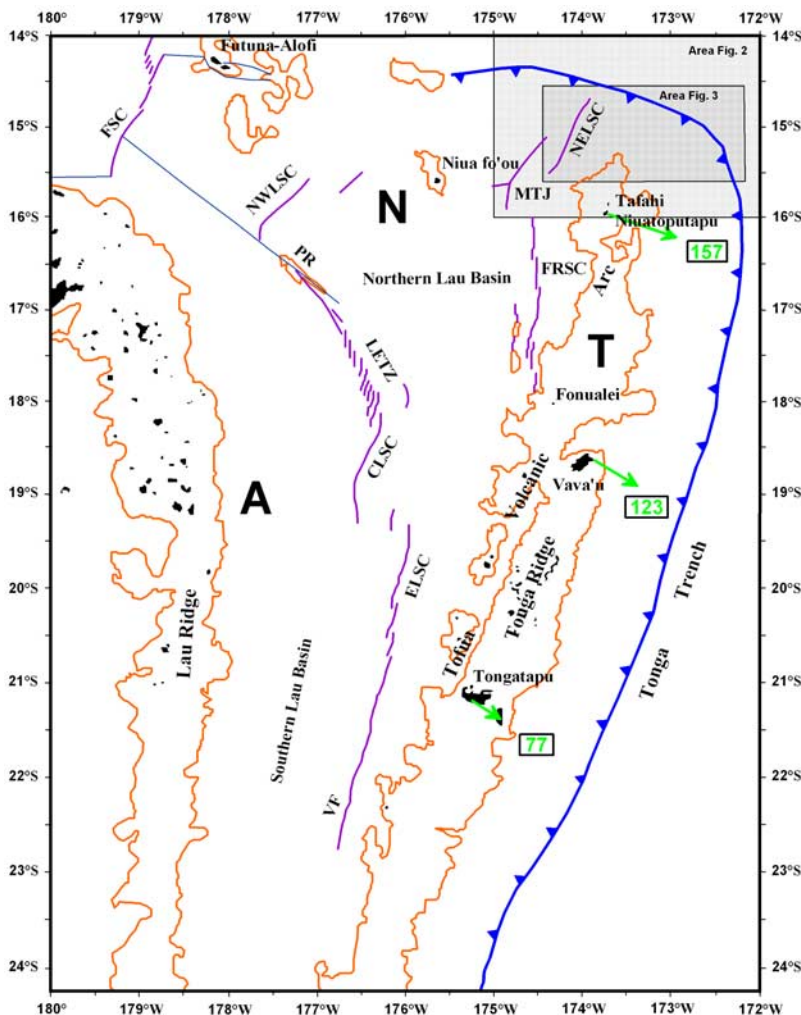


Figure 1. Schematic locality map of the Lau-Tonga supra-subduction zone, showing the regional setting of the north Tongan submarine volcanic localities. Tectonic interpretation is based on the work of *Zellmer and Taylor* [2001]. The shaded rectangles delineate the areas covered by Figures 2 and 3. Orange line is a 1500 meter bathymetric contour which outlines the Lau and Tonga Ridges and surrounds the islands (solid black) in the region. Plate boundaries (purple for spreading ridges, blue for fracture zones) are labeled as follows: CLSC, Central Lau Spreading Center; ELSC, East Lau Spreading Center; FRSC, Fonualei Rift and Spreading Center; FSC, Futuna Spreading Center; LETZ, Lau Extensional Transform Zone; PR, Peggy Ridge Transform Fault; MTJ, Mangatolu Triple Junction; NELSC, Northeast Lau Spreading Center; NWLSC, Northwest Lau Spreading Center. The three plates outlined by *Zellmer and Taylor* [2001] for this area are labeled: A, Australian Plate; T, Tongan Plate; N, Niua fo'ou Plate. Large bold green arrows are GPS velocities of Tonga relative to Australia, from *Zellmer and Taylor* [2001] (number next to arrows is rate in mm/yr).

1997; *Turner and Hawkesworth*, 1997; *Turner et al.*, 1997; *Wendt et al.*, 1997; *Ewart et al.*, 1998]. In particular these studies have demonstrated that the geochemistry of island arc tholeiites from the northern Tonga islands of Tafahi and Niuatoputapu (Figure 1) have a clear involvement of subducted volcanoclastic sediment from the Louisville Ridge, itself formed by the Louisville mantle plume. In addition, more recent work on the Samoan plume itself [*Acland*, 1996; *Workman et al.*, 2004] has

provided a better understanding of the geochemical complexity of the Samoan mantle plume source.

[4] In this study we present geochemical analyses of new sampling of submarine volcanic rocks (including boninites) from the northern Tonga Ridge and northern Lau Basin obtained during the 1996 voyage of the R/V *Melville* [*Bloomer et al.*, 1996; *Wright et al.*, 1996]. We also present new ICP-MS and isotope (Nd, Sr and Pb) analyses for

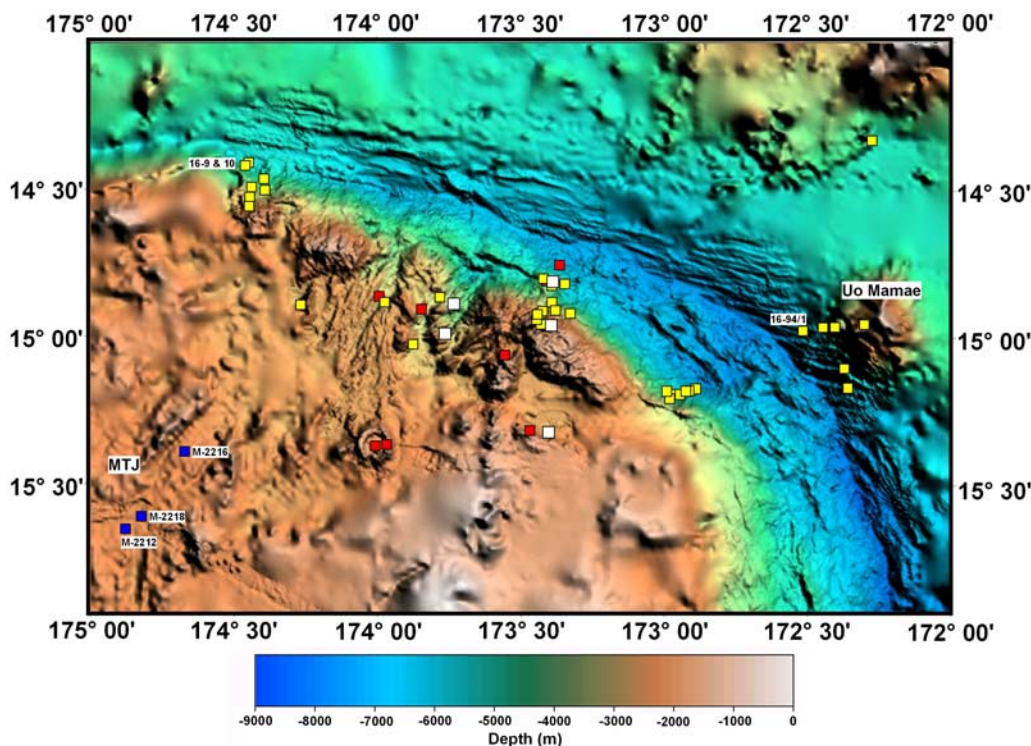


Figure 2. Shaded relief bathymetric map, created from a 200 meter SeaBeam 2000 grid (Boomerang 8 [Wright *et al.*, 2000]) of the northern termination of the Tonga Trench and northern Lau Basin. Seabeam bathymetry has been combined with the satellite bathymetry of Smith and Sandwell [1997]. Map projection is Mercator. Dredge and dive localities are indicated as follows: yellow squares, R/V *Kallisto*, 1982; white squares, R/V *Natsushima*, 1984; blue squares, R/V *Keldysh/Mir*, 1990; and red squares, R/V *Melville*, 1996.

key samples from pre-1996 voyages in this area (1982, R/V *Kallisto*; 1984, R/V *Natsushima*; 1990, R/V *Keldysh/Mir*). The data from more recent studies in this area (see above), combined with our new data, give us the opportunity to re-evaluate the model of Danyushevsky *et al.* [1995] in a more specific and quantitative manner. Our aim is to confirm the number and identify the nature of the D1, E1 and E2 components in the general model of Danyushevsky *et al.* [1995]. A particular focus of this study is to identify the number of independent mantle plume components (E2) which must be invoked to explain the isotopic composition of subduction-related magmas in this area.

[5] Our study suggests that, in addition to the previously identified mantle plume components (EMII, Samoa and subducted volcanoclastic sediments from the Louisville Ridge), an EMI-like component and a HIMU mantle plume component are also required to explain the isotopic geochemistry of the magmatic rocks investigated. Our geochemical modeling demonstrates that the model of Danyushevsky *et al.* [1995] successfully

accounts for the petrogenesis of boninites in this area.

2. Geological Setting and Dredge Locations

[6] At the northern termination of the Tonga Trench and northern Lau Basin (Figures 1–3), a wide variety of boninite and tholeiitic-dacitic-rhyolitic magmas have been recovered by rock dredging or submersible sampling by four research vessels: (1) voyage 16 of the R/V *Kallisto* in 1982 [Sharaskin *et al.*, 1983]; (2) the 1984 voyage of the R/V *Natsushima* [Honda *et al.*, 1985]; (3) the 1990 voyage of the R/V *Keldysh/Mir* [Malahoff and Falloon, 1991]; and (4) the 1996 voyage of the R/V *Melville* [Bloomer *et al.*, 1996; Wright *et al.*, 1996].

[7] The location of our study area and general tectonic features are shown schematically in Figure 1. The Tonga intraoceanic arc is recognized as a type example of an extension-dominated, non-accretionary convergent margin [Tappin, 1994; Tappin *et al.*, 1994; MacLeod, 1996], with active

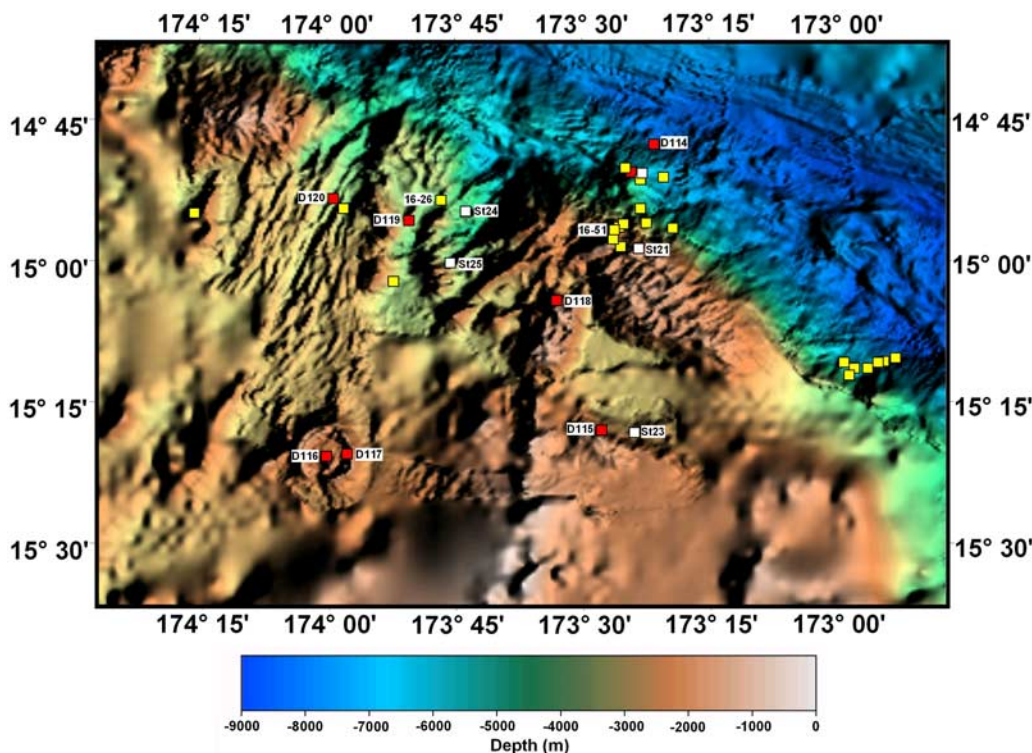


Figure 3. As for Figure 2. Figure 3 shows in more detail the locations of previous dredges in this area.

extensional tectonism throughout the forearc and landward trench slopes. The Tonga Trench is the site of westward subduction of the Pacific Plate beneath the northeastern corner of the Australian Plate. Recently, *Zellmer and Taylor* [2001], on the basis of detailed study of acoustic reflectivity and morphology, have identified three microplates to explain the kinematics of the Lau Basin–Tonga Trench system in the northern part of the Lau Basin. The three plates identified (Figure 1) are named the Niua fo’ou Plate, the Tonga Plate and the Australian Plate itself, in the southern part of the Lau Basin. The Peggy Ridge in the northern Lau Basin marks the southern boundary between the Australian and Niua fo’ou Plates.

[8] GPS measurements indicate that the instantaneous plate convergence across the northern Tonga Trench is 24 cm/yr, the fastest recorded convergence velocity on the modern Earth [*Bevis et al.*, 1995]. At the northern terminus of the trench near 15°S (Figure 1), plate convergence gives way to complex strike-slip motion along a transform fault and backarc extension in the northern Lau Basin. The trench-transform fault transition forms a slab-edge, the geometric consequences of which are the ongoing rupture and rifting of oceanic lithosphere [*Govers and Wortel*, 2005; *Millen and Hamburger*, 1998]. The tearing of the Pacific plate at the

northern terminus of the Tonga Trench (Figure 2) is evident at 15°–16° S, where the landward trench slope steepens significantly, the forearc narrows, and the trench axis is “pinched” by the presence of the Uo Mamae seamount. The Pacific plate displays striking WNW-trending lineaments which were interpreted by *Wright et al.* [2000] to be older Pacific Plate structures that have been reactivated by hinge-faulting at the bend in the trench.

[9] A consequence of the slab edge is the presence of a “slab window” which has allowed the flow of hot mantle from the Samoan plume into the northern Lau Basin above the subducting Pacific Plate [*Danyushevsky et al.*, 1995; *Smith et al.*, 2001; *Millen and Hamburger*, 1998]. Hot refractory Samoan mantle fluxed by slab-derived fluids is the primary cause for the presence of high-Ca boninite magmas at the termination of the Tonga Trench and northern Lau Basin [*Danyushevsky et al.*, 1995]. *Lupton et al.* [2004] found the highest $\delta(^3\text{He})$ reading of 43.4% detected at a depth of 1726 m, 15.0°S, 173.1°W, within the study area indicating significant hydrothermal venting of mantle He from extensional zones of the northern Lau Basin.

[10] Multibeam mapping along this boundary and the termination of the trench (Figures 2 and 3) reveals a tectonically complex terrain, including

Table 1. Major and Trace Element Geochemistry of Samples Recovered by Dredging by the R/V *Melville* and the R/V *Natsushima*^a

Location Voyage	Forearc ^b		Ridge		Ridge		Ridge		Ridge		Backarc		Backarc	
	Melville 96 D114	Melville 96 D114-3-6	Melville 96 D115	Melville 96 D115-1-1	Melville 96 D115-1-2	Melville 96 D115-1-8	Melville 96 D115	Melville 96 D115-1-5	Melville 96 D115-2-5	Melville 96 D115-2-7	Melville 96 D115	Melville 96 D116	Melville 96 D116	Melville 96 D116
Dredge station	Boninite	Basalt	Boninite	Boninite	Boninite	Boninite	Boninite	Andesite	Andesite	Andesite	Boninite	Dacite	Dacite	Dacite
Sample	114-3-1	114-3-6	115-1-2	115-1-1	115-1-2	115-1-8	115-1-5	115-2-5	115-2-7	115-2-7	5-10	116-1-1	116-1-3	116-2-1
Lithology	Boninite	Basalt	Boninite	Boninite	Boninite	Boninite	Boninite	Andesite	Andesite	Andesite	Boninite	Dacite	Dacite	Dacite
SiO ₂	52.57	52.00	54.83	54.75	56.57	56.40	56.71	56.99	53.14	66.22	66.37	67.33	67.33	67.33
TiO ₂	0.38	1.58	0.12	0.15	0.21	0.17	0.31	0.32	0.15	0.55	0.55	0.56	0.56	0.56
Al ₂ O ₃	14.34	14.60	6.29	8.20	12.33	9.91	16.93	16.44	7.00	13.73	13.59	13.68	13.68	13.68
FeO ^d	7.35	11.48	9.03	10.07	10.33	10.60	9.77	9.88	9.36	7.42	7.48	6.70	6.70	6.70
MnO	0.14	0.20	0.20	0.21	0.19	0.21	0.17	0.17	0.18	0.14	0.14	0.12	0.12	0.12
MgO	12.44	8.31	17.29	14.62	8.29	10.28	3.66	3.82	22.84	1.76	1.73	1.72	1.72	1.72
CaO	10.79	8.54	11.55	11.04	10.52	11.17	10.74	10.61	6.41	5.66	5.62	5.50	5.50	5.50
Na ₂ O	1.63	3.03	0.52	0.71	1.15	0.90	1.32	1.42	0.78	3.33	3.33	3.23	3.23	3.23
K ₂ O	0.25	0.14	0.16	0.22	0.36	0.34	0.35	0.32	0.11	1.00	0.99	0.97	0.97	0.97
P ₂ O ₅	0.10	0.14	0.01	0.01	0.03	0.02	0.03	0.03	0.03	0.19	0.19	0.17	0.17	0.17
LOI ^e	1.61	2.83	0.00	0.24	0.69	0.51	0.02	0.00	-0.14	0.96	1.08	1.17	1.17	1.17
Total ^f	99.88	100.13	99.78	99.54	99.85	99.88	100.21	99.39	99.48	99.97	99.62	99.50	99.50	99.50
Rb	3.1	1.6	2.1	5.0	5.7	5.4	5.2	5.0	2.0	17.1	17.7	16.8	16.8	16.8
Ba	26	21	44	58	79	87	79	80	27	227	227	233	233	233
Nb	<1.0	4.0	<1.0	<1.0	1.3	1.4	1.3	<1.0	<1.0	5.9	6.1	5.6	5.6	5.6
Sr	93	90	81	106	201	157	201	190	42	244	244	252	252	252
Zr	26	128	7	8	15	11	15	15	6	57	57	58	58	58
Y	12	47	4	2.8	5	4.8	7	8	4	20	20	17	17	17
V	210	354	202	244	386	276	386	365	171	179	175	170	170	170
Sc	35	44	51	56	45	59	45	48	33	26	27	26	26	26
Cr	723	183	1354	896	44	656	44	20	2212	3	2	2	2	2
Ni	335	65	135	125	51	58	13	12	558	3	2	2	2	2

Table 1. (continued)

Location	Backarc	Ridge	Ridge	Backarc	Backarc	Backarc	Backarc	Backarc	NELSC ^c	NELSC	NELSC	NELSC
Dredge station	Melville 96	Melville 96	Melville 96	Melville 96								
Sample	D117	D118	D118	D119	D119	D119	D119	D119	D120	D120	D120	D120
Lithology	Rhyolite	Rhyolite	Rhyolite	Boninite	Boninite	Boninite	Boninite	Boninite	Basalt	Basalt	Basalt	Basalt
SiO ₂	73.39	73.51	73.81	73.77	47.18	52.95	55.76	57.98	53.18	53.30	53.98	54.07
TiO ₂	0.41	0.41	0.28	0.30	0.31	0.16	0.22	0.26	0.97	0.98	0.90	0.90
Al ₂ O ₃	12.49	12.40	12.93	12.99	7.06	9.02	10.79	13.61	16.91	16.83	16.90	16.90
FeO ^d	4.35	4.33	3.29	3.28	8.59	8.37	8.67	7.52	8.23	8.28	8.51	8.45
MnO	0.09	0.10	0.07	0.07	0.15	0.16	0.16	0.14	0.15	0.15	0.15	0.15
MgO	0.65	0.65	1.09	1.12	28.70	20.79	13.87	8.33	6.16	6.07	5.84	5.81
CaO	3.16	3.21	3.61	3.59	6.60	7.29	8.88	9.89	10.95	10.87	10.29	10.39
Na ₂ O	3.47	3.61	3.41	3.38	0.98	0.98	1.33	1.77	2.48	2.51	2.50	2.39
K ₂ O	1.91	1.69	1.44	1.43	0.32	0.24	0.22	0.44	0.77	0.80	0.74	0.76
P ₂ O ₅	0.08	0.09	0.06	0.06	0.09	0.03	0.08	0.06	0.20	0.20	0.18	0.18
LOI ^e	3.08	1.67	1.47	1.36	0.08	0.91	0.05	0.37	1.22	1.39	1.08	1.47
Total ^f	99.66	99.78	100.28	99.94	99.80	99.81	99.70	99.86	99.42	100.20	100.16	100.10
Rb	30.6	30.1	28.4	28.8	7.0	4.0	30.0	7.4	19.7	20.5	17.9	19.3
Ba	355	361	342	337	102	58	71	99	194	194	183	179
Nb	8.2	7.9	15.8	15.7	5.3	3.0	4.4	5.9	9.7	9.5	9.6	9.2
Sr	227	224	242	238	138	89	141	158	294	290	278	279
Zr	74	75	75	76	21	15	19	30	71	72	66	67
Y	23	23	14	14	6	6	9	9	20	21	20	19
V	11	12	47	48	135	160	208	213	262	259	292	296
Sc	16	15	12	13	24	30	34	36	33	33	34	34
Cr	2	4	17	19	1957	1659	848	411	84	85	34	33
Ni	1	1	3	3	957	472	212	77	51	51	44	44

^aMajor element geochemistry is in wt%, and trace element geochemistry is in ppm.

^bFor locations of dredge stations refer to Table A1 and Figure 3.

^cNELSC refers to the Northeast Lau Spreading Center.

^dTotal iron calculated as FeO.

^eLOI refers to loss on ignition.

^fTotal refers to original analysis sum. Major elements have been resumed to 100% on an anhydrous basis.

Table 2. Major Element Geochemistry of Glasses Recovered by Dredging by the R/V *Melville*^a

Location	NELSC	NELSC	NELSC	NELSC	Backarc	Ridge	Ridge	Ridge	Ridge
Voyage	Melville 96								
Dredge station	D120	D120	D120	D120	D117	D118	D115	D115	D115
Sample	120-2-3	120-2-1	120-1-3	120-1-1	117-2-3	118-2-8	115-1-11	115-1-10	115-1-8
SiO ₂ ^b	55.66	55.68	54.77	54.57	75.5	80.53	54.10	57.17	59.31
TiO ₂	1.11	1.11	1.15	1.14	0.41	0.29	0.34	0.24	0.25
Al ₂ O ₃	15.70	15.75	16.05	16.03	11.88	11.51	14.35	14.12	14.04
FeO	9.51	9.55	9.42	9.24	4.22	2.41	12.96	11.74	11.13
MnO	0.17	0.16	0.16	0.17	0.09	0.04	0.21	0.21	0.09
MgO	4.77	4.72	5.08	5.12	0.45	0.26	4.42	4.00	3.78
CaO	9.46	9.39	9.79	9.99	2.83	1.78	11.43	10.30	9.49
Na ₂ O	2.52	2.49	2.41	2.57	2.88	1.43	1.48	1.48	1.27
K ₂ O	0.89	0.90	0.91	0.90	1.63	1.72	0.50	0.55	0.47
P ₂ O ₅	0.21	0.20	0.24	0.22	0.05	0.03	0.18	0.16	0.10
Cr ₂ O ₃	0.00	0.01	0.02	0.02	0.02	0.00	0.03	0.01	0.06
NiO	0.01	0.03	0.02	0.02	0.02	0.00	0.03	0.01	0.0

^aMajor element geochemistry is in wt%.

^bMajor elements have been resumed to 100% on an anhydrous basis.

the transition from subduction to strike-slip motion, and the northeast and southeast limbs of the Mangatolu Triple Junction (MTJ). This terrain contains (1) new seafloor generated by backarc spreading; (2) a deep, well-defined graben structure cutting across the Tonga Arc crust; (3) extensional rift zones associated with large caldera-like features; and (4) young volcanic seamounts located within extensional domains and graben structures. In Appendix A, we describe in detail the locations of our new and older sampling relative to the new seafloor mapping in this area, and provide a brief petrographic summary of our new sampling.

3. Geochemistry: Results and Discussion

[11] In Tables 1–4 and Figures 4–13 we present our new major and trace element and isotopic geochemistry for samples from the northern termination of the northern Tonga Ridge and the northern Lau Basin. In Appendix B, we present in detail our analytical techniques. Previous isotopic data on the Tongan boninites was presented by *Falloon et al.* [1989] and *Danyushevsky et al.* [1995] and our new data is consistent with this work, with the exception of sample 5–24 from dredge station St23 (Figure 3) [*Falloon et al.*, 1987]. Sample 5–24 is the most depleted boninite in terms of REE and HFSE, and was considered by *Danyushevsky et al.* [1995] to be close to the depleted component end-member (D1) required in the petrogenesis of these boninites. The depleted component D1 was considered to be refractory OIB mantle (Samoan

plume) on the basis of (1) low ¹⁴³Nd/¹⁴⁴Nd isotopes in sample 5–24 (0.51277 [*Falloon et al.*, 1989]) within the range of Samoan OIB, and (2) very high temperatures established for the primary melt for this depleted component (~1480°C at ~45 km) confirmed by two independent experimental studies [*Sobolev and Danyushevsky*, 1994; *Falloon and Danyushevsky*, 2000]. In our new work we have reanalyzed sample 5–24 (3 repeat separate dissolutions, Table 4) and have obtained an average ¹⁴³Nd/¹⁴⁴Nd value of 0.512973, significantly higher than previously analyzed by *Falloon et al.* [1989]. To confirm our new result we also analyzed sample 5–28 from dredge station St23, a depleted boninite similar to 5–24, which has a similar ¹⁴³Nd/¹⁴⁴Nd value of 0.512959. The reasons for the difference in results between this study and *Falloon et al.* [1989] is most likely related to the difficulty of determining ¹⁴³Nd/¹⁴⁴Nd values on very depleted boninite samples (5–24 has ~0.8 ppm Nd, Table 3) with the instrumentation and techniques available at that time, as the ⁸⁷Sr/⁸⁶Sr values determined in this study are essentially identical to those obtained by *Falloon et al.* [1989] (5–24 has ~48 ppm Sr, Table 3; av. ⁸⁷Sr/⁸⁶Sr this study 0.704436 ± 0.000031, Table 4, versus 0.704422 obtained by *Falloon et al.* [1989]). The other Tonga samples analyzed by *Falloon et al.* [1989] all have higher Nd abundances (2.7–17.3 ppm [*Falloon et al.*, 1989]) and their ¹⁴³Nd/¹⁴⁴Nd values are consistent with our new analyses of rocks sampled by the R/V *Melville* from the same areas as sampled by the R/V *Natsushima* (Table 4; T. J. Falloon, unpublished data, 1997). As we will demonstrate in section 4.1

Table 3. Trace Element Geochemistry of Rock Samples Dredged From the Northern Lau Basin-Tonga Area^a

Location	Voyage	Station	Sample	Lab	Rb	Ba	Th	U	Nb	Pb	Sr	Zr	Hf	Y
Backarc	Kall 82 ^b	16-9	16-9/1	ANU ^c	37.52	688.1	6.096	1.609	45.504	5.727	689.1	180.15	3.900	23.24
Backarc	Kall 82	16-10	16-10/4	ANU	27.66	842.1	4.175	1.267	51.717	5.210	862.1	181.99	4.224	22.32
Backarc	Kall 82	16-94	16-94/1	ANU	24.28	603.1	4.342	1.215	47.396	4.929	705.2	280.36	6.119	21.35
Backarc	Kall 82	16-26	16-26/1	ANU	6.27	59.4	0.577	0.185	3.113	1.345	100.5	18.19	0.469	6.44
Backarc	Kall 82	16-26	16-26/2	ANU	6.80	63.9	0.713	0.202	4.005	1.327	96.8	20.54	0.509	5.30
Backarc	Nat 84 ^d	St25	7-18	ANU	13.46	213.8	2.109	0.596	16.052	3.086	337.1	53.39	1.173	9.48
Backarc	Nat 84	St24	6-3	ANU	7.85	93.9	0.893	0.259	8.190	1.995	150.0	32.85	0.806	6.92
Ridge	Nat 84	St23	5-25	ANU	2.22	33.4	0.089	0.065	0.671	0.819	66.0	19.98	0.558	10.15
Ridge	Nat 84	St23	5-24	UTAS ^e	2.35	32.8	0.079	0.065	0.650	0.733	70.6	20.46	0.562	9.32
Ridge	Nat 84	St23	5-24	ANU	1.92	26.1	0.041	0.038	0.280	0.727	43.0	5.83	0.193	5.06
Ridge	Nat 84	St23	5-28	UTAS (2)	2.24	27.9	0.028	0.033	0.280	0.608	47.6	6.39	0.188	4.99
Ridge	Nat 84	St23	5-27	UTAS (2)	2.34	28.4	0.028	0.033	0.295	0.620	49.8	6.76	0.205	5.19
Ridge	Nat 84	St23	5-20	UTAS	3.49	47.9	0.111	0.086	0.980	0.930	107.1	26.60	0.760	12.70
Forearc	Nat 84	St21	3-44	ANU	2.91	49.7	0.174	0.116	1.495	1.255	120.7	38.87	1.092	17.65
Forearc	Nat 84	St21	3-51	ANU	6.15	92.1	0.327	0.156	2.060	1.813	143.5	12.61	0.372	6.36
Forearc	Nat 84	St21	3-24	ANU	5.42	98.4	0.339	0.176	1.630	1.259	166.7	13.21	0.396	5.63
Forearc	Nat 84	St21	3-36	ANU	9.46	128.0	0.600	0.246	1.873	2.580	167.2	19.66	0.592	8.15
Forearc	Nat 84	St21	3-36	ANU	18.08	265.1	2.078	0.694	4.592	5.012	377.1	43.83	1.204	12.15
Peggy Ridge ^f	Nat 84	St31	11-3	UTAS										
MTJ ^g	Kel/M 90 ^h	M-2212	M-2212-2(g) ⁱ	ANU	6.06	39.6	0.247	0.117	2.430	0.804	127.0	60.38	1.609	22.30
MTJ	Kel/M 90	M-2218	M-2218-2	ANU	5.35	42.1	0.283	0.129	2.791	0.923	119.6	75.19	1.946	24.06
MTJ	Kel/M 90	M-2218	M-2218-4(g)	ANU	2.47	23.7	0.221	0.076	2.243	0.940	130.1	72.08	1.808	27.01
MTJ	Kel/M 90	M-2218	M-2218-9	ANU	2.37	24.6	0.212	0.080	2.256	1.074	122.9	70.93	1.792	23.67
MTJ	Kel/M 90	M-2218	M-2218-10	ANU	4.86	31.1	0.261	0.120	2.140	0.806	120.3	60.91	1.592	24.86
Forearc	Mel 96 ^j	D114	114-3-1	UTAS		24.7	0.11	0.067	0.62	0.35		25.9	0.723	
Forearc	Mel 96	D114	114-3-6	UTAS		21.2	0.335	0.211	3.69	0.5			2.675	
Ridge	Mel 96	D115	115-1-1	UTAS		37.5	0.232	0.089	0.41	1.01		7.5	0.21	
Ridge	Mel 96	D115	115-2-7	UTAS		76	0.446	0.159	0.88	1.53		15.2	0.469	
Backarc	Mel 96	D116	116-1-3	UTAS		233.8	1.519	0.575	5.46	3.03		59.7	1.665	
Backarc	Mel 96	D117	117-2-3	UTAS		357.5	2.021	0.732	7.61	5.01		77.2	2.182	
Ridge	Mel 96	D118	118-2-5	UTAS		335.1	2.47	0.875	14.97	5.31		76.3	1.988	
Backarc	Mel 96	D119	119-1-1	UTAS		95.8	0.908	0.263	4.56	1.24		22.6	0.601	
Backarc	Mel 96	D119	119-2-5	UTAS		53.4	0.842	0.261	2.8	1.33		16.1	0.451	
NELSC ^k	Mel 96	D120	120-1-1	UTAS		196.1	1.371	0.475	9.03	1.6		71.3	1.849	
NELSC	Mel 96	D120	120-2-1	UTAS		186.5	1.421	0.435	9.34	2.16		66.9	1.74	

Table 3. (continued)

Location	Voyage	Station	Sample	Lab	La	Ce	Pr	Nd	Sm	Eu	Gd	Tb	Dy	Ho	Er	Yb	Lu
Backarc	Kall 82 ^b	16-9	16-9/1	ANU	46.352	90.105	10.497	38.987	7.214	2.163	6.040	0.888	4.424	0.827	2.143	1.702	0.245
Backarc	Kall 82	16-10	16-10/4	ANU	48.884	103.091	12.669	49.566	9.421	2.799	7.657	1.073	5.144	0.920	2.323	1.749	0.249
Backarc	Kall 82	16-94	16-94/1	ANU	42.938	87.271	10.436	39.988	7.580	2.369	6.263	0.903	4.378	0.788	1.928	1.398	0.197
Backarc	Kall 82	16-26	16-26/1	ANU	3.024	5.813	0.724	2.973	0.734	0.245	0.827	0.149	0.942	0.219	0.675	0.736	0.118
Backarc	Kall 82	16-26	16-26/2	ANU	4.065	7.660	0.942	3.756	0.819	0.262	0.825	0.137	0.810	0.174	0.510	0.521	0.079
Backarc	Nat 84 ^d	Si25	7-18	ANU	16.117	32.904	3.978	15.613	3.022	0.860	2.101	0.341	1.685	0.333	0.917	0.853	0.133
Backarc	Nat 84	Si24	6-3	ANU	5.662	11.215	1.381	5.530	1.218	0.379	1.178	0.194	1.123	0.250	0.727	0.735	0.118
Ridge	Nat 84	Si23	5-25	ANU	1.021	2.720	0.442	2.325	0.827	0.312	1.189	0.234	1.521	0.355	1.080	1.095	0.175
Ridge	Nat 84	Si23	5-24	UTAS	1.057	2.699	0.455	2.424	0.842	0.319	1.165	0.233	1.582	0.360	1.078	1.140	0.165
Ridge	Nat 84	Si23	5-28	ANU	0.322	0.788	0.133	0.718	0.286	0.113	0.477	0.102	0.698	0.169	0.543	0.605	0.100
Ridge	Nat 84	Si23	5-27	UTAS (2)	0.361	0.822	0.147	0.794	0.311	0.126	0.508	0.106	0.756	0.183	0.565	0.620	0.097
Ridge	Nat 84	Si23	5-20	UTAS (2)	0.363	0.876	0.151	0.823	0.327	0.131	0.533	0.111	0.791	0.191	0.576	0.639	0.101
Forearc	Nat 84	Si21	3-44	ANU	1.445	3.878	0.625	3.354	1.139	0.409	1.561	0.300	2.037	0.480	1.402	1.469	0.230
Forearc	Nat 84	Si21	3-24	ANU	2.031	5.441	0.880	4.571	1.569	0.573	2.157	0.416	2.680	0.614	1.862	1.851	0.287
Forearc	Nat 84	Si21	3-36	ANU	1.976	5.467	0.895	4.620	1.627	0.592	2.130	0.408	2.757	0.626	1.874	1.846	0.275
Peggy Ridge ^f	Nat 84	Si31	11-3	UTAS	1.08	1.08	0.64	3.48	1.57	0.62	2.74	0.577	3.76	0.793	2.50	2.39	0.308
MTJ ^g	Kel/M 90 ^h	M-2212	M-2212-2(g)	ANU	3.241	8.975	1.426	7.398	2.404	0.874	3.166	0.577	3.601	0.793	2.296	2.097	0.308
MTJ	Kel/M 90	M-2218	M-2218-2	ANU	3.740	10.410	1.651	8.491	2.755	0.934	3.480	0.632	3.882	0.854	2.412	2.160	0.316
MTJ	Kel/M 90	M-2218	M-2218-4(g)	ANU	3.351	9.630	1.603	8.235	2.755	1.009	3.673	0.678	4.314	0.955	2.804	2.586	0.384
MTJ	Kel/M 90	M-2218-9	M-2218-9	ANU	3.305	9.493	1.545	8.036	2.651	0.981	3.508	0.658	4.078	0.900	2.609	2.397	0.354
MTJ	Kel/M 90	M-2218	M-2218-10	ANU	3.258	9.100	1.483	7.478	2.501	0.938	3.375	0.643	3.987	0.879	2.623	2.420	0.365
Forearc	Mel 96 ⁱ	D114	114-3-1	UTAS	1.405	2.872	0.482	2.563	0.876	0.354	1.35	0.259	1.721	0.394	1.172	1.238	0.196
Forearc	Mel 96	D114	114-3-6	UTAS	4.614	12.856	2.126	11.534	4.067	1.308	5.53	1.038	6.592	1.46	4.139	4.034	0.614
Ridge	Mel 96	D115	115-1-1	UTAS	1.431	2.182	0.29	1.251	0.349	0.126	0.43	0.073	0.463	0.109	0.339	0.373	0.061
Ridge	Mel 96	D115	115-2-7	UTAS	2.398	4.527	0.6	2.768	0.768	0.3	0.98	0.178	1.132	0.269	0.786	0.889	0.146
Backarc	Mel 96	D116	116-1-3	UTAS	9.244	18.815	2.459	10.999	2.741	0.839	2.95	0.497	3.105	0.694	1.974	2.15	0.351
Backarc	Mel 96	D117	117-2-3	UTAS	12.163	23.892	3.101	13.374	3.118	0.926	3.35	0.563	3.434	0.766	2.248	2.446	0.399
Ridge	Mel 96	D118	118-2-5	UTAS	13.892	26.08	3.01	11.868	2.358	0.659	2.16	0.35	2.075	0.45	1.352	1.501	0.247
Backarc	Mel 96	D119	119-1-1	UTAS	5.787	11.582	1.45	6.033	1.268	0.421	1.28	0.201	1.09	0.236	0.644	0.667	0.104
Backarc	Mel 96	D119	119-2-5	UTAS	3.712	6.321	0.711	2.848	0.645	0.224	0.76	0.138	0.843	0.194	0.601	0.642	0.106
NELSC ^k	Mel 96	D120	120-1-1	UTAS	9.813	20.82	2.757	12.252	2.965	1.009	3.19	0.543	3.206	0.678	1.92	1.89	0.296
NELSC	Mel 96	D120	120-2-1	UTAS	10.138	20.541	2.66	11.676	2.827	0.956	3.05	0.516	3.054	0.653	1.81	1.84	0.285

^aTrace element geochemistry is in ppm.

^bKall 82 refers to the 1982 voyage of the RV *Kallisto*.

^cANU, Australian National University.

^dNat 84 refers to the 1984 voyage of the RV *Natsushima*.

^eUTAS, University of Tasmania.

^fREE data are presented for sample 11-3, a Lau Basin backarc basalt from the Peggy Ridge recovered by the Natsushima 84 cruise. REE abundances for this sample were incorrectly reported as chondrite normalized values by Falloon et al. [1987, 1989]. The correct values for 11-3 in ppm are provided in Table 3.

^gMTJ refers to the Mangatolu Triple.

^hKel/M 90 refers to the 1990 voyage of the RV *Keldysh* and submersible *Mir*.

ⁱ(g) refers to glass.

^jMel 96 refers to the 1996 voyage of the RV *Melville*.

^kNELSC refers to the Northeast Lau Spreading Center.

Table 4. Isotope Geochemistry of Rock Samples Dredged From the Northern Lau–Tonga Area

Location	Voyage	Station	Sample	Lab	⁸⁷ Sr/ ⁸⁶ Sr	¹⁴³ Nd/ ¹⁴⁴ Nd	²⁰⁶ Pb/ ²⁰⁴ Pb	²⁰⁷ Pb/ ²⁰⁴ Pb	²⁰⁸ Pb/ ²⁰⁴ Pb
Backarc	Kall 82	16-9	16-9/1	MELB ^a	0.704155	0.512757	19.215	15.644	39.154
	Kall 82	16-10	16-10/4	MELB	0.704299	0.512743	19.143	15.632	39.064
	Kall 82	16-26	16-26/2	MELB			18.921	15.623	38.893
Ridge	Nat 84	St23	5–24	MELB	0.704465	0.512977	18.625	15.570	38.435
				MELB	0.704404	0.512979			
				MELB	0.704439	0.512964			
				MELB					
Ridge	Nat 84	St23	5–28	MELB	0.704439	0.512959	18.639	15.566	38.450
Ridge	Nat 84	St23	5–20	ANU ^b	0.703844	0.512961	18.583	15.541	38.329
Ridge	Nat 84	St21	3–24	ANU	0.704384	0.512785	18.740	15.585	38.676
Ridge	Nat 84	St21	3–22	ANU			18.757	15.575	38.711
Ridge	Nat 84	St21	3–52	ANU			18.795	15.583	38.748
Ridge	Nat 84	St21	3–36	ANU			18.827	15.596	38.789
Peggy Ridge	Nat 84	St31	11-3	ANU	0.703364	0.512963	18.074	15.503	38.117
Forearc	Mel 96	D114	114-3-1	MELB	0.703582	0.513041	18.432	15.558	38.112
Forearc	Mel 96	D114	114-3-6	MELB	0.703595	0.512999	18.603	15.549	38.462
Ridge	Mel 96	D115	115-1-1	MELB	0.704603	0.512812	18.766	15.591	38.717
Backarc	Mel 96	D116	116-1-3	MELB	0.704076	0.512865	19.229	15.616	38.940
Backarc	Mel 96	D119	119-2-5	MELB	0.704884	0.512755	18.883	15.619	38.911
				MELB	0.704849	0.512760			
				MELB	0.704884	0.512755			
MTJ	Mel 96	D120	120-1-1	MELB	0.703839	0.512861	19.026	15.602	38.908

^aMELB, University of Melbourne.

^bANU, Australian National University.

(see below), the new ¹⁴³Nd/¹⁴⁴Nd value obtained for sample 5–24 in this study is, in fact, more consistent with the model of *Danyushevsky et al.* [1995] than the previously reported value by *Falloon et al.* [1989].

3.1. Northern Tongan Boninite Compositions

[12] Figure 4 shows that the north Tongan boninites (blue, red and green circles; see caption to Figure 4) have significantly higher whole rock SiO₂ at a given MgO content compared to young island arc series volcanics from the Tofua Volcanic arc (TVA; the northern section of the Tonga Arc), backarc basin basalts from the northern Lau Basin, and MORB (see calculated liquid line of descent for Siqueiros Fracture Zone, East Pacific Rise, Figure 4) (Figure 4a). Boninite compositions are exceptionally picritic with MgO contents ranging to 29 wt% (sample 119-1-1, Table 1), reflecting accumulation of magnesian olivine phenocrysts (range Fo 89–94, Table A4 and *Falloon and Green* [1986] and *Sobolev and Danyushevsky* [1994]). Detailed mineralogy of the boninites from this area is reported in detail by *Falloon et al.* [1989] and *Sobolev and Danyushevsky* [1994]. The boninites also have exceptionally low TiO₂ contents (range ~0.1–0.3 wt%, Table 1) at a given MgO content compared to other magma suites in the area (Figure 4b).

[13] The Tongan boninites have been broadly divided into two groups by *Sobolev and Danyushevsky* [1994]. The eastern group boninites (from dredge stations St21, St23, D114, D115 and D118, Figure 3; blue and red circles in Figure 4; blue and red symbols for individual samples Figures 5–20) are associated with rifting of the north Tongan Ridge and generally have higher FeO^T contents (Figure 4d) compared to the western group boninites (from dredge stations St24, St25, 16–26, D116, D117 and D119, Figure 3; green circles in Figure 4; green symbols for individual samples Figures 5–20), which are associated with rifting of the northern Lau Basin immediately adjacent to the north Tonga Ridge (Figures 2 and 3). *Danyushevsky et al.* [1995] recognized that the compositions of Tongan boninites could be explained by magma mixing between a “depleted” and an “enriched” end-member boninite composition. The results of this study suggest that a third, intermediate boninite end-member is also required to explain the full range in major, trace and isotopic compositions of the north Tongan boninites. In Figure 5, the normalized abundance patterns of the three identified boninite end-member compositions are presented along with the general model for boninite petrogenesis of *Danyushevsky et al.* [1995].

[14] The most depleted boninite end-member is represented by boninite 5–24 from the eastern group boninites recovered from dredge station

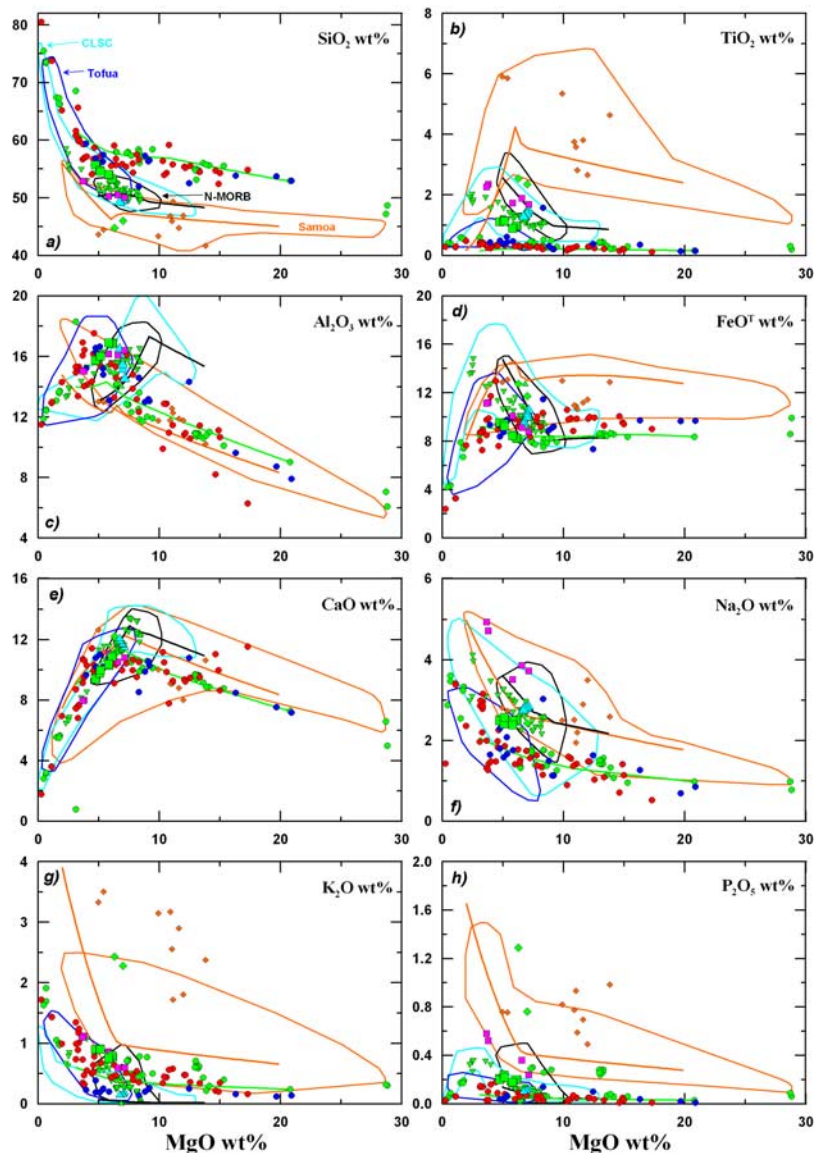


Figure 4. Major elements (a) SiO_2 , (b) TiO_2 , (c) Al_2O_3 , (d) FeO^T , total iron as FeO , (e) CaO , (f) Na_2O , (g) K_2O , and (h) P_2O_5 wt% versus MgO wt% for dredged volcanic rocks from the north termination of the Tonga Trench and northern Lau Basin. All analyses have been resummed to 100 wt% on an anhydrous basis. Plotted symbols, fields, and lines are as follows: Eastern group boninites and related rocks, red and blue circles. The red circles are samples with enriched REE patterns and the blue circles are samples with flat to depleted REE patterns (see section 3.2). Western group boninites and related rocks, green circles; D120, green squares; Coriolis Trough, magenta squares; Niua fo'ou, cyan triangles; Uo Mamae, orange diamonds; 16-9 and 16-10, green diamonds; Mangatolu Triple Junction (MTJ) type I lavas, green triangles; MTJ type II lavas, green inverted triangles; orange field, Samoa; black field, N-MORB; blue field, Tofua Arc; cyan field, Central Lau Spreading Center (CLSC); orange line, liquid line of descent (LLD) for Samoa; black line, LLD for N-MORB; green line, LLD for D119 western group boninites. Data sources are as follows: Samoan Plume, *Workman et al.* [2004]; S. R. Hart (personal communication, 2004); MTJ, *Falloon et al.* [1992]; CLSC, *Falloon et al.* [1992], *Hawkins* [1976, 1995], *Hawkins and Melchior* [1985], *Sunkel* [1990], *Loock et al.* [1990], *Fouquet et al.* [1991], *Boespflug et al.* [1990], *Volpe et al.* [1988], and *Pearce et al.* [1995]; Tofua arc, including Tafahi and Niuatoputapu and the backarc island of Niua fo'ou, *Ewart et al.* [1973, 1977, 1994, 1998], *Ewart and Hawkesworth* [1987], *Turner et al.* [1997], *Wendt et al.* [1997], and *Regelous et al.* [1997]; Coriolis Trough, *McConachy et al.* [2005]; Uo Mamae, *Zlobin et al.* [1991]; Tongan boninites, this study, *Falloon et al.* [1987, 1989], *Falloon and Crawford* [1991], *Sobolev and Danyushevsky* [1994], and *Danyushevsky et al.* [1995]; and N-MORB, *Danyushevsky* [2001]. Liquid lines of descent for representative whole rock compositions from Samoa, Siqueiros, and D119 were calculated using PETROLOG software [*Danyushevsky*, 2001].

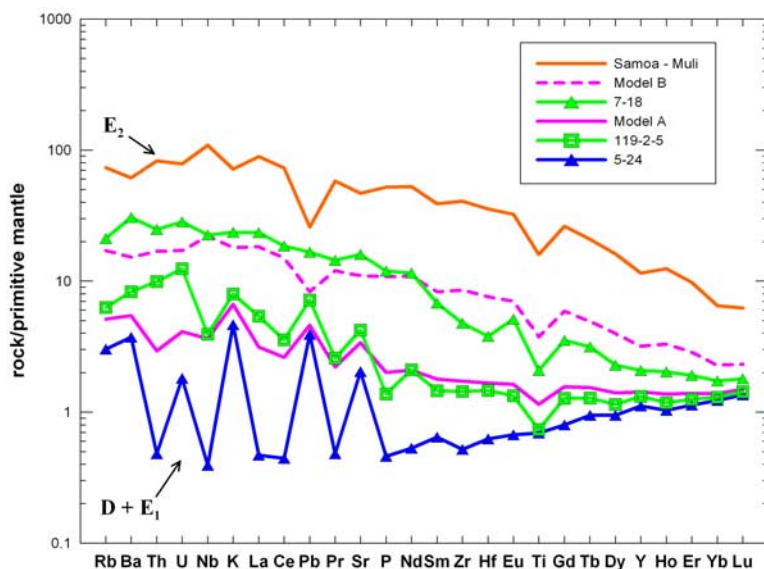


Figure 5. Primitive mantle normalized trace element abundance patterns of end-member boninites from northern termination of the Tonga ridge and Lau Basin. D + E₁ and E₂ are the components in the petrogenetic model of *Danyushevsky et al.* [1995]; see text for discussion. Mixing model A, 3 wt% av Muli lava composition from Samoa [Workman et al., 2004] and 97 wt% boninite 5–24. Mixing model B, 20 wt% av Muli lava composition and 80 wt% boninite 5–24. Primitive mantle normalizing values from *Sun and McDonough* [1989].

St23 (Figure 3) [Falloon et al. [1987]. In the model of *Danyushevsky et al.* [1995], this end-member is considered to be the result of a subduction component (E₁), most likely a slab-derived fluid, flux-

ing and causing melting of a refractory OIB source mantle (D₁, the Samoan plume). The depleted end-member has a gently sloping, LREE-depleted REE pattern ($La_N/Sm_N = 0.73$, Figure 5) and very low

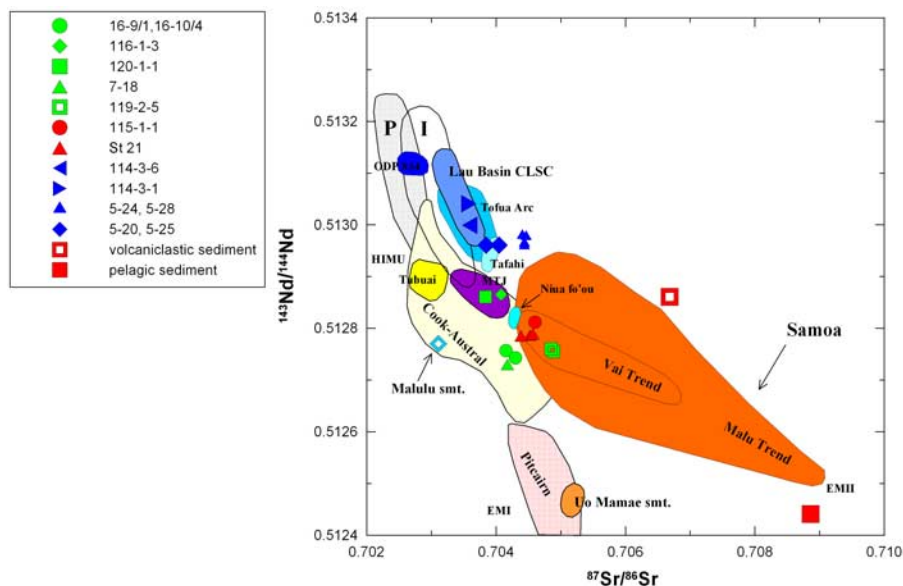


Figure 6. The $^{143}\text{Nd}/^{144}\text{Nd}$ versus $^{87}\text{Sr}/^{86}\text{Sr}$ isotopic compositions of submarine volcanics from the northern termination of the Tonga ridge and Lau Basin compared to the isotopic compositions of relevant magmatic suites. Data sources are as follows: Samoa, including Malulu seamount, *Workman et al.* [2004] and S. R. Hart (personal communication, 2004); Tafahi and Niua fo'ou, *Turner et al.* [1997]; Uo Mamae seamount, *Acland* [1996]; volcaniclastic and pelagic sediment, see Table C2 (Appendix C); and ODP 834, *Hergt and Hawkesworth* [1994]. All other data sources are from this study and the GEOROC reference database (<http://georoc.mpch-mainz.gwdg.de/georoc/>). P refers to Pacific MORB. I refers to Indian MORB. MTJ refers to the Mangatolu Triple Junction center in the northern Lau Basin.

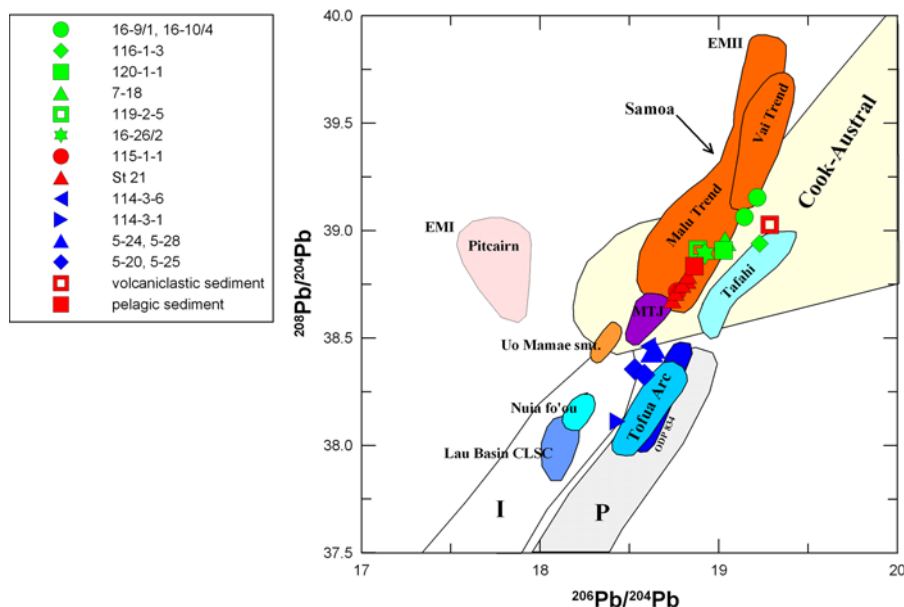


Figure 7. The $^{208}\text{Pb}/^{204}\text{Pb}$ versus $^{206}\text{Pb}/^{204}\text{Pb}$ isotopic compositions of submarine volcanics from the northern termination of the Tongan arc and northern Lau Basin compared to the isotopic compositions of relevant magmatic suites. Data sources as for Figure 6.

abundances of HFSE and HREE (e.g., Nb = 0.28 ppm; Yb = ~0.61, Table 3) reflecting the refractory D1 source component. The influence of the E1 component (slab-derived fluid) is reflected in the typical subduction zone enrichment in LILE elements (Rb, Ba, U, K, Pb and Sr) seen in the depleted end-member (Figure 5). The depleted

end-member has $^{143}\text{Nd}/^{144}\text{Nd}$ values within the range shown by Pacific MORB and TVA, but displaced to significantly higher $^{87}\text{Sr}/^{86}\text{Sr}$ values (5–24, Figure 6, Table 4). The depleted end-member also has Pb isotope values which are close to those displayed by Pacific MORB and the TVA (Figure 7 and Table 4).

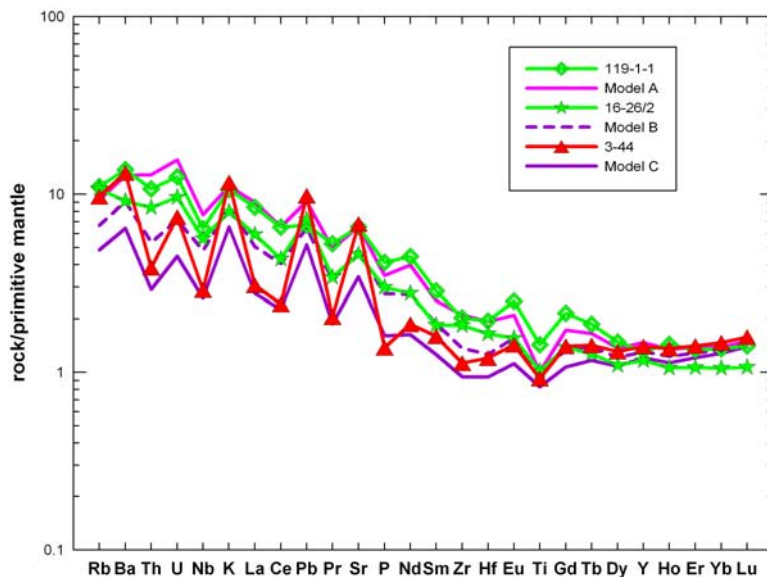


Figure 8. Primitive mantle normalized trace element abundance patterns of selected boninites from the north Tonga Ridge and northern Lau Basin, and mixing models (models A, B, and C) between the identified boninite end-members (types 1–3; see text for discussion). Model A, 20 wt% type 2 boninite 7–18 and 80 wt% type 3 boninite 119-2-5. Model B, 20 wt% type 2 boninite 7–18 and 80 wt% type 1 boninite 5–24. Model C, 10 wt% type 2 boninite 7–18 and 90 wt% type 1 boninite 5–24. Primitive mantle normalizing values from *Sun and McDonough* [1989].

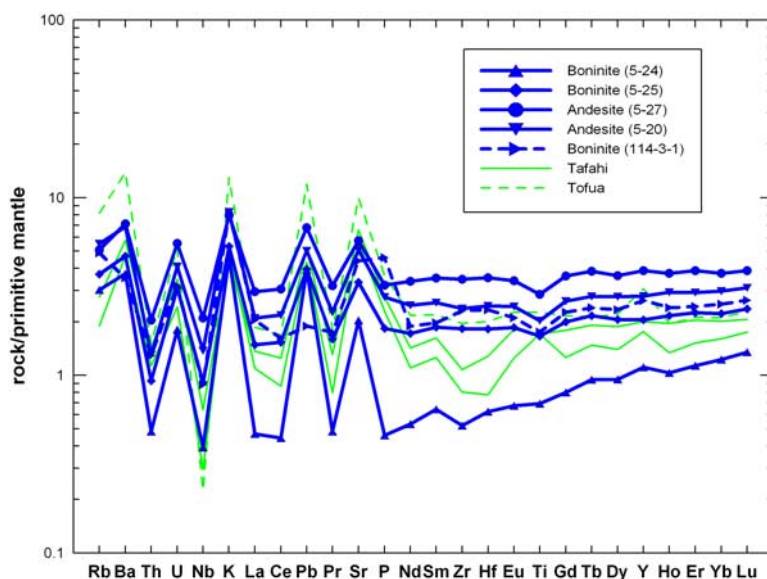


Figure 9. Primitive mantle normalized trace element abundance patterns with normal subduction zone enrichments. Representative patterns for the Tongan islands of Tofua and Tafahi in the Tofua Volcanic arc are from *Turner et al.* [1997] and *Eggins et al.* [1997]. Primitive mantle normalizing values from *Sun and McDonough* [1989].

[15] The enriched boninite end-member is represented by boninite 7–18 from the western group boninites recovered at dredge station St25 (Figure 3) [*Falloon et al.*, 1987]. In the model of *Danyushevsky et al.* [1995], this end-member is considered to be the result of the addition of the E2 (OIB) component into the depleted end-member. Quantitative mixing models A and B (Figure 5) demonstrate that mixing between an enriched OIB

melt composition from Samoa (e.g., Muli, Figure 5) progressively swamps the subduction zone signature seen in the depleted end-member as more of the E2 component is added (see quantitative models A and B, Figure 5). The enriched end-member can be modeled by the addition of ~20 wt% (Model B, Figure 5) of the E2 component mixed into the depleted end-member represented by 5–24. The enriched end-member has a LREE-

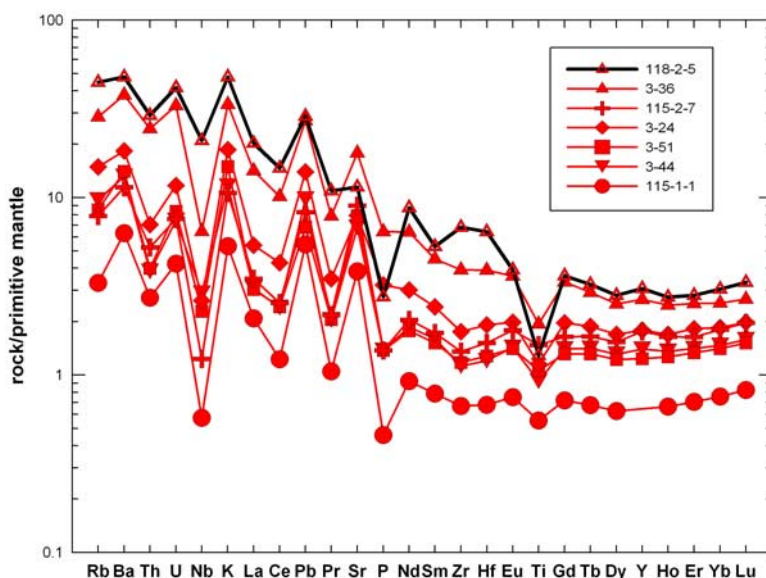


Figure 10. Primitive mantle normalized trace element abundance patterns for enriched boninites associated with rifting of the northern Tongan ridge at its northern termination. Primitive mantle normalizing values from *Sun and McDonough* [1989].

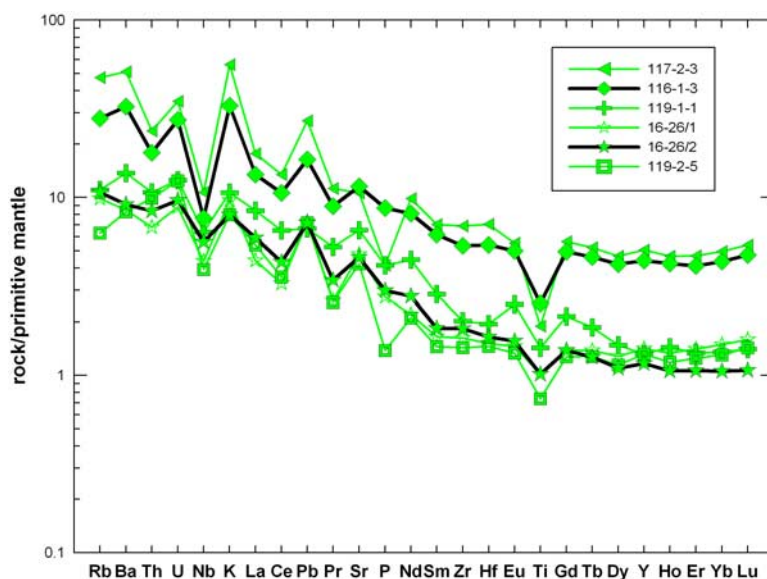


Figure 11. Primitive mantle normalized trace element abundance patterns for enriched boninites associated with rifting in the northern Lau Basin. Primitive mantle normalizing values from *Sun and McDonough* [1989].

enriched REE pattern ($La_N/Sm_N = 3.5$, Figure 5), with relatively low HREE abundances ($Yb = 0.85$ ppm, Table 3), and enrichment in HFSE ($La_N/Nb_N = 1.0$; except TiO_2 , which remains relatively low) and LILE. The enriched end-member has low $^{143}Nd/^{144}Nd$ values within the range of those of the Samoan lavas, but does not have the same high $^{87}Sr/^{86}Sr$ values as Samoan lavas (Figure 6). However, the enriched end-member has Pb isotope values which fall within the range displayed by Samoan lavas (Figure 7).

[16] The intermediate boninite end-member is represented by boninite 119-2-5 from the western group boninites recovered at dredge station D119 (Figure 3). This end-member is intermediate in character between the depleted and enriched end-members. It has a normalized abundance pattern which shows enrichment in LREE and HFSE relative to the depleted end-member (creating a U-shaped REE pattern), but still retains a subduction zone LILE enrichment normalized abundance pattern (Figure 5). The intermediate end-member

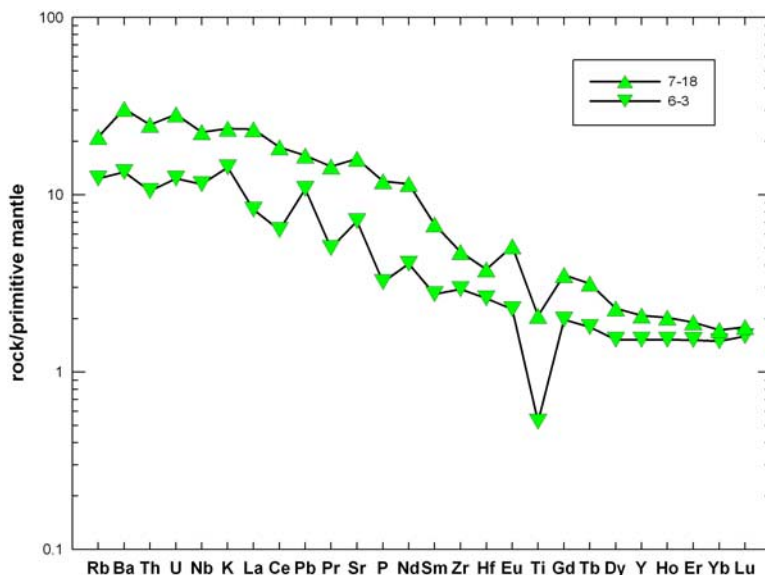


Figure 12. Primitive mantle normalized trace element abundance patterns for enriched boninites from stations 24 and 25, northern Lau Basin. Primitive mantle normalizing values from *Sun and McDonough* [1989].

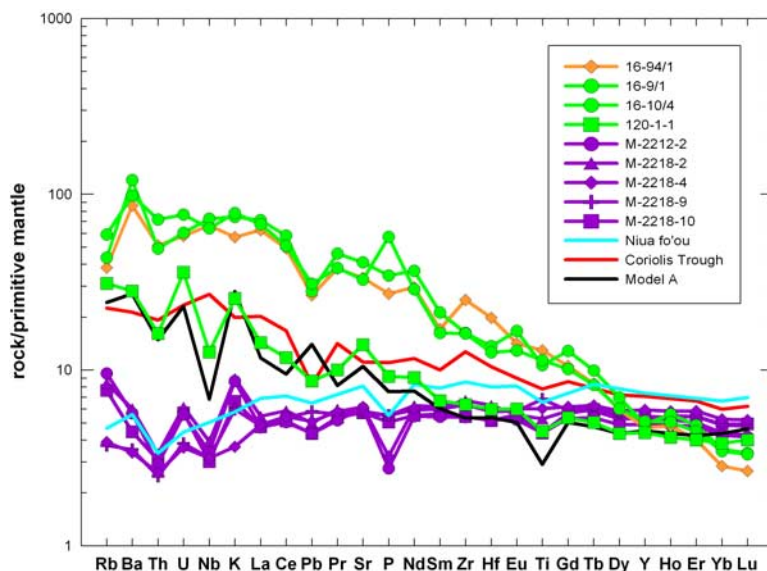


Figure 13. Primitive mantle normalized trace element abundance patterns for backarc basin lavas from the northern Lau Basin, compared with representative patterns from the Central Lau spreading center (CLCS, sample GC51 [Sunke], 1990); Niua fo'ou Island (average 1946 eruption lava composition [Turner et al., 1997]); Coriolis Trough (Nifonea Ridge sample 143635 [McConachy et al., 2005]); and Uo Mamae seamount (sample 16–94/1, this study). Samples M-2212-2, M-2218-2, M-2218-4, M-2218-9, and M-2218-10 are from the Mangatolu Triple Junction spreading center. Mixing model A, 80 wt% evolved boninite 116-1-3 with 20 wt% glass M-2212-2. Primitive mantle normalizing values from Sun and McDonough [1989].

normalized abundance pattern (NAP) can be modeled by the addition of ~3 wt% (Model A, Figure 5) of the E2 component mixed into the depleted end-member represented by 5–24. The intermediate end-member has Nd, Sr and Pb isotope values within the range displayed by lavas from Samoa (Figures 6 and 7) and has the highest Sr isotope value of the Tongan boninites (Figure 6).

[17] Mixing between these three boninite end-members can explain the geochemistry of all the enriched (in terms of LREE and $^{143}\text{Nd}/^{144}\text{Nd}$ values) boninites recovered from both the north Tonga Ridge and northern Lau Basin. This is demonstrated by quantitative mixing models in Figure 8, where three different models are presented (Models A–C, Figure 8). Although the match between the mixing models and NAPs is not perfect, it is sufficiently close to support the hypothesis that mixing between a restricted range of end-members can explain the geochemistry of boninites recovered from this area. Mixing of magmas is also supported by the mineral- and olivine-hosted melt inclusion chemistry of the boninites [Falloon et al., 1989; Sobolev and Danyushevsky, 1994].

[18] In the following section, we show that volcanic rocks recovered from the northern termination

of the Tonga Ridge (the eastern group) can be divided into two broad sub-groups, based on REE patterns and isotopic composition.

3.2. Volcanics Associated With Rifting of the Tonga Ridge and Forearc

3.2.1. Boninites and Andesites With Flat to Depleted REE Patterns

[19] NAPs of boninites and andesites with flat to depleted REE patterns are presented in Figure 9. These boninites and andesites are most like the young TVA volcanics in terms of their REE patterns and enrichments in LILE (Figure 9), and they also have Nd and Sr isotope values similar to the young TVA, except the depleted end-member 5–24 which has distinctly higher Sr isotope values (Figure 6, blue symbols). This group of boninites and andesites also has similar $^{206}\text{Pb}/^{204}\text{Pb}$ values to volcanics from the southern TVA, but significantly lower $^{206}\text{Pb}/^{204}\text{Pb}$ values compared to the northern Tongan island of Tafahi, which is located to the south of the graben structure cutting the northern Tongan Ridge (Figure 7, blue symbols).

[20] One of the dredge station St23 boninites, sample 5–25, has a number of odd features which indicates that it has a more complex petrogenesis

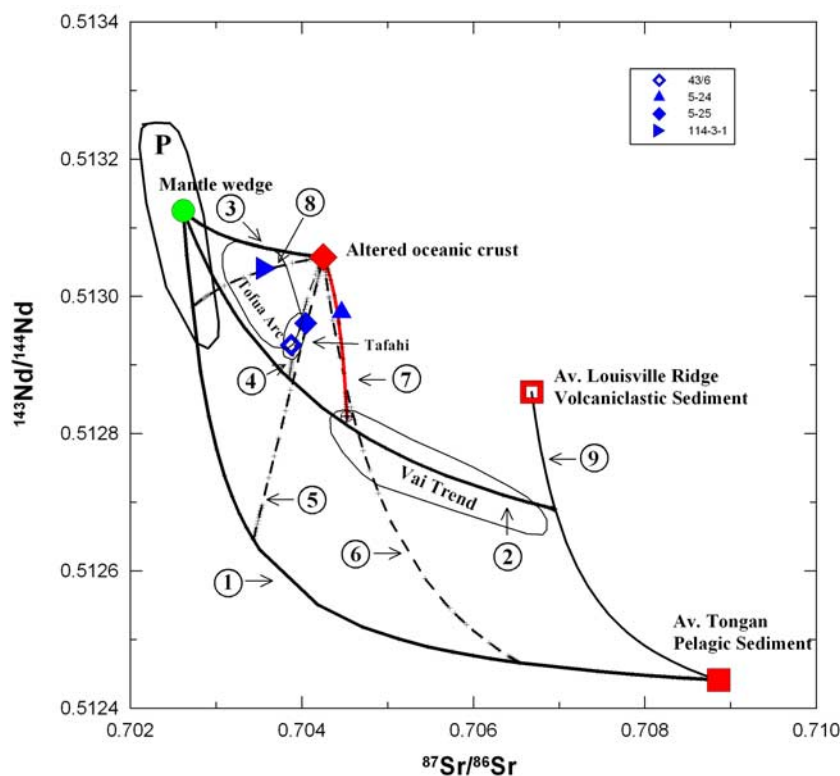


Figure 14. The $^{143}\text{Nd}/^{144}\text{Nd}$ versus $^{87}\text{Sr}/^{86}\text{Sr}$ isotopic compositions of submarine volcanics from the northern termination of the Tonga ridge and Lau Basin compared to the isotopic compositions of relevant magmatic suites and model mixing curves (see text for discussion). Fields and data sources as for Figure 6. End-member compositions for mixing models are presented in Appendix C (Tables C2 and C4). Numbered mixing models are as follows: 1, mixing between a fluid derived from subducted pelagic sediment and a refractory wedge composition; 2, mixing between a fluid derived from a 90:10 mix of volcaniclastic sediment and pelagic sediment and refractory mantle wedge; 3, mixing between fluid derived from subducted oceanic crust and refractory mantle wedge; 4 and 7, mixing between a modified (addition of a fluid from a 90:10 mix of volcaniclastic sediment and pelagic sediment) mantle wedge composition and fluid from subducted oceanic crust; 5, 6, and 8, mixing between a modified (addition of a fluid from subducted pelagic sediment) and a fluid from subducted oceanic crust; and 9, bulk mixing between volcaniclastic and pelagic sediment.

than other boninites from this area. Melt and spinel inclusions in olivine indicate that this sample is a mixed magma [Falloon *et al.*, 1989; Danyushevsky *et al.*, 1995]. The most magnesian olivines (FO_{94}) have spinel and melt inclusion compositions identical to the other depleted dredge station St23 boninites (e.g., 5–24, 5–28); however, the more evolved olivines have melt inclusions indicating a melt with lower SiO_2 and higher FeO contents and spinels with significantly lower Al_2O_3 contents. The chemical features of this sample may reflect interaction of high-Ca boninite melts or mantle sources with the modern Tofua Arc magmatic system. Unfortunately the small size of the sample itself precludes any detailed chemical, mineralogical and experimental study of melt inclusions, which are necessary to clarify its origin.

3.2.2. Boninites, Andesites, and Rhyolites With U-Shaped REE Patterns

[21] NAPs of boninites, andesites and rhyolites with U-shaped REE patterns are presented in Figure 10. New sampling at dredge station D115 recovered boninite lavas similar to boninites previously recovered from dredge station St21 (Figures 3 and 10). Whole rock compositions from dredge station D118 (Table 1), located on a large volcanic edifice within the graben at the northern end of the Tonga Ridge (Figure 3), are rhyolitic. The glass composition from sample 118-2-8 (Table 2) is strongly enriched in SiO_2 . Falloon and Crawford [1991] demonstrated that, in general, the variation in the dredge station St21 lavas from primitive high-Ca boninites (e.g., sample 3–44, Figure 10) to andesites (e.g., sample 3–36, Figure 10) is consistent with the process of fractional crystallization.

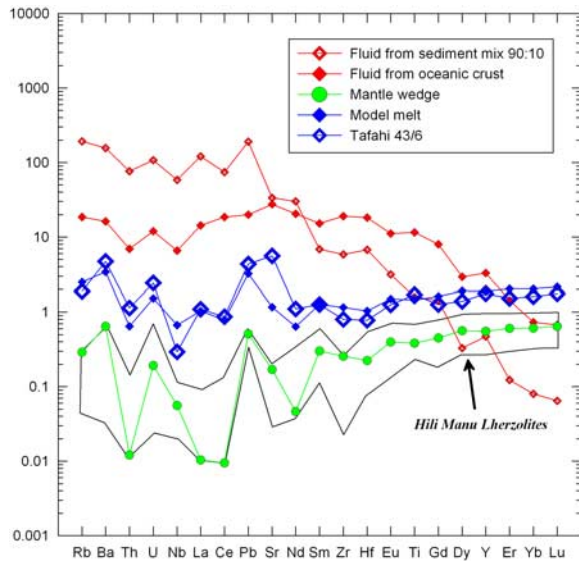


Figure 15. Primitive mantle normalized trace element abundance patterns for end-member components (Table C2, Appendix C) and lava composition 43/6 from Tafahi [Turner *et al.*, 1997]; see text for discussion. Data for Hili Manu Lherzolites from Falloon *et al.* [2006]. Primitive mantle normalizing values from Sun and McDonough [1989].

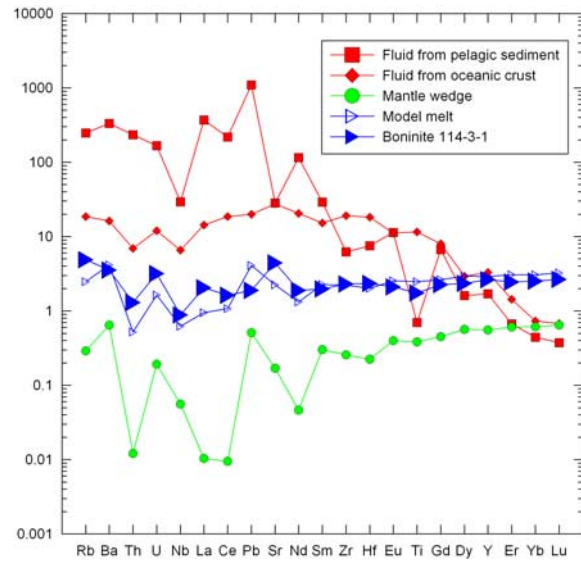


Figure 17. Primitive mantle normalized trace element abundance patterns for end-member components (Table C2, Appendix C) and boninite composition 114-3-1; see text for discussion. Primitive mantle normalizing values from Sun and McDonough [1989].

Compositions of rhyolites from dredge station D118 are consistent with being highly evolved magma compositions derived from parental compositions similar to those for dredge station St21 lavas. The NAP of rhyolite sample 118-2-5 paral-

els those for boninites and andesites from dredge station St21 with relative depletions in Sr, P and Ti consistent with crystal fractionation involving plagioclase, apatite and Ti-magnetite (Figure 10). We therefore infer that the large volcanic edifice occu-

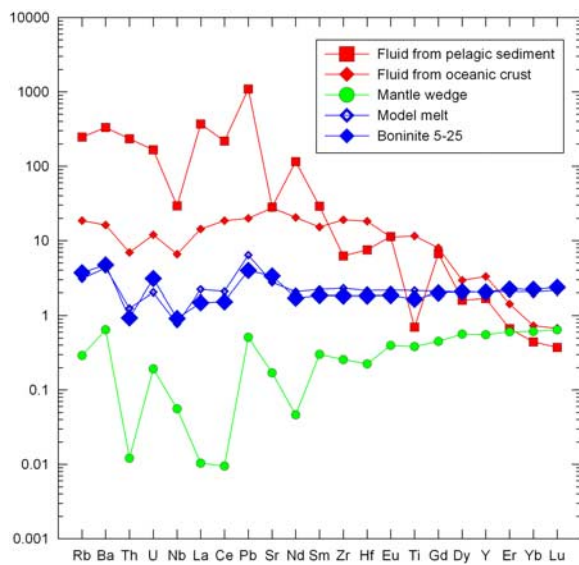


Figure 16. Primitive mantle normalized trace element abundance patterns for end-member components (Table C2, Appendix C) and boninite composition 5-25; see text for discussion. Primitive mantle normalizing values from Sun and McDonough [1989].

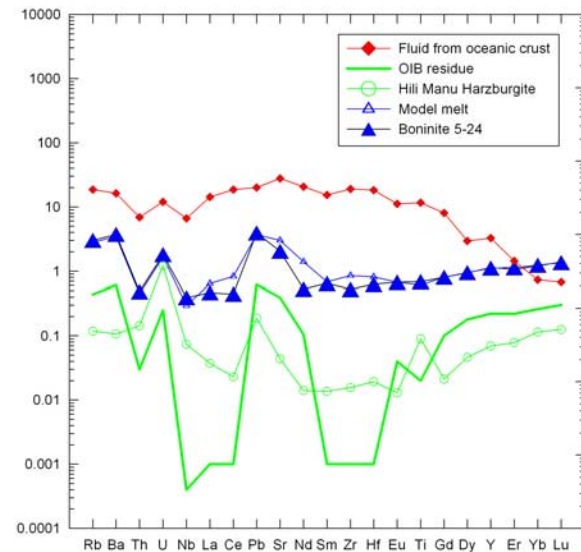


Figure 18. Primitive mantle normalized trace element abundance patterns for end-member components (Table C2, Appendix C) and boninite composition 5-24; see text for discussion. Average Hili Mau harzburgite composition from Falloon *et al.* [2006]. Primitive mantle normalizing values from Sun and McDonough [1989].

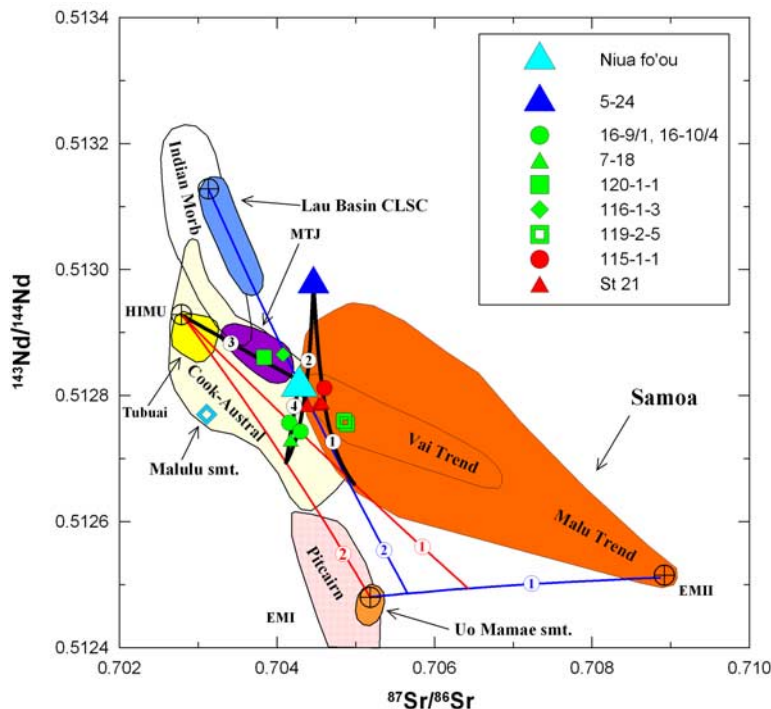


Figure 19. The $^{143}\text{Nd}/^{144}\text{Nd}$ versus $^{87}\text{Sr}/^{86}\text{Sr}$ isotopic compositions of submarine volcanics from the northern termination of the Tonga ridge and Lau Basin compared to the isotopic compositions of relevant magmatic suites and model mixing curves (see text for discussion). Fields and data sources as for Figure 6. End-member compositions for mixing models are presented in Appendix C (Tables C4 and C5). Numbered mixing models are colored coded as follows: 1, blue line, bulk mixing between mantle source compositions for Uo Mamae and Malumalu; 2, blue line, bulk mixing between the mantle source for the Central Lau spreading center (CLSC) and OIB mantle comprising a mix between Uo Mamae and Malumalu; 1, red line, bulk mixing between melts from Tubuai and OIB melt 1 (Table C5); 2, red line, bulk mixing between melts derived from Tubuai and Uo Mamae; 1, black line, bulk mixing between boninite 5–24 and OIB melt 3 (Table C5); 2, black line, bulk mixing between boninite 5–24 and OIB melt 2 (Table C5); 3, black line, bulk mixing between melts derived from Niuva fo'ou and Tubuai; and 4, black line, bulk mixing between melts derived from Niuva fo'ou and OIB melt 2 (Table C5).

pying the graben at the northern end of the Tonga Ridge is related to boninitic magmatism associated with rifting at the northern termination of the Tonga Trench. The volcanics with U-shaped REE patterns have Nd, Sr and Pb isotopic values (Figures 6 and 7, red symbols) displaced from young TVA volcanics, overlapping values for volcanics from the nearby Samoan plume (Figures 6 and 7).

3.3. Volcanics Associated With Backarc Rifting in the Northern Lau Basin

[22] Seafloor imaging immediately to the west of, and in a relative backarc position to, the northern Tonga Ridge reveals a number of small rifted basins with associated volcanic features (Figures 2 and 3). Samples recovered from this area include the enriched western group boninite compositions and

backarc basin basalts, as outlined in sections 3.3.1 and 3.3.2.

3.3.1. Boninites

[23] The western group boninites recovered from this area all display strong enrichment in LREE (Figures 11 and 12). Boninites from dredge station D119 have strongly enriched REE patterns (samples 119-1-1, 119-2-5, Figure 11) consistent with boninites recovered at dredge stations 16–26 (R/V *Kallisto*, samples 16–26/1, 16–26/2, Figure 11), and St24-St25 (R/V *Natsushima*, samples 6-3, 7–18, Figure 12). Volcanic rocks recovered from the large backarc caldera (dredge stations D116 and D117, Figure 3) are evolved dacites and rhyolites (Tables 1 and 2). Figure 11, shows that NAPs of samples 116–1–3 and 117–2–3 parallel those of the enriched boninites, suggesting that the parental

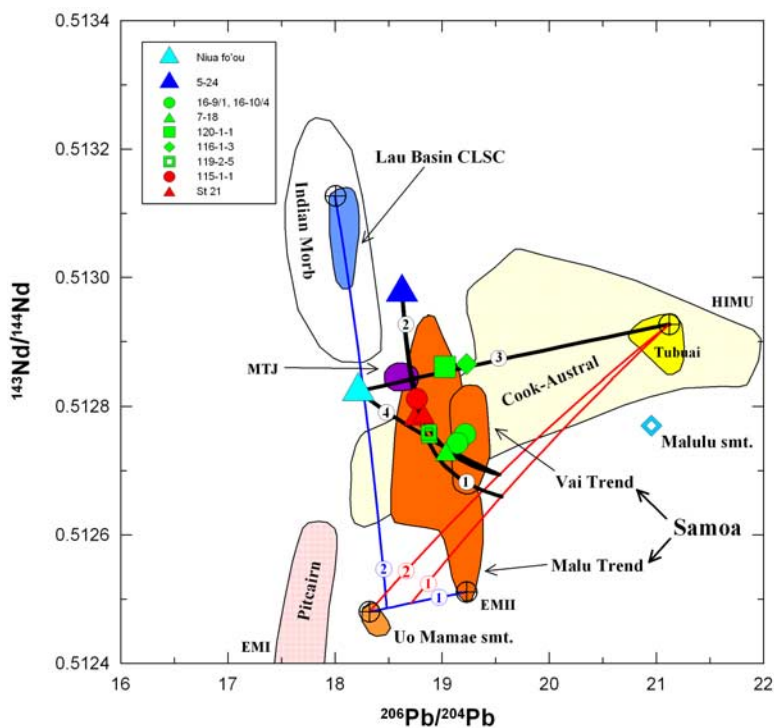


Figure 20. The $^{143}\text{Nd}/^{144}\text{Nd}$ versus $^{206}\text{Pb}/^{204}\text{Pb}$ isotopic compositions of submarine volcanics from the northern termination of the Tonga ridge and Lau Basin compared to the isotopic compositions of relevant magmatic suites and model mixing curves (see text for discussion). Fields and data sources as for Figure 6. End-member compositions for mixing models are presented in Appendix C (Tables C4 and C5). Colored-coded and numbered mixing curves as for Figure 19.

magmas to these dacites and rhyolites were boninitic in composition. The isotopic compositions of these western group boninites associated with backarc rifting are displaced to lower Nd and Sr values compared to the eastern group boninites associated with rifting of the north Tonga Ridge (Table 4, green symbols versus red symbols in Figure 6). Only the intermediate end-member boninite 119-2-5 has Nd and Sr isotopic values overlapping volcanics from Samoa (Figure 6). All the backarc western group boninites, however, have Pb isotopic values overlapping volcanics from Samoa (Table 4, green symbols in Figure 7). The isotopic values (Table 4) for the dacite composition 116-1-3 from the backarc caldera (D116, Figure 3) are distinctive, in having similar Pb isotopic values to volcanics from the northern Tonga island of Tafahi (Figure 7), but having lower Nd values (Figure 6).

3.3.2. Backarc Basin Basalts

[24] NAPs of representative backarc basin basalts from the MTJ and new sampling at dredge station D120 on the Northeast Lau Spreading Center (Figures 1 and 3) are presented in Figure 13.

The geochemistry of pillow lavas recovered by *Mir* submersible from the MTJ (dives M-2212, M-2216, M-2218, Figure 2) have been presented by Falloon *et al.* [1992]. Pillow lavas range from basalt to andesite (Figure 4), and Falloon *et al.* [1992] distinguished two geochemical groups of lavas. Type I lavas most closely resemble N-MORB in terms of major and trace element geochemistry, whereas the type II lavas more closely resemble E-MORB or BABB, the distinctive primary magma type identified by Sinton and Fryer [1987]. The type I and II designation is equivalent to the “depleted” and “enriched” types respectively of Volpe *et al.* [1988] for lavas dredged from the central parts of the Lau Basin, and the (N)-type and (T)-type Lau backarc basin basalts respectively of Hawkins and Melchior [1985]. Type I lavas from the MTJ have very low K_2O (<0.14wt%), LREE-depleted REE patterns, and similar incompatible element abundances to N-MORB, except for slightly higher Rb and Ba contents (representative examples are glasses M-2218-4 and M-2218-9, Figure 13). Type II lavas from the MTJ have higher K_2O (>0.14wt%), LREE-depleted to enriched REE patterns, and significant enrichments in LILE com-

pared to N-MORB, but similar to those observed in the BABB magma type (representative glasses are samples M-2212-2, M-2218-2, M-2218-10, Figure 13). The type II lavas have Al_2O_3 and FeO contents intermediate between trends displayed by BABB and N-MORB suites of glasses [Falloon *et al.*, 1992]. Figures 4 and 13 show that the geochemistry of pillow lavas from the MTJ are very similar to lavas from the backarc island of Niua fo'ou (Figure 4 and 13).

[25] Pillow lavas recovered at dredge station D120 on the Northeast Lau Spreading Center are basaltic andesites (Table 1). The major element chemistry of whole rocks (Table 1) and glasses (Table 2) from dredge station D120 are very different from backarc basin lavas from the MTJ [Falloon *et al.*, 1992], having at a given MgO content higher SiO_2 , Al_2O_3 , and K_2O and lower TiO_2 , FeO^T , and Na_2O contents (Figure 4). The NAPs of the D120 pillow lavas show that compared to MTJ pillow lavas they are enriched in both LREE and LILE (sample 120-1-1, Figure 13). The major element chemistry of the D120 pillow lavas is intermediate between the basaltic pillow lavas from MTJ and the boninites recovered from the backarc rifts immediately to the east of D120 (Figure 4). This suggests the possibility that boninite magmas are being generated under the spreading ridge, and mixing with normal backarc basin basalt magmas. This possibility is tested in Figure 13 which demonstrates that a simple mix between an evolved boninite pattern and a MTJ pillow lava can produce a reasonably close fit to basaltic andesite sample 120-1-1 (Model A, Figure 13). As can be seen from Figure 6, the pillow lava 120-1-1 has Nd and Sr isotope values (Table 4) that fall within the range of values of pillow lavas from the MTJ. However, Figure 7 demonstrates that sample 120-1-1 has significantly higher $^{206}\text{Pb}/^{204}\text{Pb}$ and $^{208}\text{Pb}/^{204}\text{Pb}$ values than MTJ lavas overlapping those of boninites from backarc rifts immediately toward the east. Thus the Pb isotope values support the hypothesis that boninite magmas are currently involved in magma generation beneath this active backarc spreading center. If this hypothesis is correct, it demonstrates for the first time in an active setting, an association between boninite magmas with backarc spreading centers.

[26] Pillow lavas recovered from dredge stations 16-9 and 16-10 lavas compared to MTJ pillow lavas at a given MgO content have significantly lower SiO_2 , slightly lower Al_2O_3 , higher TiO_2 , FeO^T , and significantly higher K_2O and P_2O_5

contents (Figure 4), compositions intermediate between pillow lavas from the MTJ and lavas from the Samoan plume, especially pillow lavas recovered from the Uo Mamae seamount (Figure 4). The NAPs of pillow lava samples 16-9/1 and 16-10/4 pillow lavas show significant enrichment in all incompatible elements compared to MTJ pillow lavas (Figure 13) but have NAP patterns almost identical to pillow lavas from the Uo Mamae seamount (sample 16-94/1, Figure 13). Clearly, these pillow lavas are “OIB-like” yet they were clearly erupted on the backarc side of the trench (and not accreted from the Pacific plate), as they contain cumulate xenoliths related to boninite magmas [Zlobin *et al.*, 1991]. As Figures 6 and 7 demonstrate, the pillow lava samples 16-9/1 and 16-10/4 have significantly lower Nd isotopic and significantly higher Pb isotope values than pillow lavas from the MTJ (Table 4). Although the NAP patterns for 16-9/1 and 16-10/4 are similar to lavas from Samoa, their Nd and Sr isotopic values plot away from Samoan lavas in Figure 6 and plot just on the margin of the field of Samoan lavas in terms of Pb isotope values (Figure 7). Clearly, the OIB component involved in their petrogenesis cannot simply be a pure Samoan plume component.

[27] Recently, McConachy *et al.* [2005] reported alkalic pillow lavas enriched in LREE, Nb and Zr from young incipient rift basins (Coriolis Troughs) behind the Vanuatu Island arc. The NAP of a representative pillow from the Nifonea Ridge within the Coriolis Troughs is very similar to the NAP of the D120 pillow lava sample 120-1-1 but not as enriched as pillow lavas 16-9/1 and 16-10/4. In terms of major element chemistry, the Coriolis Trough pillow lavas are intermediate in composition between dredge station D120 and dredge stations 16-9 and 16-10 lavas, except for Na_2O contents, which are significantly higher in the Coriolis Trough lavas. Both the Coriolis Trough and the dredge station 16-9 and 16-10 pillow lavas have relatively high TiO_2 contents which are normally associated with intraplate magmatism. McConachy *et al.* [2005] argued that the Coriolis Trough lavas despite having strong alkali enrichment do not belong to the within-plate magma type but represent a globally unique end-member of backarc basin magmatism associated with incipient backarc basin rifting. McConachy *et al.* [2005] proposed that the alkali and associated LREE enrichment (Figures 4 and 13) seen in the Coriolis Trough lavas is the result of low-degree partial melting of a relatively fertile mantle source in response to incipient rifting behind the volcanic

front. In contrast to the Coriolis Trough lavas, pillow lavas from dredge stations 16-9 and 16-10, although having similar TiO_2 contents to the Coriolis Trough lavas, are significantly enriched in K_2O (Figure 4g) and LREE (samples 16-9/1 and 16-10/4, Figure 13) compared to normal backarc basin lavas, such as those from the MTJ, and have clear isotopic evidence for the involvement of an OIB component (samples 16-9/1 and 16-10/4, Figures 6 and 7). This suggests that there is a variety of ways in which enriched backarc basin lavas may obtain the enriched, within-plate magma characteristics.

3.4. Volcanics Associated With the Samoan Plume

[28] In this study we have reanalyzed one pillow lava from Uo Mamae seamount from dredge station 16-94 (Figure 2, sample 16-94/1, Table 3) recovered by the R/V *Kallisto* and reported by *Zlobin et al.* [1991]. Sr, Nd and Pb isotopic composition of Uo Mamae seamount lavas have been determined by *Acland* [1996]. In terms of major element chemistry, the Uo Mamae lavas, in general, overlap compositions produced by the Samoan plume (Figure 4). However, the Uo Mamae lavas are distinctive in having the highest K_2O contents so far identified from Samoan plume lavas (Figure 4g) and in having a distinctive isotopic composition similar to an EMI mantle end-member component, unlike the EMII dominated isotopic compositions of the Samoan plume (Figures 6 and 7). The Uo Mamae lavas have significantly lower Nd isotopic values at a given Sr isotopic value than other Samoan lavas (Figure 6) and significantly lower $^{208}\text{Pb}/^{206}\text{Pb}$ and $^{206}\text{Pb}/^{204}\text{Pb}$ values compared to other Samoan lavas (Figure 7). Although the Pb isotopic values of the Uo Mamae lavas fall just within the range of lavas from the HIMU dominated Cook-Austral plume (Figure 7), they have Nd and Sr isotopic values well outside the range of Cook-Austral plume lavas (Figure 6). Similarly, although Uo Mamae lavas have Nd and Sr isotopic values within the range of the EMI-dominated lavas from Pitcairn, they have Pb isotopic values well outside the range of Pitcairn lavas (Figure 7). Thus it appears that Uo Mamae lavas are derived from a unique component of the Samoan plume, which has as yet not been recovered from islands and seamounts forming the two main lineaments of the plume (the Malu and Vai trends, Figures 6 and 7). However, as we demonstrate in sections 4.2 and 4.3, the plume composition which produced the Uo Mamae seamount pillow lavas is a vital component

involved in the petrogenesis of the boninites and associated lavas in the northern Lau Basin and termination of the north Tonga Ridge.

4. Geochemical Modeling

[29] In this section we present petrogenetic quantitative models to explain the geochemistry of volcanics from our study area. Our modeling is explained in more detail in Appendix C, and will be presented in three sections. In section 4.1, we present quantitative modeling of boninites and associated volcanics which are the result of “normal” subduction zone processes, involving simply a depleted mantle wedge composition and a subduction-related fluid components derived from the down going slab. In section 4.2, we present modeling for boninites and related volcanics which have enriched isotopic compositions indicating the involvement of an OIB component in their petrogenesis. In section 4.3, we present modeling to explain the range of isotopic compositions present in the northern Lau backarc basin lavas.

4.1. Boninites Generated by “Normal” Subduction Processes

[30] Quantitative modeling of the elemental and isotopic variations in normal subduction-related magmas suggests that in general a minimum of three independent components are required to explain their petrogenesis [*Ellam and Hawkesworth*, 1988; *Turner et al.*, 1997; *Hawkesworth et al.*, 1997a, 1997b; *Haase et al.*, 2002; *Kimura and Yoshida*, 2006], the depleted mantle wedge, a fluid derived from the dehydration of subducted basaltic oceanic crust and a fluid/melt from terrigenous sediment. Previous workers have demonstrated that the presence of these three components is required to successfully model the geochemistry of young TVA lavas [*Ewart and Hawkesworth*, 1987; *Turner and Hawkesworth*, 1997; *Turner et al.*, 1997; *Ewart et al.*, 1998]. In the case of young TVA lavas, *Turner et al.* [1997] presented a detailed geodynamic and quantitative three component model to explain their petrogenesis. In this model, three components identified are (1) the mantle wedge, (2) a melt from subducted sediments, and (3) a dehydration fluid from subducted basaltic oceanic crust. The sediment contribution to the northern TVA lavas from Tafahi and Niuatoputapu consists of a ~90:10 mixture between volcanoclastic sediment derived from the subducted Louisville Ridge and pelagic sediment. In the model of *Turner et al.* [1997], a sediment melt derived from the subducting oceanic plate enriches

the overlying mantle wedge (see discussion by *Turner et al.* [1997]) at relatively shallow depths. The mantle wedge is then dragged to greater depths in response to viscous drag along the upper surface of the subducting oceanic plate, arriving at the melt generation area after $\sim 2\text{--}4$ Myr [*Turner et al.*, 1997]. At the melt generation zone, the enriched mantle wedge undergoes partial melting in response to fluxing by fluids derived from dehydration reactions occurring within the subducted oceanic crust. The time interval between fluid release and partial melting is $\sim 30\text{--}50,000$ yrs based on Th-U isotopic data [*Turner et al.*, 1997]. In this section, we model quantitatively the Nd and Sr values and NAPs of boninites which have a subduction zone signature similar to TVA and the representative depleted boninite end-member 5–24 using the model of *Turner et al.* [1997] and the new experimental data of *Kessel et al.* [2005] on element partitioning between eclogite and supercritical fluids (see Appendix C for further details). Our modeling results are presented in Figures 14 to 18.

[31] In order to demonstrate that our modeling approach and methodology (see Appendix C) is consistent with previous work, we first model the lava composition 43/6 from the northern Tonga island of Tafahi [*Turner et al.*, 1997]. *Turner et al.* [1997] have previously demonstrated that the mantle wedge source for Tafahi lavas requires a small enrichment (~ 0.15 wt% addition) of a $\sim 90:10$ mixture of volcanoclastic and pelagic sediment. The presence of Louisville volcanoclastic sediment is required to explain the distinctive Pb isotope values of lavas from Tafahi compared to the rest of the TVA (e.g., Figure 7) [*Turner et al.*, 1997; *Regelous et al.*, 1997; *Wendt et al.*, 1997; *Ewart et al.*, 1998]. This model is presented in Figures 14 and 15. We have chosen a mantle wedge composition based on natural lherzolite samples from the ultrafresh Hili Manu peridotite [*Falloon et al.*, 2006] as representative of a depleted mantle wedge source (see Appendix C). This mantle wedge source is first enriched by the addition of a sediment melt derived from a bulk composition comprising a 90:10 mixture between an average Louisville Ridge volcanoclastic sediment and an average Tongan pelagic sediment (bulk mixing between these two sediments is shown by model 9 in Figure 14). The NAP of the sediment melt as calculated using the *Kessel et al.* [2005] experimental data is shown in Figure 15 (see Appendix C for details). Mixing between the depleted mantle wedge and this sediment melt is shown by model 2 in Figure 14. The addition of 0.2 wt% of this model

sediment melt to the mantle wedge causes the mantle wedge Nd and Sr isotope values to move to a position directly below the field defined by lavas from the island of Tafahi (model 2, Figure 14). If the enriched mantle wedge source is then fluxed by a fluid from altered subducted oceanic crust, then the addition of $\sim 0.13\text{--}0.68$ wt% fluid will raise the Nd and Sr isotope values of the previously enriched mantle wedge to encompass the range displayed by lavas from the island of Tafahi (model 4, Figure 14). The NAP of the fluid from the altered subducted oceanic crust, as calculated using the *Kessel et al.* [2005] experimental data is presented in Figure 15 (see Appendix C for details). To quantitatively match the Nd and Sr values of lava sample 43/6 requires the addition of 0.2 wt% of the sediment melt followed by 0.42 wt% addition of fluid from the altered oceanic crust. If we apply these mass balance constraints derived from the Nd and Sr isotope modeling, we can get a good match to the NAP of sample 43/6 if the modified depleted mantle wedge source is melted to a high degree ($F = 0.3$; see “model melt,” Figure 15).

[32] In Figure 14 we present quantitative modeling of Nd and Sr values for eastern group boninite samples 5-25 and 114-3-1 which have strong subduction zone signature, similar to the depleted end-member boninite 5-24. Boninite 114-3-1 has Nd and Sr and Pb isotope values similar to young lavas from the TVA (Figures 6 and 7), whereas boninite 5–25 has Nd and Sr values similar to the island of Tafahi (Figure 6) but with Pb isotope values similar to young TVA lavas (Figure 7). Both boninites 114-3-1 and 5–25 have Nd and Sr isotope values which can be successfully modeled by the addition of differing amounts of a pelagic sediment melt to the mantle wedge source. The Nd and Sr isotope values of boninite 5–25 can be successfully matched if the mantle wedge source was first enriched by the addition of 0.09 wt% pelagic sediment derived melt (model 1 in Figure 14 is a bulk mixing curve between a pelagic sediment melt and the mantle wedge) followed by the addition of 2.3 wt% of fluid from the altered oceanic crust (model 5, Figure 14). If this modified source undergoes a high degree of melting then we can closely match the NAP of boninite 5–25 ($F = 0.3$; see “model melt,” Figure 16). Similarly the Nd and Sr isotope values of boninite 114-3-1 can be successfully matched if the mantle wedge source was first enriched by the addition of 0.01 wt% pelagic sediment derived melt, followed by the addition of 1.0 wt% fluid (model 8,

Figure 14). If this modified wedge source undergoes a moderate degree of melting we can closely match the NAP of boninite 114-3-1 ($F = 0.2$, see “model melt,” Figure 17). Note that the modeling confirms that boninite melts require significantly higher fluid addition compared to basaltic andesites from Tafahi (1–2.3 wt% versus 0.42 wt%), consistent with the higher H_2O contents present in boninite magmas compared to other subduction-related magmas [Sobolev and Chaussidon, 1996].

[33] The depleted boninite end-member 5–24, as previously mentioned (see section 3.1), has significantly higher $^{87}Sr/^{86}Sr$ values compared to young TVA lavas (Figure 6 and 14). To achieve these high $^{87}Sr/^{86}Sr$ values using the model of Turner *et al.* [1997] requires a petrologically unreasonable amount of fluid to be added to the modified mantle wedge source (~ 34 wt%, model 6, Figure 14). In the petrological model of Danyushevsky *et al.* [1995], however, the depleted end-member is derived not from fluid-fluxed melting of the mantle wedge with Pacific isotopic composition, but instead from fluid-fluxed melting of refractory OIB mantle related to the Samoan plume. If we assume that the isotopic composition of the OIB mantle residue is similar to the more depleted part of the range displayed by Samoan lavas of the Vai Trend (e.g., Tau’u Island [Workman *et al.*, 2004]; Figure 14), then a more petrologically reasonable amount of added fluid (~ 1 wt%) can explain the high $^{87}Sr/^{86}Sr$ values of boninite 5–24 (model 7, Figure 14).

[34] In the model of Danyushevsky *et al.* [1995] it was assumed that the middle REE were not transported by the slab-derived fluid, as this fluid (which should have a Nd isotopic value of the subducted Pacific ocean crust with $\sim >0.5129$) appeared not to have changed the isotopic composition of the refractory OIB mantle residue (based on the reported data of Falloon *et al.* [1989]). However, recent experimental work on likely subduction zone fluid compositions [Kessel *et al.*, 2005] demonstrates that middle-REE are fluid mobile. Our quantitative modeling (Figures 14 and 18, Appendix C) using the new Nd isotopic values obtained in this study for the depleted boninite end-member 5–24 demonstrates that the new values are in fact more consistent with the model of Danyushevsky *et al.* [1995] than the previously published values. This is because the subduction zone fluid (derived from altered subducted Pacific crust) will impose its isotopic value onto a refractory OIB source, as our modeling demonstrates (see model 7, Figure 14).

[35] In Figure 18 we present quantitative modeling of the NAP for the depleted boninite end-member 5–24. As explained in more detail in Appendix C, we could only get a close matching to the NAP of boninite 5–24, if we arbitrarily changed the trace element abundances of the residue, so that a partial melt of the residue plus added fluid component would produce a close match to boninite 5–24 ($F \sim 0.22$, Figure 18, Appendix C). The resulting NAP of the OIB residue is similar to an average depleted harzburgite from the Hili Manu peridotite, apart from significant depletions in HFSE. Similar HFSE depletions have been observed in mantle xenoliths from Samoan lavas [Hauri *et al.*, 1993], and could possibly be due to metasomatism by carbonatite melts [Hauri *et al.*, 1993; Danyushevsky *et al.*, 1995].

4.2. Boninites Generated by the Involvement of OIB Plume Components

[36] Danyushevsky *et al.* [1995] have previously demonstrated that the LREE and isotopically enriched Tongan boninites can be explained by mixing of an OIB component (E2 in the model of Danyushevsky *et al.* [1995]) into the depleted end-member represented by boninite 5–24 (D+E1 in the model of Danyushevsky *et al.* [1995]). In this study we have previously demonstrated that the geochemistry of the enriched Tongan boninites can be explained by mixing of three boninite end-members (see section 3.1). In general the Pb isotopic composition of the enriched boninites can be simply explained by mixing of a Samoan EMII component(s) into the depleted end-member 5–24. For example, Figure 7 shows that the enriched boninites (samples 115-1-1, St21, 16-26/2, 119-2-5, and 7-18, Figure 7) and the depleted boninite 5–24 form a \sim linear array overlapping with Samoan lavas. This array could potentially be explained by mixing of a pure EMII component of the Samoan plume into boninite 5–24 (Figure 7). However, this simple model cannot explain the Nd and Sr isotopic values of the enriched boninites. This is because any mixing of an EMII component into the boninite 5–24 end-member will produce mixing arrays which will not pass through the enriched boninites. In fact, some of the enriched boninites (e.g., dredge station St25, sample 7–18) have Nd and Sr isotopic values which fall outside the main field of Samoan lavas from the Vai and Malu Trends (Figure 6). Even if the lavas from Uo Mamae seamount are included in the Samoan field, in Figure 6, the Sr isotopic value of boninite 7–18 is too low for Uo Mamae to be the enriching

component. In addition, the Uo Mamae lavas have depleted Pb isotopic compositions compared to the enriched boninites (Figure 7), making it impossible for Uo Mamae to be the enriching E2 component. Similar arguments apply to the role of subducted pelagic sediment and volcanoclastic Louisville Ridge derived sediment. Both the average pelagic sediment component and Louisville volcanoclastic sediment do not have appropriate Pb isotopic compositions to be the enriched E2 component mixing into the depleted boninite 5–24 end-member (Figure 7). As well, mixing arrays of these sedimentary components into boninite 5–24 will not pass through the enriched boninites in Nd and Sr isotopic space (Figure 6). In summary, it is clear from simple inspection of Figures 6 and 7 that the proposed E2 component that mixes into the depleted boninite end-member 5–24 cannot be correlated with any known isotopic composition from the Samoan plume or subducted sediment.

[37] Of particular significance therefore is the observation that not all seamounts located close to the line of the Samoan plume are associated with it [Workman *et al.*, 2004]. In particular, Workman *et al.* [2004] noted that the Malulu seamount and Rose Atoll, located immediately to the east of the active Vailulu'u seamount, are most likely part of the Cook-Austral mantle plume [Workman *et al.*, 2004]. This observation is of significance as it allows the possibility that a HIMU mantle plume component is also involved in the petrogenesis of lavas at the northern termination of the Tonga Ridge and Lau Basin. The Cook-Austral Islands and associated seamounts are assumed to have been formed by the same hot spot volcanism currently located on the MacDonalld Seamount ($\sim 29^\circ\text{S}$, $\sim 140^\circ\text{W}$) in the South Pacific [Jordahl *et al.*, 2004; Bideau and Hekinian, 2004]. The Cook-Austral chain, which although in general conforms to an absolute plate motion relative to the hot spot reference frame [Duncan and Clague, 1986], has a complex age progression [Jordahl *et al.*, 2004] making it unlikely that a single hot spot could explain the entire chain. The oldest parts of the Cook-Austral chain (20–25 Ma), however, overlap the positions of seamounts and islands formed by the Samoan hot spot [Norton, 2000], which is currently located at the active submarine Vailulu'u volcano at $\sim 14^\circ\text{S}$ $\sim 169^\circ\text{W}$ [Hart *et al.*, 2000]. We propose that in addition to the Samoan EMII plume component, HIMU mantle sources related to the Cook-Austral plume have also penetrated across into the northern Lau Basin mantle. As can be seen from Figures 6 and 7 the isotopic

compositions of lavas from the Cook-Austral islands encompass the entire range of isotopic compositions of the Tongan boninites. In particular, the Cook-Austral Islands have significantly lower $^{87}\text{Sr}/^{86}\text{Sr}$ values than the EMII-dominated Samoan lavas (Figure 6). Malulu seamount plots within the range of Cook-Austral lavas in Sr and Nd isotopic space, with significantly lower $^{87}\text{Sr}/^{86}\text{Sr}$ values than Samoan lavas. Both Falloon *et al.* [1989] and Falloon and Crawford [1991] have previously suggested on the basis of Nd and Sr isotopes that an OIB component other than the Samoan plume must be involved in mantle sources of northern Tongan boninites, and that the mantle sources derived from the Cook-Austral plume was the most likely extra OIB component.

[38] In this section, we present quantitative modeling of the Sr, Nd and Pb isotopic composition of the enriched boninites, demonstrating that it is possible to explain the isotopic compositions of the enriched boninites if components other than Samoan EMII are included. The results of our modeling are presented in Figures 19 and 20. Compositions of end-members used in mixing calculations are presented in Appendix C. In order to achieve an internally consistent quantitative model for all of the Sr, Nd and Pb values of the enriched boninites based on the assumption that the isotopic compositions are the result of mixing of an OIB component (E2) into the depleted boninite end-member 5–24, three distinct OIB “end-member” components are required. These components are (1) the Samoan EMII component, represented by the compositions from Malumalu seamount [Workman *et al.*, 2004]; (2) the distinctive Samoan EMI-like plume component represented by the Uo Mamae seamount [Acland, 1996; this study]; and (3) a HIMU component from the Cook-Austral plume, represented by lavas from Tubuai [Hauri and Hart, 1993]. The required mixing lines between these end-members components necessary to explain the enriched boninites are presented in Nd versus Sr isotopic space in Figure 19 and in Nd versus Pb isotopic space in Figure 20.

[39] The isotopic composition of enriched boninites can be explained if the E2 component of Danyushevsky *et al.* [1995] is either an OIB melt (e.g., OIB melt 1, Table C5, Appendix C) which is derived from a mixture of HIMU, Uo Mamae and EMII components (model 1, black line, Figures 19 and 20), or alternatively, an OIB melt (e.g., OIB melt 2, Table C5, Appendix C) which is derived from a mixture of HIMU and Uo Mamae components (model 2, black line, Figures 19 and 20). The

mixing lines are illustrative only, as a unique line could be calculated to match exactly the isotopic composition of any individual boninite. Our modeling suggests that a significant (~25–35%) HIMU plume component is required in the E2 component of the *Danyushevsky et al.* [1995] model. Only in the enriched boninites from the northern Tonga ridge and the intermediate boninite end-member (119-2-5; see section 3.1) is a significant contribution (~37%) from Samoan EMII required in the E2 component.

4.3. Northern Lau Basin

[40] A distinctive feature of the lavas currently erupting from spreading ridges in the Lau backarc basin is that their isotopic composition is related to geographical position reflecting distinctive mantle sources. *Volpe et al.* [1988] demonstrated that the Sr and Nd isotopic compositions of Lau Basin basalts display a bimodal distribution related to geographic location within the Lau Basin. They defined two types of basalt comprising both N- (similar to N-MORB) and E-types (similar to E-MORB); Type I basalts ($^{87}\text{Sr}/^{86}\text{Sr} \leq 0.7037$, $^{143}\text{Nd}/^{144}\text{Nd} \geq 0.51297$) occur along the Peggy Ridge and seafloor to the south, and Type II basalts ($^{87}\text{Sr}/^{86}\text{Sr} \geq 0.7038$, $^{143}\text{Nd}/^{144}\text{Nd} \leq 0.51288$), which have been recovered from spreading ridges and seafloor north of the Peggy Ridge. *Volpe et al.* [1988] noted that the Sr-Nd compositions of Type II lavas are similar to OIB, including recent alkali basalts from Fiji [*Gill*, 1984], and from the South Pandora Ridge in the North Fiji Basin [*Sinton et al.*, 1991]. *Volpe et al.* [1988] also noted that the restriction of Type II basalts to the northeastern portion of the Lau Basin indicates that there are localized mantle domains with distinct compositions. Further work [*Loock et al.*, 1990; *Falloon and Crawford*, 1991; *Hergt and Hawkesworth*, 1994; *Ewart et al.*, 1998] subsequent to *Volpe et al.* [1988] has confirmed these observations, and it is clear that the Peggy Ridge lies on the boundary between two mantle domains, MORB-like to the south (Pacific evolving to Indian [*Hergt and Hawkesworth*, 1994]) and OIB-like to the north. This is also supported by $^3\text{He}/^4\text{He}$ ratios of northern Lau Basin basalts [*Poreda*, 1985; *Poreda and Craig*, 1993]. The isotopic data of Lau Basin backarc lavas indicate that there is a generalized influence of the Samoan Plume mantle within the Lau Basin. However, so far, this influence is only reflected in the isotopic compositions of erupted lavas, and is not reflected in their major or trace element compositions, which are typical for the

range expected for backarc spreading centers. This observation is consistent with mixing of sources in the mantle (the Samoan mantle flowing into the northern Lau Basin across the “slab edge”).

[41] The Island of Niua fo’ou in the northern Lau Basin has also long been recognized as having a distinctive mantle source in terms of its isotopic values. Lava compositions from Niua fo’ou are MORB-like tholeiites very similar to lavas from the MTJ (see section 3.3.2). *Ewart and Hawkesworth* [1987] noted the similarities of the isotopic compositions between lavas from Niua fo’ou and lavas from the Samoan and Cook Island chains, and suggested that Niua fo’ou may be tapping a mixed asthenosphere source. *Ewart et al.* [1998] suggested that Niua fo’ou represents a separate “mini-plume” from deeper within the Lau Basin, possibly involving mixing of the “new” (Indian) Lau Basin MORB-source with a restricted isotopic subset of the Samoan plume arrays. In Figures 6 and 7 the Sr, Nd and Pb isotopic compositions of lavas erupting from the Central Lau Spreading Center (CLSC), Niua fo’ou Island and the MTJ are plotted. Lavas erupting from the CLSC have Indian MORB isotopic values (Figures 6 and 7), and it can be seen from Figure 6 that the Nd and Sr isotopic values for the MTJ and Niua fo’ou plot toward lavas from the Samoan plume. In terms of Nd and Sr isotopic values, the lavas from Niua fo’ou would appear to have more of a Samoan plume component in their mantle source (Figure 6). However, in terms of Pb isotopic values, the lavas from the MTJ would appear to have more of a Samoan plume influence (Figure 7). This observation strongly suggests that different OIB components other than the Samoan plume must be involved in causing the enriched isotopic values of northern Lau Basin backarc lavas.

[42] In Figures 19 and 20 we demonstrate that it is possible to explain the mantle source of the Niua fo’ou island as a simple mixture between a Samoan plume component dominated by the distinctive EMI-like Uo Mamae component (~78%) and Indian MORB mantle (source mixing model 2, blue line, Figures 19 and 20). This result is consistent with the conclusion of *Ewart et al.* [1998] that the mantle source for Niua fo’ou lavas must involve a mixing with a subset of the Samoan plume. We propose that this “subset” plume component is represented by the distinctive EMI-like Uo Mamae lavas. In Figures 19 and 20 we also demonstrate that the isotopic values of the MTJ lavas, and lavas from the backarc caldera (sample 116-1-3) and the NELSC (sample 120-1-1) are

consistent with mixing of a pure HIMU component (Tubuai) into the distinctive mantle source represented by Niua fo'ou Island (mixing model 3, black line, Figures 19 and 20). This mixing is well defined in Nd and Pb isotopic space where Niua fo'ou, MTJ, NELSC and sample 116-1-3 from the large caldera are all co-linear (Figure 20) and this array projects directly to Tubuai. Mixing between the HIMU component and Niua fo'ou Island causes backarc spreading lavas to move to higher Nd and Sr isotopic values (Figure 19).

[43] The enriched OIB-like backarc lavas from dredge stations 16-9 and 16-10 (samples 16-9/1, 16-10/4) do not fall on a mixing line between Niua fo'ou and a HIMU component. However, the isotopic composition of lavas 16-9/1 and 16-10/4 are consistent with the E2 component involved in the petrogenesis of the backarc enriched boninites (OIB melt 2, Table C5, Appendix C) being mixed into the Niua fo'ou mantle source (model 4, black line, Figures 19 and 20). The presence of cumulate xenoliths derived from boninite melts in these lavas supports a possible close petrogenetic relationship between these OIB-like lavas and enriched boninites.

4.4. Summary

[44] The complex tectonic setting at the northeastern corner of the Lau backarc basin is responsible for the simultaneous eruptions of a large variety of subduction-related magmas. The main features of this setting are the roll-back of the Tonga trench, the transition from subduction to transform fault tectonics at the northern termination of the Tonga arc, and the presence of two separate mantle hot spot trails on the Pacific plate immediately to the north of the Tonga trench.

[45] Extension in the backarc region, generated by the trench rollback, is accommodated by two processes. The first is propagation of the backarc spreading into the area (the NELSC), which results in the adiabatic upwelling of "Indian"-type mantle under the spreading center. The second is inflow of the sub-Pacific mantle from the north through the slab window formed due to the subduction/transform fault transition. This sub-Pacific mantle contains variable components of the Samoan and Cook-Austral mantle plumes.

[46] Thus the mantle sources in the area are a complex mixture of (1) the "normal" Tongan mantle wedge source that has "Pacific"-type isotopic signature with (2) the plume-related components and (3) an "Indian"-type source upwelling

beneath the backarc spreading. Some of these sources, such as the "normal" mantle wedge and variably depleted residual plume mantle are fluxed by subduction components from the slab, which produces boninites, tholeiites and their mixtures. Other mantle sources, such as "Indian"-type backarc mantle and also some of the plume mantle produce melts due to adiabatic decompression. These melts are variably mixed with each other and the fluxed melts to form the observed spectrum of magma compositions.

5. Conclusions

[47] 1. New multibeam mapping [Wright *et al.*, 2000] reveals that the boninites erupted at the northern termination of the Tonga Trench and Lau Basin are clearly related to recent rifting along the trench-transform wall. The boninite dredge locations are located on either young volcanic cones associated with rift grabens in the northern Lau Basin, or recovered from the rifted walls of a prominent graben which cuts the North Tonga Ridge at its northern terminus. This study confirms the association of boninitic magmas with active backarc spreading ridges and rifting in a backarc setting inferred from previous studies [Crawford *et al.*, 1989; Falloon *et al.*, 1992].

[48] 2. The geochemistry of enriched boninites can be explained by mixing between three end-member compositions. The depleted end-member is derived by fluid-fluxed melting of refractory OIB mantle source, which is inferred to be hot Samoan plume mantle which has penetrated across the trench-transform boundary above the subducting Pacific oceanic crust. The enriched end-member geochemistry is dominated by an OIB component, inferred to be a melt, and is equivalent to the E2 component in the model of Danyushevsky *et al.* [1995]. The third boninite end-member is intermediate between types 1 and 2, and is slightly more enriched in $^{87}\text{Sr}/^{86}\text{Sr}$ values.

[49] 3. Quantitative modeling of isotopic values of the enriched boninites requires that the OIB melt component (E2) is a combination of up to three distinct components, these being the Samoan EMII mantle, an EMI-like component, represented by lavas from the Uo Mamae seamount and a HIMU component, represented by lavas from Tubuai.

[50] 4. Quantitative modeling of boninites which have normal "subduction" zone enrichments of LILE, are consistent with the geodynamic and quantitative geochemical model of Turner *et al.*

Table A1. Summary of Dredging Results in the Northern Lau Basin—Tonga Area During Boomerang Leg 8 of the 1996 Voyage of the R/V *Melville*

Dredge Station	Location/Comments	Start			Finish			Recovery/Deck Log
		Latitude, °S	Longitude, °W	Depth, m	Latitude, °S	Longitude, °W	Depth, m	
D114	Base of fault scarp, lower nearshore flank of Tonga Trench.	14 44.99	173 21.49	6563	14 46.17	173 21.72	5796	160 kg of gabbros, serpentinized ultramafics, volcanics, and sediments, about 8 buckets, mostly cobble to pebble size.
D115	North end of Tonga Ridge, north facing fault wall, just east of active arc.	15 18.7	173 27.49	2128	15 19.85	173 28.06	1200	260 kg of vesicular oliv-phyric and plag-phyric volcanics.
D116	Central edifice of 10 km wide caldera, about 40 km west of Tofua Arc.	15 22.24	174 00.19	1541	15 22.58	174 00.19	1327	350–400 kg of glassy andesitic to dacitic flow pieces.
D117	Eastern caldera wall of caldera.	15 22.10	173 58.18	1793	15 22.1	173 57.46	1339	800 kg of dacitic-rhyolitic material.
D118	Northernmost seamount in Tofua Arc.	15 03.78	173 32.92	1380	15 04.24	173 33.18	900	500 kg of plag-, quartz-phyric rhyolite, pumice.
D119	West side of NNE trending graben cutting trench slope. West side of a structure which parallels the north arm of the Lau spreading center.	14 54.99	173 50.31	3173	14 54.20	173 50.6	2613	400 kg of oliv-phyric boninites. Picritic to basaltic in character.
D120	Northern end of the Northeast Lau Spreading Center. Volcanic part of rift.	14 51.79	173 59.1	3084	14 52.11	173 59.75	2929	65 kg of slightly Mn-coated and weathered glassy basalts, both pillow and more tabular, pahoehoe type pieces.

Table A2. Radiometric Age Determinations for Rock Samples Dredged From the Northern Lau Basin – Tonga Area

	Sample	Rock Type	Lab/Data Source	Method	Age, Ma	(\pm)1 σ	
Kallisto 82							
	Station 16–51	16–51/9	boninite	<i>Acland</i> [1996]	K-Ar	2.54	0.74
	Station 16–51	16–51/16	boninite	<i>Acland</i> [1996]	K-Ar	3.09	0.48
	Station 16–26	16–26/1	boninite	<i>Acland</i> [1996]	K-Ar	0.58	0.20
	Station 16–26	16–26/2	boninite	<i>Acland</i> [1996]	K-Ar	0.89	0.04
Natsushima 84							
	Station St21	3–23	boninite	OSU ^a	K-Ar	1.40	0.03
	Station St23	5–27	basaltic andesite	OSU	K-Ar	2.03	0.11
Tafahi							
	TT1		basaltic andesite	UCSC ^b	K-Ar	0	0
Niuatoputapu							
	TN3		basaltic andesite	UCSC	K-Ar	3.00	0.10

^aOSU, Oregon State University, R. Duncan analyst.

^bUCSC, University of California Santa Cruz, J. B. Gill personal communication, 1986.

[1997]. However, unlike the northern Tonga Islands of Tafahi and Niuatoputapu, there appears to be no involvement of subducted volcanoclastic sediment derived from the Louisville Ridge.

[51] 5. Backarc pillow lavas recovered from the northern most nascent spreading center in the northern Lau Basin, the NELSC, at dredge station D120, are basaltic andesites with LREE-enriched patterns. The basaltic andesites have major element geochemistry intermediate between those of MTJ lavas and enriched boninites sampled from rifts in the northern Lau Basin. This suggests that boninite magmas are being mixed into normal backarc spreading ridge lavas at the northern end of the NELSC. Volcanics recovered from a large backarc caldera (dredge stations D116 and 117) are dacites and rhyolites with major and trace element geochemistry consistent with being derived by crystal fractionation from boninitic parents.

[52] 6. The isotopic composition of backarc lavas from the island of Niua fo'ou can be explained by source mixing between the EMI-like Samoan plume component represented by Uo Mamae lavas and Indian MORB represented by lavas from the CLSC. Mixing of a pure HIMU plume component into this distinctive Niua fo'ou source can explain the isotopic compositions of spreading ridge lavas from the MTJ, NELSC and the large boninite-derived backarc caldera sampled at dredge stations D116 and D117 by the *R/V Melville*.

[53] 7. Lavas sampled from rifts located to the west of the NELSC (dredge stations 16-9 and 16-10) have major element chemistry intermediate between MTJ and Samoan plume lavas, and have strong enrichments in LREE similar to Samoan lavas. The isotopic composition of these lavas

suggests that the enrichment seen in these OIB like lavas is similar to the E2 component present in enriched boninites associated with rifting in the northern Lau Basin.

Appendix A: Geological Setting of Dredged Samples

[54] Locations from dredging or submersible sampling from the *R/V Melville*, *R/V Kallisto*, *R/V Keldysh*, and *R/V Natsushima* voyages are presented in Figures 2 and 3. Dredging results from the *R/V Melville* voyage are summarized in Table A1. Available radiometric age dating of rocks from the area is presented in Table A2. Brief petrographic descriptions and mineral chemistry of the samples collected from the *R/V Melville* voyage are presented in Tables A3 and A4. In Table A5 we present corrected sample numbers for the data from the study of *Falloon and Crawford* [1991].

[55] The sampling covers seven specific tectonomagmatic elements of the northern Lau Basin-Tonga Trench termination as outlined below moving west to east in Figures 2 and 3. Radiometric ages and radiogenic isotope analyses from a number of samples from both the *R/V Keldysh* and *R/V Kallisto* cruises are reported by *Acland* [1996].

A1. Inner Slope of the Westernmost Extent of the Tonga Trench

[56] During the 1982 voyage of the *R/V Kallisto* fresh pillow lavas were recovered from dredge stations 16-9 and 16-10 [*Sharaskin et al.*, 1983; *Zlobin et al.*, 1991] located within a backarc rift

Table A3. Petrographic Summary of Samples Studied

Petrographic Group	Samples	Comments
Olivine – phyric boninite	114-3-1	Quenched strongly oliv-phyric picritic rock lacking opx phenocrysts, and having a quenched groundmass, assemblage of fan spherulites with small opx microlites and strongly zoned clinopyroxene.
Olivine + clinopyroxene + plagioclase – phyric basalt	114-3-6	
Orthopyroxene + clinopyroxene ± olivine – phyric boninite	115-1-1,115-1-2, 115-1-8,115-1-10, 115-1-11,115-1-5	Strongly porphyritic vesicular boninitic high-Mg andesite dominated by large opx and cpx phenocrysts, with abundant evidence of magma mixing, including partially reacted grains, opx with strong reverse zoned rims. Very little chromite.
Orthopyroxene + plagioclase ± clinopyroxene – phyric andesite	115-2-5,115-2-7	
Orthopyroxene + clinopyroxene + plagioclase + titanomagnetite ± apatite – phyric dacite	116-1-1,116-1-3	Highly vesicular, glassy.
Plagioclase + orthopyroxene + clinopyroxene + titanomagnetite + apatite – phyric rhyolite	117-1-1,117-2-3	Vesicular, glassy groundmass.
Plagioclase + quartz + orthopyroxene + clinopyroxene + titanomagnetite – phyric rhyolite	118-2-5,118-2-8	Massive, vesicular, glassy groundmass.
Olivine + orthopyroxene + Cr-spinel ± clinopyroxene – phyric Boninite	119-1-1,119-2-5, 119-3-5,119-3-6	Vesicular and strongly to moderately porphyritic very fresh boninite with common large oliv and opx phenocrysts, in a quenched groundmass of glass charged with small cpx and opx microlites. Samples 119-3-5, –6 are sparsely phyric to aphyric.
Olivine + plagioclase + clinopyroxene – phyric basalts	120-1-1,120-1-3, 120-2-1,120-2-3	Both pillow and tabular pahoehoe pieces.

zone associated with the transition from a trench to a transform plate boundary in this area.

A2. Northeast Lau Spreading Center

[57] The mapping reveals a nascent spreading center, the Northeast Lau Spreading Center (Figure 3, the location is identified by dredge station D120), featuring a series of parallel, or closely-spaced ridges and troughs [Wright *et al.*, 2000; Langmuir *et al.*, 2005; German *et al.*, 2006]. The spreading center can be clearly identified to within about 30km of the trench axis and it is likely that the spreading center intersection with the trench forms a ridge-transform-transform triple junction between the Tonga Plate, the Pacific Plate and the Niua fo’ou Plate. This spreading center is a continuation of the northeastern limb of the Mangatolu Triple Junction, MTJ (Figure 2, dive sites M-2212, M-2218, M-2216), a backarc ridge-ridge-ridge junction. Hydrothermal activity along this spreading center is reported by German *et al.* [2006]. The Mangatolu Triple Junction is located $\sim 15^{\circ} 37'S$, $174^{\circ} 52'W$, and is characterized by intense deformation and neovolcanism [Parson and Tiffin, 1993].

[58] The detailed geological structure of the Lau Basin including the MTJ is presented by Zellmer

and Taylor [2001]. During the 1990 voyage of the R/V *Keldysh*, three *Mir* dives were conducted on the MTJ. Two dives (M-2212, M-2218 [Falloon *et al.*, 1992]) were conducted close to the center of the triple junction, and one dive (M-2216 [Falloon *et al.*, 1992]) was conducted on the northeastern branch of the triple junction (Figure 2). During the 1996 R/V *Melville* voyage one dredge (dredge station D120, Table A1, Figure 3) was conducted on the northern part of the Northeast Lau Spreading Center which appears to intersect the Tonga Trench to form a triple junction [Wright *et al.*, 2000].

A3. Backarc Caldera

[59] To the south of dredge station D120 (~ 50 km) and on the eastern side of the spreading ridge lies a 10km wide caldera with a significant breach on its southern rim (Figure 3, dredge stations D116 and D117). Dredges D116 and D117 (Table A1) were conducted respectively on the central volcanic cone and eastern wall of this large backarc caldera (Figure 3).

A4. Rift-Related Boninite Lavas: “Western Group Boninites”

[60] The multibeam mapping reveals that the boninites sampled during voyage 16 of the R/V

Table A4. Selected Mineral Analyses

Sample	Mineral	Type	Analysis	SiO ₂	TiO ₂	Al ₂ O ₃	Cr ₂ O ₃	FeO	MnO	MgO	CaO	Na ₂ O	K ₂ O	NiO	Mg#	An
115-1-8	Cpx	Ph	24	52.81	0.06	1.56	0.48	7.95	0.22	17.13	19.71	0.08				79.3
	Opx	Ph	27	54.92	0.03	0.93	0.14	14.30	0.36	27.08	2.24	0.01				77.1
	Opx	Ph	28	56.55	0.00	0.40	0.24	9.18	0.22	31.14	2.24	0.02				85.8
115-1-10	Plag	mcl	17	47.51		30.09		2.46		0.50	17.07	2.20	0.17			80.3
	Cpx	Ph	23	53.60	0.03	0.54	0.56	5.03	0.21	19.35	20.56	0.12				87.3
	Cpx	Ph	22	51.60	0.06	1.34	0.24	8.50	0.26	17.97	19.94	0.08				79.0
115-1-11	Opx	Ph	16	52.23	0.03	1.25	0.14	16.24	0.45	27.45	2.17	0.04				75.1
	Oliv	Ph	29	38.79			0.01	13.65	0.27	47.00	0.20			0.08		86.0
	Opx	Ph	28	53.29	0.04	0.97	0.08	15.27	0.47	27.67	2.22	0.01				76.4
115-2-5	Cpx	Ph	25	52.72	0.06	1.49	0.16	8.34	0.33	17.28	19.55	0.08				78.7
	Cpx	Ph	20	54.58	0.07	0.93	0.06	16.87	0.43	24.80	2.24	0.02				72.4
	Plag	Ph	24	44.28		34.55		0.68		0.06	19.72	0.68	0.03			94.0
116-1-1	Cpx	mPh	41	51.44	0.28	1.85	0.01	11.55	0.41	14.61	19.69	0.16				69.3
	Opx	mPh	44	52.73	0.24	1.04	0.00	22.35	0.80	20.87	1.95	0.02				62.5
	Plag	mPh	39	55.64		26.81		1.60		0.15	11.79	3.79	0.23			62.3
116-3-1	Ti-mag	mPh	43	0.23	7.02	3.42	0.00	87.62	0.31	1.37	0.02					
	Opx	Ph rim	30	53.38	0.16	0.95	0.05	20.71	0.50	22.30	1.89	0.06				65.7
	Cpx	Ph	38	51.18	0.32	1.90	0.04	11.87	0.37	13.98	20.09	0.24				67.7
117-2-3	Plag	Ph	43	47.73		32.37		0.99		0.11	16.91	1.85	0.04			83.3
	Ti-mag	mPh	37	0.10	6.16	3.26	0.11	87.99	0.24	2.14	0.00					
	Cpx	Ph	4	51.00	0.26	0.98	0.00	16.50	0.53	11.45	19.14	0.15				55.3
118-2-8	Opx	Ph	30	50.41	0.24	0.65	0.01	31.22	0.90	14.64	1.94	0.00				45.5
	Plag	Ph	3	50.21		31.03		0.61		0.03	15.12	2.94	0.06			73.7
	Ti-mag	mPh		0.12	15.28	1.97	0.03	80.94	0.54	1.11	0.01					
119-1-1	Opx	Ph	11	52.71	0.17	0.51	0.02	24.16	0.60	20.51	1.30	0.02				60.2
	Cpx	Ph	20	51.96	0.21	0.97	0.00	11.38	0.36	13.65	21.28	0.19				68.1
	Plag	Ph	52	48.20		32.41		0.58		0.03	16.19	2.53	0.06			77.7
120-1-1	Ti-mag	mPh	25	0.11	8.67	2.15	0.23	87.15	0.31	1.30	0.08					
	Cpx	Ph r	6	54.04	0.14	1.18	0.57	4.01	0.11	19.05	20.78	0.11				89.4
	Oliv	Ph r	19	41.23			0.14	7.03	0.10	50.99	0.21			0.31		92.8
120-1-1	Oliv	Ph c	18	40.69			0.05	10.45	0.14	48.16	0.31			0.21		89.1
	Cr-sp	incl	21	0.08	0.33	9.76	58.59	16.82	0.22	14.21	0.00					
	Oliv	Ph	64	38.79				18.78	0.31	41.75	0.27			0.11		79.8
120-1-1	Oliv	mPh	47	38.71				17.62	0.29	43.02	0.20			0.16		81.3
120-1-1	Plag	Ph	60	49.33		31.22		0.78		0.26	15.63	2.68	0.10			75.9
120-1-1	Plag	Ph	61	46.19		33.66		0.55		0.14	18.05	1.36	0.04			87.8
120-2-3	Plag	Ph c	23	44.40		34.99		0.57		0.12	18.98	0.92	0.02			91.8
120-1-1	Cpx	Ph	59	52.19	0.38	2.09	0.07	6.78	0.18	17.75	20.45	0.13				82.3
120-2-1	Cpx	mPh	17	50.21	0.81	5.00	0.10	8.13	0.22	16.11	19.24	0.18				77.9
120-2-1	Cpx	mPh	19	50.92	0.63	4.07	0.15	7.13	0.34	16.51	20.09	0.17				80.5

Kallisto in 1982 at dredge station 16-26 (samples 16-26/1 and 16-26/2) and the 1984 voyage of the R/V *Natsushima* in 1984 at dredge stations St24 and St25 (samples 6-3, 7-18) were derived from young volcanic cones associated with a rift graben immediately to the east of the Northeast Lau Spreading Center sampled by dredge station D120 (Figures 2 and 3). The cones are young based on their undisturbed shape despite being in a tectonically active area, lack of alteration and Mn coating on pillow rinds of the erupted lavas and radiometric dating (Table A2) [Falloon *et al.*, 1987; Acland, 1996]. These boninites were referred to as the “western group” boninites by Sobolev and Danyushevsky [1994] and Danyushevsky *et al.* [1995]. During the 1996 R/V *Melville* voyage

dredge station D119 (Table A1) was conducted on a small volcanic cone on the western side of the rift graben where boninite lavas were also recovered (Figure 3).

A5. Tonga Trench at the Northern Termination of the Tofua Volcanic Arc

[61] Boninite lavas were recovered at dredge stations 16–51 (R/V *Kallisto*) and St21 (R/V *Natsushima*) from this area (Figure 3, Table A1). The boninites from this area belong to the “eastern group” boninites of Sobolev and Danyushevsky [1994] and Danyushevsky *et al.* [1995]. The radiometric ages obtained for boninites from dredge stations 16-51 and St21 give relatively young ages (~1–3 Ma, Table A2) which overlap the age of

Table A5. Corrected Table 2 From *Falloon and Crawford [1991]*^a

Group Sample	I 3-44	I 3-39	II 3-21	II 3-51	II 3-49	III 3-45	III 3-47	III 3-25	III 3-46	IV 3-53	IV 3-22	IV 3-34	IV 3-41
SiO ₂	54.35	54.53	54.35	53.95	52.41	55.39	55.18	55.79	55.58	57.51	56.01	59.06	55.84
TiO ₂	0.2	0.22	0.23	0.23	0.21	0.29	0.31	0.3	0.24	0.29	0.29	0.34	0.33
Al ₂ O ₃	10.67	11.43	12.88	12.88	11.12	10.85	10.94	11.45	10.58	13.18	13.88	13.29	14.47
FeO	9.41	9.3	9.88	9.81	9.54	9.87	10	9.87	9.96	9.22	9.7	9.23	9.84
MnO	0.19	0.18	0.16	0.16	0.18	0.18	0.19	0.18	0.19	0.18	0.19	0.18	0.19
MgO	14.99	13.34	10.59	10.4	14.87	12.05	12.14	11.08	12.54	8.14	7.78	6.26	6.93
CaO	8.66	9.53	9.87	10.5	9.99	9.36	9.24	9.29	9.48	9.53	9.98	9.13	9.98
Na ₂ O	1.14	1.09	1.56	1.6	1.41	1.48	1.48	1.42	1.03	1.35	1.63	1.78	1.74
K ₂ O	0.35	0.34	0.44	0.45	0.2	0.48	0.48	0.58	0.36	0.54	0.47	0.64	0.61
P ₂ O ₅	0.03	0.03	0.04	0.03	0.05	0.05	0.05	0.05	0.04	0.06	0.06	0.09	0.07
LOI	0.05	0.36	1.07	1.33	1.46	0.59	0.98	1.08	0.28	-0.07	-0.15	-0.04	0.5
Ba	106	86	112	104	98	108	113	117	93	140	131	163	161
Rb	6	7	4	5	2	7	7	9	5	8	7	10	12
Sr	151	161	172	175	264	177	172	190	156	202	236	223	271
Zr	12	11	10	9	9	18	20	18	11	17	14	19	18
Nb		2				1		1		1	1		1
Y	7	7	5	6	8	9	8	10	8	9	10	11	9
Sc	50	51	48	53	45	48	51	46	53	50	49	47	47
V	247	261	326	343	253	247	259	252	256	275	281	275	292
Ni	275	215	122	123	233	150	153	132	143	84	78	47	67
Cr	1095	814	435	445	935	729	762	607	774	365	281	196	196
Hf	0.61			0.3			0.55			0.6	0.72		
Ta	<0.3			<0.3			<0.3			<0.3	<0.3		
Th	0.48			0.54			0.53			0.82	0.47		

Table A5. (continued)

Group	IV	IV	IV	IV	V	VI	VI	VI							
Sample	3–28	3–52	3–40	3–26	3–31	3–24	3–27	3–36	3–30	3–23	3–29	3–32	3–42		
SiO ₂	54.4	56.77	56.74	55.66	57.27	59.19	55.59	60.17	60.8	59.81	60.19	60.01	60.73		
TiO ₂	0.27	0.3	0.34	0.3	0.34	0.25	0.31	0.42	0.43	0.41	0.42	0.41	0.43		
Al ₂ O ₃	14.81	14.59	16.18	15.31	15.39	10.96	15.51	15.21	14.95	15.3	15.2	15.32	15.27		
FeO	10.02	9.32	9.38	9.61	9.34	8.83	9.82	8.9	8.72	8.82	8.94	8.88	8.7		
MnO	0.17	0.18	0.15	0.17	0.17	0.18	0.17	0.15	0.15	0.14	0.14	0.15	0.14		
MgO	7.82	6.42	4.55	6.39	5.15	10.8	6.01	3.35	3.11	3.34	3.33	3.35	3.14		
CaO	10.69	10.35	9.95	10.57	9.72	7.78	10.71	7.68	7.48	7.65	7.67	7.64	7.45		
Na ₂ O	1.38	1.52	1.98	1.45	1.86	1.37	1.41	2.96	2.86	3.16	2.79	2.85	2.99		
K ₂ O	0.4	0.46	0.64	0.47	0.67	0.56	0.43	1.01	1.35	1.21	1.17	1.24	0.99		
P ₂ O ₅	0.04	0.09	0.09	0.06	0.08	0.07	0.04	0.14	0.14	0.14	0.14	0.14	0.15		
LOI	0.04	0.03	0.04	0.45	0.13	0.01	0.3	0.83	2.23	2.04	1.73	2.02	-0.03		
Ba	107	116	180	123	170	140	104	271	278	268	270	267	274		
Rb	8	10	9	8	12	10	7	19	21	20	21	20	13		
Sr	189	206	319	212	260	175	196	385	379	387	389	384	396		
Zr	15	14	20	16	23	19	16	44	41	40	43	40	41		
Nb	1	2	1	2	2	2	2	4	4	4	5	3	3		
Y	8	8	11	10	11	7	9	13	12	12	12	13	14		
Sc	51	52	42	50	45	43	52	34	32	33	32	32	32		
V	323	338	288	345	333	251	330	309	274	305	310	307	247		
Ni	99	63	40	64	43	117	50	21	16	19	19	17	18		
Cr	287	180	88	159	94	605	78	17	17	14	13	13	16		
Hf		0.48				0.84	0.9	1.51							
Ta		<0.3				<0.3	<0.3	<0.3							
Th		0.62				0.9	0.7	2.3							

^aThe correct Table 2 from *Falloon and Crawford* [1991], giving the major and trace element geochemistry for dredge station S21 high-Ca boninite lavas, northern Tonga (see [*Falloon and Crawford*, 1991] for other details). The original published table was missing sample numbers for petrographic groups IV–VI.

Table B1. Major Element Analyses of Tasmanian Standard Rocks Obtained During This Study

	TASBAS, <i>n</i> = 9		TASDOL, <i>n</i> = 8		TASDIOR, <i>n</i> = 5		TASGRAN, <i>n</i> = 6	
	This Study	Published	This Study	Published	This Study	Published	This Study	Published
SiO ₂	44.46	44.55	53.03	53.19	64.73	65.11	72.83	72.78
TiO ₂	2.42	2.32	2.44	2.43	0.61	0.61	0.29	0.29
Al ₂ O ₃	14.13	14.15	13.20	13.10	14.94	14.80	13.69	13.66
Fe ₂ O ₃	12.64	12.65	12.50	12.57	5.59	5.61	2.26	2.26
MnO	0.17	0.17	0.18	0.18	0.12	0.11	0.04	0.04
MgO	8.34	8.29	2.84	2.79	3.07	3.02	0.71	0.68
CaO	7.86	7.84	6.19	6.20	4.78	4.79	1.83	1.84
Na ₂ O	5.42	5.37	3.18	3.16	1.93	1.97	2.79	2.74
K ₂ O	1.93	1.93	1.82	1.81	2.23	2.20	4.61	4.59
P ₂ O ₅	0.93	0.94	0.94	0.95	0.15	0.17	0.11	0.12
Loss	1.56	1.56	3.28	3.28	1.35	1.35	0.73	0.73
Sum	99.77	99.77	99.68	99.72	99.56	99.74	99.85	99.73
S	0.04	0.04	0.11	0.11	0.02	0.03	0.00	0.00

modern Tofua Arc volcanism on the islands of Tafahi and Niuatoputapu (Table A2).

A6. Large Rift Graben Cutting the North Tonga Ridge at Its Northern Termination

[62] This rift graben was first identified by the R/V *Natsushima* voyage which sampled the north facing wall of the graben at dredge station St23 (Figure 3) [Falloon *et al.*, 1987]. During the R/V *Melville* voyage the rift wall was again sampled at dredge station D115 and boninite lavas recovered (Figure 3, Table A2). Also sampled at dredge station D118 was a large submarine volcanic edifice which completely fills the central part of the graben (Figure 3). Boninites from this rift graben are also part of the “eastern group” boninites.

A7. Uo Mamae Seamount

[63] The R/V *Kallisto* voyage sampled the most southerly seamount of the Samoan plume, Uo Mamae (dredge stations 16–94 to 16–100 [Sharaskin *et al.*, 1983]). This seamount is starting to be pulled apart by the rifting of the Pacific Plate at the termination of the Tonga Trench [Wright *et al.*, 2000]. Hawkins and Natland [1975] report a K-Ar age of 940,000 yrs for a phonolite dredged from the summit of this seamount.

Appendix B: Analytical Techniques

B1. Major Element Analysis

[64] Samples were ground in an agate mill to avoid any possible trace element contamination. Major element analyses were performed at the School of Earth Sciences (UTAS) using X-ray fluorescence

spectrometry (XRF) and the methods of Robinson [2003]. Whole rock sample powders were fused with 12–22 flux (a pre-fused mixture consisting of 12 parts Li₂B₄O₇ and 22 parts LiBO₂) using a sample:flux ratio of 1:9 at 1100°C. All fusions are performed in a non-wetting 5% Au–95% Pt alloy crucible. The following quantities are used to make 32 mm diameter discs: –12–22 flux (4.5000 g), sample (0.5000 g) and LiNO₃ (0.0606 g, added as 100 μl of 60.6% LiNO₃). The mix is fused with agitation at 1100°C for 15 minutes before being cast in a 5% Au–95% Pt mould. Ignition loss was determined on ~2 grams of sample powder ignited overnight at 1000°C in 5 mL platinum crucibles. Major elements were determined with a ScMo 3kW side window X-ray tube and a Philips PW1480 x-ray spectrometer. Corrections for mass absorption are calculated using Philips X40 software with De Jongh’s calibration model and Philips (or CSIRO) alpha coefficients. Compton scattering is also used for many trace elements (see below). Calibrations are on pure element oxide mixes in pure silica, along with international and Tasmanian standard rocks are used. Analyses of a range of secondary standards are presented in Table B1.

B2. Trace Element Analysis

B2.1. XRF

[65] Trace element analyses in Table 3 (Rb, Ba, Nb, Sr, Zr, Y, V, Sc, Cr, Ni) were determined by using pressed powder pill analysis (10 grams, 32 mm) using a combination of ScMo (Y, Rb, Ni) and Au (Ba, Nb, Sr, Zr, V, Sc, Cr) 3kW side window X-ray tubes and a Philips PW1480 x-ray spectrometer. Analyses of international and secondary standards and detection limits are presented in Table B2.

Table B2. Trace Element Analyses of International and Tasmanian Standard Rocks Obtained During This Study

Detection Limits	BIR-1, n = 10		ENDV, n = 10		BHVO1, n = 2		Tafahi, n = 9		TASBAS, n = 9		TASGRAN, n = 10		AGV1		BCR1	
	This Study	Published	This Study	Published	This Study	Published	This Study	Published	This Study	Published	This Study	Published	This Study	Published	This Study	Published
Nb	<1	0.5	6.3	6.35	17.5	17.2	0.5	0.5	54.6	54.5	13.0	13.1				
Zr	14.3	14.5	111.1	111.0	171.6	167	11.6	12.1	258.3	259.0	160.0	160.0				
Sr	106.9	106	162.6	162.0	393.7	388	138.7	138.9	1006.5	1008.0	145.8	147.0				
Cr	389.1	389	315.7	314	301.1	289.0	54.2	53.0	182.5	181.0	9.4	9.0				
Ba	6.2	6.4	65.2	70	130.8	130	44.2	40.3	191.7	186.5	447.4	450				
Sc	37.8	38	43.8	41.0	32.9	32.7	46.3	45.5	13.7	14	6.6	6.9				
V	308.7	313.0	292.4	289	298.3	312	316.5	315	146.5	156.0	24.1	24.0				
n	6				12	14	14	14	14	14	10	10			3	3
Y	16.4	14.8			9.1	9.2	9.1	9.2	21.1	19.5	36.0	33	20.2	20.0	37.8	38
Rb	0.2	0.2			1.7	1.8	1.7	1.8	16.0	16.4	251.7	251.0	68.7	67.3	48.0	47.2
Ni	157.8	159			22.1	23	22.1	23	147.6	150.0	3.5	3.5	15.5	16	11.1	13

B2.2. ICP-MS

[66] ICP-MS trace element analyses at UTAS were obtained using the methods of *Robinson et al.* [1999] and *Yu et al.* [2000]. ICP-MS analyses were performed on duplicate high-pressure HF-HClO₄ digestions. Sub-boiling double distilled acids and ultrapure water were used, as were clean sampler and skimmer cones, ICP torch, spray chamber, nebulizer and sample introduction tubes (including auto-sampler tubing). Prior to sample analysis the instrument was purged for at least 24 hours with 5% v/v HNO₃ and 0.05% v/v HF rinse solution. Analyses of international and secondary standards and detection limits are presented in Table B3.

[67] ICP-MS analyses were also performed at the ANU using the multiple enriched isotope internal standard, solution ICP-MS method of *Eggins et al.* [1997]. Trace and minor element concentrations for several basaltic international reference materials and the ANU in-house secondary standard (Tafahi) that were determined during the same analytical runs as the unknowns measured in this study are reported in Table B4.

B3. Electron Microprobe Analyses

[68] Electron Microprobe Probe Analysis (EMPA) of interstitial glass and pillow rind glass are presented in Table 4 and were obtained using a Cameca SX50 electron microprobe at the Central Science laboratory, University of Tasmania, Hobart, at 15 kV and 20 nA. Each element was calibrated against a relevant oxide standard. In the case of glass analyses we analyzed the international standard USNM 111240/2 (basaltic glass) from *Jarosewich et al.* [1980] to derive correction factors, which were applied to the glass analyses. Counting times for all elements except Na and K were 10s for the peak and 5s for the background on both sides of the peak. K and Na was analyzed for 20s on the peak and 10s on the background. Standard electron microprobe accuracy is as follows: 2% for Si, Al, Fe, Mg and Ca; 5% for Na and Ti; and 5–50% for K depending on absolute content. A beam size of 5 μm was routinely used.

B4. Isotope Analyses

B4.1. Sr-Nd-Pb Isotopes: The Australian National University

[69] Sample powders were first acid washed in hot 6N HCl for around 30 minutes, rinsed in milli-Q water and finally dissolved in HF/HNO₃ acids. Pb, Sr, and Nd were then separated by conventional

Table B3. Analyses of Standard Rocks by ICP-MS at UTAS

	BIR-1, <i>n</i> = 1		TASBAS, <i>n</i> = 3		Tafahi, <i>n</i> = 2	
	This Study	Published	This Study	Published	This Study	Published
La	0.796	0.58	40.43	44.58	0.90	0.938
Ce	1.74	1.85	79.34	85.24	2.19	2.22
Pr	0.34	0.37	9.51	10.12	0.35	0.361
Nd	2.20	2.35	37.67	41.68	1.85	1.93
Sm	1.05	1.1	7.55	8.24	0.70	0.722
Eu	0.50	0.52	2.41	2.63	0.30	0.305
Gd	1.80	1.97	6.54	6.79	1.05	1.069
Tb	0.36	0.38	0.92	1.01	0.20	0.207
Dy	2.44	2.5	4.45	4.76	1.36	1.384
Ho	0.56	0.57	0.76	0.80	0.31	0.322
Er	1.60	1.7	1.73	1.79	0.93	0.98
Yb	1.60	1.6	1.26	1.27	0.98	0.992
Lu	0.25	0.25	0.18	0.17	0.16	0.153

	BIR-1, <i>n</i> = 4		TASBAS, <i>n</i> = 2		Tafahi, <i>n</i> = 4	
	This Study	Published	This Study	Published	This Study	Published
Zr	14.8	14.5	255.5	260	12.7	12.07
Nb	0.533	0.55	54.7	54.5	0.458	0.456
Ba	7.1	6.4	186	186.5	42.5	40.3
Hf	0.547	0.56	5.51	5.43	0.392	0.395
Pb	2.99	3	4.64	4.6	0.69	0.95
Th	0.029	0.03	4.816	4.8	0.118	0.12
U	0.01	0.01	1.91	1.89	0.072	0.0728

ion-exchange techniques. Total procedural blanks were negligible in all cases, with Pb blanks typically less than 100 pg.

[70] All samples were run on a Finnigan MAT261 mass spectrometer operating in static multicollector mode. $^{87}\text{Sr}/^{86}\text{Sr}$ and $^{143}\text{Nd}/^{144}\text{Nd}$ were normalized to $^{86}\text{Sr}/^{88}\text{Sr} = 0.1194$ and $^{144}\text{Nd}/^{146}\text{Nd} = 0.7219$ respectively, using a linear fractionation law. Repeated analysis of the NBS 987 Sr and nNd-1 (the ANU “in-house” Nd standard) Nd standards over a 3 year period provided long-term mean values of $^{87}\text{Sr}/^{86}\text{Sr} = 0.710198 \pm 4$ (2 s.e. for $n = 96$) and $^{143}\text{Nd}/^{144}\text{Nd} = 0.512200 \pm 3$ (2 s.e. for $n = 60$), the latter corresponding to a $^{143}\text{Nd}/^{144}\text{Nd}$ value for La Jolla Nd of 0.511899. Typical in-run precisions (2se) are ± 0.000010 (Nd) and ± 0.000015 (Sr). Measured Pb isotope ratios were routinely corrected for mass fractionation using a $^{207}\text{Pb}/^{204}\text{Pb}$ double spike. Samples were split for spiking immediately prior to filament loading and mass spectrometry thus avoiding any potential problem due to variable blank composition in spiked and unspiked aliquots. This technique provides consistently high quality data with improvement in both precision and accuracy over conventional correction procedures (an external precision in $^{206}\text{Pb}/^{204}\text{Pb}$, $^{207}\text{Pb}/^{204}\text{Pb}$ and

$^{208}\text{Pb}/^{204}\text{Pb}$ ratios of ± 0.003 , 0.003 and 0.01 ($2 \times$ S.D.) respectively is routinely obtainable independent of minor variations in loading and run parameters); for further details readers are referred to *Woodhead et al.* [1995].

B4.2. Sr-Nd-Pb Isotopes: University of Melbourne

[71] Sample preparation techniques for isotopic analysis at the University of Melbourne differ from those used at the ANU. Hand-picked rock chips were acid washed in hot 6N HCl for 15 minutes and then dissolved in HF/HNO₃ acids. After extraction of Pb using conventional anion exchange using HBr-HCl media, Sr and LREE were extracted on EICHRON Sr. resin and RE.resin, respectively, followed by Nd purification on EICHRON LN resin [*Pin et al.*, 1994; *Pin and Santos-Zaldugui*, 1997]. Total procedural blanks were negligible in all cases with Pb blanks typically less than 20 pg.

[72] All isotopic analyses were carried out on a Nu Instruments multicollector ICP-MS coupled to a CETAC Aridus desolvating nebulizer [*Belshaw et al.*, 1998; *Woodhead*, 2002]. Instrumental mass bias was corrected by normalizing to $^{146}\text{Nd}/^{145}\text{Nd} =$

Table B4. Analyses of USGS Reference Materials and ANU in-House Standard Tafahi Measured by Solution Nebulization ICPMS at the ANU^a

	AGV-1 (n = 2)	BIR-1 (n = 4)	%RSD	Tafahi (n = 4)	%RSD	W-2 (n = 1)
Li	11.30	3.309	1.1	4.00	0.8	9.57
Be	2.60	0.115	0.8	0.185	0.9	0.74
Sc	12.4	44.1	1.6	46.1	1.8	35.5
Ti	5986	5841	7.5	2294	9.2	7296
V	129.8	325	2.0	283	3.3	268
Cr	8.93	416	1.1	50.6	9.2	90.9
Co	15.48	53.2	0.6	39.6	0.4	44.4
Ni	15.95	175.6	0.5	24.6	0.8	73.1
Cu	58.28	112.8	1.4	126.3	1.2	100.7
Zn	85.0	65.9	1.1	62.2	2.5	71.5
Ga	20.23	15.10	0.9	13.02	1.1	17.23
As	0.91	0.330	10.6	0.61	12.3	0.53
Rb	68.6	0.195	2.2	1.73	1.3	20.0
Sr	654	105.9	0.6	137.7	0.5	189.0
Y	21.01	16.28	0.9	9.15	0.3	22.61
Zr	237.5	14.37	0.7	11.97	0.4	88.5
Nb	14.84	0.554	0.7	0.45	1.0	7.84
Cs	1.304	0.0053	4.0	0.067	3.0	0.898
Ba	1226	6.450	0.7	40.37	1.0	170.5
La	38.91	0.603	0.7	0.942	1.1	10.49
Ce	68.90	1.888	0.2	2.224	0.7	22.82
Pr	8.429	0.375	0.8	0.363	1.5	3.014
Nd	31.35	2.360	0.9	1.932	1.4	12.93
Sm	5.877	1.115	1.7	0.721	2.2	3.301
Eu	1.573	0.521	0.9	0.306	0.9	1.090
Gd	4.766	1.864	0.7	1.074	0.7	3.688
Tb	0.693	0.379	1.4	0.212	0.2	0.646
Dy	3.553	2.520	0.7	1.386	0.5	3.840
Ho	0.692	0.580	0.9	0.322	0.5	0.803
Er	1.865	1.731	0.9	0.983	0.2	2.257
Yb	1.647	1.643	1.2	0.990	1.0	2.030
Lu	0.249	0.248	1.3	0.154	1.6	0.296
Hf	2.742	0.559	1.8	0.395	1.7	2.279
Ta	0.876	0.041	1.1	0.022	3.5	0.478
Pb	38.07	2.946	0.1	0.96	1.7	7.96
Th	6.49	0.0306	3.5	0.119	2.9	2.155
U	1.89	0.0100	3.4	0.073	1.0	0.496

^aUsing the method of *Eggins et al.* [1997]. Units are ppm.

2.0719425 (equivalent to $^{146}\text{Nd}/^{144}\text{Nd} = 0.7219$ [Vance and Thirlwall, 2002]) and $^{86}\text{Sr}/^{88}\text{Sr} = 0.1194$, using the exponential law. Further details are given by *Maas et al.* [2005]. In the case of MC-ICPMS data, where mass bias is generally highly constant during a given analytical session, but can vary between sessions, data are routinely normalized to the standards of the day. In this case, data are reported relative to La Jolla Nd = 0.511860 and SRM987 = 0.710230. This secondary normalization yields the following results for international standards ($\pm 2\text{sd}$): BCR-1 = 0.512641 ± 18 , BHVO-1 = 0.512998 ± 18 , JNdi-1 = 0.512113 ± 22 ; E&A Sr carbonate = 0.708005 ± 47 , BCR-1 = 0.705016 ± 46 , BHVO-1 = 0.703478 ± 36 . These results compare well with data based on TIMS and MC-ICPMS from other laboratories [e.g., *Raczek et al.*, 2003;

Tanaka et al., 2000]. Typical in-run precisions (2se) are ± 0.000010 (Nd) and ± 0.000022 (Sr). External (2sd) precision, or reproducibility, is ± 0.000020 (Nd) and ± 0.000040 (Sr) and is based on the results for secondary standards. Mass bias for Pb was corrected using the thallium-doping technique [Woodhead, 2002]. This produces data accurate to $< \pm 0.02\%$ (with respect to the SRM981 Pb standard), with an external (2sd) precision of $\approx \pm 0.02\%$.

Appendix C: Geochemical Modeling

C1. Modeling of Subduction Components

[73] To model the subduction components according to the geodynamic model of *Turner et al.* [1997] we applied the experimentally determined

Table C1. High-Pressure Normative Compositions of Modeled Subduction Compositions

	Eclogite ^a	LR VS ^b	Pel Sed ^c	90:10 Mix ^d
<i>Major Element Compositions</i>				
SiO ₂	53.42	51.06	63.95	52.35
TiO ₂	1.45	2.6	0.9	2.43
Al ₂ O ₃	17.24	12.27	14.49	12.49
FeO ^T ^e	8.8	10.55	9.61	10.46
MgO	5.93	14.82	3.61	13.76
CaO	10.22	5.61	2.87	5.34
Na ₂ O	3.24	3.1	4.57	3.24
<i>High-Pressure Normative Compositions</i>				
Garnet	20.79	10.87	8.12	10.54
Olivine	5.78	29.51	9.54	27.09
Jadeite + diopside	19.85	14.61	11.4	14.16
Quartz	50.35	39.98	69.61	43.65
Ilmenite	3.23	5.03	1.34	4.56

^aAnhydrous bulk composition of eclogite used in the experimental study of *Kessel et al.* [2005].

^bAverage composition of volcanoclastic sediment from the Louisville Ridge. Data from *Turner et al.* [1997] and *Ewart et al.* [1998].

^cAverage composition of Tongan pelagic sediments. Data from *Turner et al.* [1997], *Ewart et al.* [1998], and *Plank and Langmuir* [1998].

^dBulk mix formed by 90:10 ratio of Louisville Ridge derived volcanoclastic sediments (LR VS) and Tongan pelagic sediments (Pel Sed).

^eTotal Fe as FeO.

fluid/solid partition coefficients for eclogite determined by *Kessel et al.* [2005]. However, in order to apply the results of *Kessel et al.* [2005] we used the high-pressure normative mineralogy (using the method of *Yaxley and Green* [1998]) of our bulk compositions (Table C1) to determine the modal amount of clinopyroxene and garnet in each model eclogite. The amount of fluid produced at the relevant experimental conditions was determined by dividing the normative quartz by a factor of 2, which gives a reasonable approximation to the amount of fluid present in the experiments of *Kessel et al.* [2005]. We used the actual eclogite bulk composition of *Kessel et al.* [2005] for the composition of subducted oceanic crust (Table C1). In the model of *Turner et al.* [1997] a sediment melt (or super-critical fluid) is first added to the mantle wedge at relatively low pressure. We used the experimental results of *Kessel et al.* [2005] at 4 GPa, 900°C to model this process. The mantle wedge is then dragged down to deeper levels by viscous drag due to the subducting oceanic crust, until a point at which fluid dehydration reactions add a fluid from the oceanic crust to the mantle wedge, initiating partial melting. We used the experimental results of *Kessel et al.* [2005] at 6 GPa, 1000°C to model this process. The resulting calculated bulk distribution coefficients are pre-

sented in Table C2. Table C2 also lists the trace element and isotopic compositions of our model bulk compositions and resulting fluid compositions at the chosen model conditions.

C2. Modeling of Residue Compositions

[74] There are two potential residual mantle compositions lying above the subducting Pacific ocean crust at the northern termination of the Tonga Ridge. The first is Pacific MORB like mantle which has been depleted by the loss of a melt fraction due to the opening of the Lau Back arc basin, according to the geodynamic model of *Ewart and Hawkesworth* [1987] and *Ewart et al.* [1998]. The second is a refractory OIB mantle which has moved across from the slab edge formed by the trench-transform boundary according to the geodynamic model of *Danyushevsky et al.* [1995].

[75] To model the Sr and Nd abundances and isotope values of these two potential mantle residues we selected a Pacific MORB like lava from the earliest phase of Lau Back arc basin, sampled at ODP 834B [*Hergt and Hawkesworth*, 1994]. A Samoan lava from Ta'u Island [*Workman et al.*, 2004] was chosen to model an OIB residue for the Samoan plume. The Sr and Nd contents of the mantle residues were calculated assuming simple batch melting. Partition coefficients and modes used are presented in Table C3. The Sr and Nd abundances and isotopic values of the residues are presented in Table C4 (Mantle wedge residue and OIB residue, Table C4).

[76] Three potential methods of modeling the full NAP of the mantle wedge and OIB refractory mantle are as follows: (1) by calculation using partition coefficients (e.g., Figure C1); (2) assuming an arbitrary smooth NAP pattern reflecting the ordering of incompatible elements (e.g., Figure C1); (3) using natural examples of refractory mantle compositions; and (4) a combination of the last three methods. In the case of both the mantle wedge and OIB residue composition we found that both a calculated NAP and an assumed smooth NAP for the mantle residue could not successfully match the NAP of the normal subduction-related boninites (section 4.1). This is because the NAP of calculated residues (see examples in Figure C1) have markedly “spikey” patterns which are not removed by the addition of the fluid components, which are generally enriched in all incompatible elements (Figures 15 and 16). An arbitrarily smooth NAP for a mantle wedge residue combined with generally “smoothly” enriched patterns from

Table C2. End-Member Compositions Used in Modeling of “Normal” Subduction Zone Enrichments

	Mantle Wedge	OIB Residue	Tongan Pelagic Sediment	Louisville Volcaniclastic Sediment	90:10 ^a Sediment Mix	Oceanic Crust	D ₁ ^b	D ₂ ^b	C _{fluid} Pelagic	C _{fluid} 90:10 Sediment Mix	C _{fluid} Oceanic Crust ^c
Rb	0.184	0.279	56	25	28.1	4	77	67	156.232	122.105	11.765
Ba	4.498	4.263	850	195	260.5	38	43	180	2328.025	1093.896	113.867
Th	0.001	0.003	9	1.47	2.223	0.2	6.4	62	19.931	6.502	0.587
U	0.004	0.005	1.6	0.701	0.7909	0.09	6	25	3.491	2.260	0.252
Nb	0.040	0.0003	11	18.8	18.02	2	3.7	7	20.925	41.828	4.698
La	0.007	0.001	104	15	23.9	3.34	11.3	74	255.201	82.691	9.851
Ce	0.017	0.002	184	34	49	11.48	5.2	35	387.368	132.432	32.881
Pb	0.095	0.115	75	1.24	8.616	1.27	31.4	47	202.320	35.190	3.689
Sr	3.582	8.299	228	177	182.1	197	21.1	82	598.731	708.652	582.546
Nd	0.063	0.142	122	19.7	29.93	10.15	1.51	19.6	156.317	40.635	27.871
Sm	0.134	0.0004	27	4.88	7.092	3.43	0.371	3.8	12.845	3.054	6.774
Zr	0.827	0.011	140	146	145.4	110	0.39	3.6	69.421	65.495	213.132
Hf	0.069	0.0003	3.7	3.57	3.583	2.56	0.52	5.3	2.313	2.083	5.609
Eu	0.067	0.007	6.6	1.59	2.091	1.23	0.208	2.05	1.899	0.527	1.873
Ti	501	26	4796	13429	12566	8572	0.132	2.8	909	2050	15057
Gd	0.269	0.060	29	4.96	7.364	4.68	0.094	1.03	3.992	0.865	4.773
Dy	0.414	0.133	26	4.2	6.38	5.53	0.03	0.301	1.181	0.243	2.164
Y	2.508	1.001	160	41	52.9	32	0.032	0.37	7.743	2.151	14.948
Er	0.291	0.106	15	2.01	3.309	3.52	0.014	0.14	0.321	0.059	0.688
Yb	0.302	0.128	13	1.68	2.812	2.75	0.011	0.092	0.219	0.040	0.361
Lu	0.048	0.022	2	0.24	0.416	0.45	0.009	0.077	0.028	0.005	0.050
⁸⁷ Sr/ ⁸⁶ Sr	0.702618	0.704528	0.70886	0.70668	0.706953	0.70425			0.70886	0.706953	0.70425
¹⁴³ Nd/ ¹⁴⁴ Nd	0.513125	0.512822	0.512441	0.512861	0.51269	0.513057			0.512441	0.51269	0.513057
T, °C							900	1000	900	900	1000
P, GPa							4	6	4	4	6
F									0.35	0.22	0.33

^aModel mix is based on the quantitative model of *Turner et al.* [1997] and comprises 10% pelagic sediment and 90% volcaniclastic sediment from the Louisville Ridge.

^bBulk distribution coefficients for eclogite-fluid equilibria are from *Kessel et al.* [2005].

^cIsotopic composition of fluid from *Ewart et al.* [1998].

the fluid components results in smooth OIB like patterns in the resulting calculated melt compositions. However, we found a much better matching of model NAP with observed NAP of the boninites if we used natural residue compositions.

[77] In the case of the mantle wedge composition we found that the NAP (Figure C1) of average lherzolite composition from the ultrafresh subduction-related Hili Manu peridotite, East Timor [*Falloon et al.*, 2006] gave a very close match to the observed NAP of the boninites when used in our modeling. However, we found that there was a mismatch in some elements. The final residue composition presented in Table C2 was derived from this average lherzolite composition from the Hili Manu peridotite, with Sr and Nd values calculated using partition coefficients and the pillow lava from ODP 834B, and values selectively raised and lowered but within the range displayed by the Hili Manu lherzolite, to give the best match to the NAP of boninites 5–25 and 114-3-1 (Figures 16 and 17). The NAP of the

mantle wedge residue composition relative to the range displayed by the Hili Manu lherzolites is shown in Figure 15. The fact that this residue composition also gives a very close matching to the Tafahi Island composition 43/6 using a different sediment fluid composition, gives us confidence that our preferred residue composition may well be a close approximation to actual mantle residue composition resulting from melting in a backarc supra-subduction environment.

[78] We used the same approach as in the previous paragraph to model the NAP of the refractory OIB residue. We modeled the Sr and Nd abundances using partition coefficients and a natural lava composition from Samoa (Ta’u; see Table C4). Because boninite 5–24 is so depleted in incompatible elements we initially used an average harzburgite composition from the Hili Manu peridotite (Figures 18 and C1). Although in general the natural harzburgite gave a reasonable fit, it was necessary to adjust the trace element abundances arbitrarily to achieve a close matching to the NAP

Table C3. Distribution Coefficients Used in Trace Element and Isotope Melting Models

	Ol ^a	Opx ^b	Ref ^c	Mode ^d Ol	Mode Opx
Rb	0.0002	0.0006	1	0.727	0.273
Ba	0.009	0.001	1	0.727	0.273
Th	0.0000024	0.0000157	2	0.727	0.273
U	0.0000056	0.0000362	2	0.727	0.273
Nb	0.001	0.01	1	0.727	0.273
La	0.0021	0.0046	1	0.727	0.273
Ce	0.0022	0.0069	1	0.727	0.273
Pb	0.0001	0.0013	3	0.727	0.273
Sr	0.0002	0.07	1	0.727	0.273
Nd	0.0022	0.0104	1	0.727	0.273
Sm	0.0023	0.0203	1	0.727	0.273
Zr	0.0005	0.05	1	0.727	0.273
Hf	0.01	0.14	4	0.727	0.273
Eu	0.0023	0.0258	1	0.727	0.273
Ti	0.01	0.25	1	0.727	0.273
Gd	0.0024	0.0651	1	0.727	0.273
Dy	0.0017	0.022	3	0.727	0.273
Y	0.015	0.15	1	0.727	0.273
Er	0.0015	0.03	3	0.727	0.273
Yb	0.015	0.2	1	0.727	0.273
Lu	0.022	0.235	1	0.727	0.273

^aDistribution coefficients between olivine and liquid used in this study.

^bDistribution coefficients between orthopyroxene and liquid used in this study.

^cData sources for partition coefficients are as follows: 1, *Ewart et al.* [1998]; 2, *Beattie* [1993]; 3, *McKenzie and O'Nions* [1991]; 4, *Ulmer* [1989].

^dOlivine and orthopyroxene modes in the residue are based on peridotite melting experiment T-4335 [*Falloon et al.*, 1999].

of boninite 5–24 (Figure 18). The resulting harzburgite NAP has significant depletions in HFSE outside the range shown by the natural examples. Thus the OIB residue to boninite 5–24 cannot be a simple residue and must have been modified by secondary mantle processes. One such process is

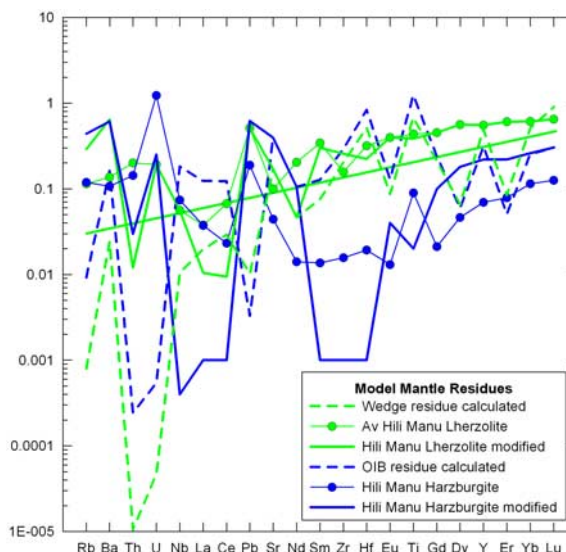


Figure C1. Primitive mantle normalized trace element abundance patterns for residual mantle compositions (see text, Appendix C for discussion). Primitive mantle normalizing values from *Sun and McDonough* [1989].

potential metasomatism by carbonatite melts which have been identified in mantle xenoliths from Samoan lavas [*Hauri et al.*, 1993]. *Danyushevsky et al.* [1995] also present discussion on the potential role of carbonatite metasomatism affecting the trace element signature of their proposed depleted mantle component D1.

C3. Modeling of OIB Source and Melt Components

[79] Our rationale in modeling the Sr, Nd and Pb isotope compositions of the enriched boninites was to use observed compositions represented by actual

Table C4. End-Member Mantle Source Compositions Used for Isotope Modeling

	Mantle Wedge Residue		OIB Residue		Lau Basin Mantle		Uo Mamae Mantle		Malumalu Mantle	
	C _L ^a	C _R	C _L ^b	C _R	C _L ^c	Co	C _L ^d	Co	C _L ^e	Co
Sr	186	3.582	431	8.299	73.9	14.735	704.2	210.4092	361	107.864
Nd	14.18	0.063	32.06	0.142	4.1	0.819	39.98	11.985	32.86	9.849
Pb					0.366	0.073195	4.929	1.478	3.77	1.131
F ^f		0.23		0.23	0.2		0.3		0.3	
⁸⁷ Sr/ ⁸⁶ Sr	0.702618	0.702618	0.704528	0.704528	0.703134	0.703134	0.705183	0.705183	0.70886	0.70886
¹⁴³ Nd/ ¹⁴⁴ Nd	0.513125	0.513125	0.512822	0.512822	0.513127	0.513127	0.513127	0.513127	0.512511	0.512511
²⁰⁶ Pb/ ²⁰⁴ Pb					18.000	18.000	18.319	18.319	19.23	19.23

^aBased on Pacific N-MORB lava composition ODP 834B 15R-2 96-104 [*Hergt and Hawkesworth*, 1994].

^bBased on OIB lava composition T30 from the Samoan Island of Ta'u [*Workman et al.*, 2004].

^cBased on Lau Basin lava composition GC51 from the Central Lau Spreading Center [*Sunkel*, 1990].

^dBased on lava composition 16–94/1 (this study and *Acland* [1996]).

^eBased on lava composition 78-3 [*Workman et al.*, 2004].

^fMelt fraction used to calculate mantle sources and residue using partition coefficients presented in Table C3.

Table C5. End-Member Melt Compositions Used for Isotope Modeling

	Tubuai ^a C _L	Uo Mamae ^b C _L	Niua fo'ou ^c C _L	Boninite 5–24 ^d C _L	OIB Melt 1 ^e C _L	OIB Melt 2 ^f C _L	OIB Melt 3 ^g C _L
Sr	1056	704.2	170.8	47.6	530.953	827.33	662.2148
Nd	68.01	39.988	11.2	0.794	36.3901	49.7957	44.29508
Pb	7	4.929	1.2	0.6675	4.34911	5.65385	5.011833
F ^h					0.3	0.3	0.3
⁸⁷ Sr/ ⁸⁶ Sr	0.7028	0.705183	0.704284	0.704465	0.706428	0.704118	0.704983
¹⁴³ Nd/ ¹⁴⁴ Nd	0.512927	0.51248	0.512824	0.512977	0.512494	0.512694	0.51266
²⁰⁶ Pb/ ²⁰⁴ Pb	21.118	18.319	18.2178	18.624	18.71381	19.5319	19.55329

^aBased on lava composition TBA-B-23 [Hauri and Hart, 1993].

^bBased on lava composition 16–94/1 (this study and Acland [1996]).

^cBased on average lava compositions [Turner et al., 1997].

^dBased on data from this study.

^eCalculated melt from a mantle source comprising a 50:50 mixture of mantle sources to Uo Mamae and Malumalu lavas.

^fCalculated melt from a mantle source comprising a 35:65 mixture of mantle sources to Tubuai and Uo Mamae lavas.

^gCalculated melt comprising a 25:75 mixture of OIB melt 1 and Tubuai.

^hMelt fraction of calculated melt compositions.

erupted lava compositions to determine the composition of the enriching E2 component which is mixed into the depleted boninite 5–24 in accordance with the petrogenetic model of *Danyushevsky et al.* [1995]. However, it was found that it was not possible to construct internally consistent mixing models using the observed compositions in all cases. For example the HIMU end-member based on an actual observed lava composition (from Tubuai) appears to be representative of a pure end-member melt composition involved in the petrogenesis of backarc basin lavas in the northern Lau Basin (Figures 19 and 20). However, the EMI-like component represented by Uo Mamae lavas, although close to being a pure end-member melt component, required the addition of an additional OIB component, either EMII or HIMU, to produce an exact match for the E2 melt component in all isotope space (OIB melts 1–3, Table C5). The resulting end-member E2 components (OIB melts 1–3, Table C5) plot into areas of isotope space that so far are not represented by actual lava compositions erupted from either the Samoan or Cook-Austral Islands. Our modeling assumes that the identified E2 melt components are available during boninite petrogenesis, but thus far no lava composition of pure E2 components has been erupted. Our modeling, if correct, predicts that such lava compositions with the isotopic composition of our E2 components may one day be sampled from the northern Tonga, Lau Basin area.

Acknowledgments

[80] This research was supported by the Australian Research Council and by NSF grants OCE-9521023 and OCE-9521039. We wish to thank all the scientists, officers, and crew who participated in all the cruises mentioned. We acknowledge

support of the Museum of Natural History, Washington, D. C., which provided electron microprobe standards. We thank Stan Hart for allowing us to use his database on Samoan volcanics. We thank Phil Robinson and Katie McGoldrick for their help with geochemical analyses. We thank editor Vincent Salters, associate editor David Hilton, Colin Macpherson, and three anonymous reviewers for their critical comments and helpful suggestions.

References

- Acland, A. S. (1996), Magma genesis in the northern Lau Basin, S.W. Pacific, Ph.D. thesis, 260 pp., Univ. of Durham, Durham, U. K.
- Beattie, P. (1993), The generation of uranium series disequilibrium by partial melting of spinel peridotite: Constraints from partitioning studies, *Earth Planet. Sci. Lett.*, *117*, 379–391.
- Belshaw, N. S., P. A. Freedman, R. K. O'Nions, M. Frank, and Y. Guo (1998), A new variable dispersion double-focusing plasma mass spectrometer with performance illustrated for Pb isotopes, *Int. J. Mass Spectrom. Ion Processes*, *181*, 51–58.
- Bevis, M. F., et al. (1995), Geodetic observations of very rapid convergence and back-arc extension at the Tonga Arc, *Nature*, *374*, 249–251.
- Bideau, D., and R. Hekinian (2004), Intraplate gabbroic rock debris ejected from the magma chamber of the Macdonald Seamount (Austral hotspot): Comparison with other provinces, in *Oceanic Hotspots: Intraplate Submarine Magmatism and Tectonism*, edited by R. Hekinian, P. Stoffers, and J. L. Cheminee, pp. 309–348, Springer, Berlin.
- Bloomer, S. H., B. Taylor, C. J. MacLeod, R. J. Stern, P. Fryer, J. W. Hawkins, and L. Johnson (1995), Early arc volcanism and the ophiolite problem: A perspective from drilling in the western Pacific, in *Active Margins and Marginal Basins of the Western Pacific*, *Geophys. Monogr. Ser.*, vol. 88, edited by B. Taylor and J. Natland, pp. 1–39, AGU, Washington, D. C.
- Bloomer, S. H., et al. (1996), Geology of the Tonga Forearc: A supra-subduction zone ophiolite, *Eos Trans. AGU*, *77*(46), Fall Meet. Suppl., F325.
- Bospflug, X., L. Dosso, H. Bougault, and J.-L. Joron (1990), Trace element and isotopic (Sr, Nd) geochemistry of volcanic rocks from the Lau Basin, *Geol. Jahrb.*, *D92*, 503–516.

- Crawford, A. J., T. J. Falloon, and D. H. Green (1989), Classification, petrogenesis and tectonic setting of boninites, in *Boninites and Related Rocks*, edited by A. J. Crawford, pp. 1–49, Unwin Hyman, London.
- Danyushevsky, L. V. (2001), The effect of small amounts of H₂O on crystallization of mid-ocean ridge and backarc basin magmas, *J. Volcanol. Geotherm. Res.*, *110*, 265–280.
- Danyushevsky, L. V., and A. V. Sobolev (1987), New data on the petrology of boninites in Tonga (in Russian), *Geol., Geophys.*, *12*, 100–103.
- Danyushevsky, L. V., A. V. Sobolev, and N. N. Kononkova (1992), Methods of studying magma inclusions in minerals during investigations on water-bearing primitive mantle melts (Tonga trench boninites), *Geochem. Int.*, *29*, 48–62.
- Danyushevsky, L. V., A. V. Sobolev, and T. J. Falloon (1995), North Tongan high-Ca boninite petrogenesis: The role of Samoan plume and subduction zone-transform fault transition, *J. Geodyn.*, *20*, 219–241.
- Duncan, R. A., and D. A. Clague (1986), Pacific plate motion recorded by linear volcanic chains, in *The Pacific Ocean: The Ocean Basins and Margins*, vol. 7A, edited by A. E. M. Nairn, F. G. Stehli, and S. Uyeda, pp. 89–121, Plenum, New York.
- Eggins, S. M., J. D. Woodhead, L. P. J. Kingsley, G. E. Mortimer, P. Sylvester, M. T. McCulloch, J. M. Hergt, and M. R. Handler (1997), A simple method for the precise determination of ≥ 40 trace elements in geological samples by ICPMS using enriched isotope internal standardization, *Chem. Geol.*, *134*, 311–326.
- Ellam, R. M., and C. J. Hawkesworth (1988), Elemental and isotopic variations in subduction related basalts: Evidence for a three component model, *Contrib. Mineral. Petrol.*, *98*, 72–80.
- Ewart, A., and C. J. Hawkesworth (1987), The Pleistocene-Recent Tonga-Kermadec arc lavas: Interpretation of new isotopic and rare earth data in terms of a depleted mantle source model, *J. Petrol.*, *28*, 495–530.
- Ewart, A., W. B. Bryan, and J. Gill (1973), Mineralogy and geochemistry of the younger volcanic islands of Tonga, southwest Pacific, *J. Petrol.*, *14*, 429–465.
- Ewart, A., R. N. Brothers, and A. Mateen (1977), An outline of the geology and geochemistry, and the possible petrogenetic evolution of the volcanic rocks of the Tonga-Kermadec-New Zealand island arc, *J. Volcanol. Geotherm. Res.*, *2*, 205–250.
- Ewart, A., W. B. Bryan, B. W. Chappell, and R. L. Rudnick (1994), Regional geochemistry of the Lau-Tonga Arc and back-arc systems, *Proc. Ocean Drill. Program Sci. Results*, *135*, 385–425.
- Ewart, A., K. D. Collerson, M. Regelous, J. I. Wendt, and Y. Niu (1998), Geochemical evolution within the Tonga-Kermadec-Lau Arc-Back-arc systems: The role of varying mantle wedge composition in space and time, *J. Petrol.*, *39*, 331–368.
- Falloon, T. J., and A. J. Crawford (1991), The petrogenesis of high-calcium boninite lavas dredged from the northern Tonga ridge, *Earth Planet. Sci. Lett.*, *102*, 375–394.
- Falloon, T. J., and L. V. Danyushevsky (2000), Melting of refractory mantle at 1.5, 2 and 2.5 GPa under anhydrous and H₂O-undersaturated conditions: Implications for the petrogenesis of high-Ca boninites and the influence of subduction components on mantle melting, *J. Petrol.*, *41*, 257–283.
- Falloon, T. J., and D. H. Green (1986), Glass inclusions in magnesian olivine phenocrysts from Tonga: Evidence for highly refractory parental magmas in the Tongan arc, *Earth Planet. Sci. Lett.*, *81*, 95–103.
- Falloon, T. J., D. H. Green, and A. J. Crawford (1987), Dredged igneous rocks from the northern termination of the Tofua magmatic arc, Tonga and adjacent Lau Basin, *Aust. J. Earth Sci.*, *34*, 487–506.
- Falloon, T. J., D. H. Green, and A. J. Crawford (1989), Petrogenesis of high-Mg and associated lavas from the north Tonga trench, in *Boninites and Related Rocks*, edited by A. J. Crawford, pp. 357–395, Unwin Hyman, London.
- Falloon, T. J., A. Malahoff, L. P. Zonenshain, and Y. Bogdanov (1992), Petrology and geochemistry of back-arc basin basalt from Lau Basin spreading ridges at 15°, 18° and 19°S, *Mineral. Petrol.*, *47*, 1–35.
- Falloon, T. J., S. H. Bloomer, and A. J. Crawford (1997), Boninites recovered from the Tonga Forearc, *Eos Trans. AGU*, *78*(46), Fall Meet. Suppl., F815.
- Falloon, T. J., D. H. Green, L. V. Danyushevsky, and U. H. Faul (1999), Peridotite melting at 1.0 and 1.5 GPa: An experimental evaluation of techniques using diamond aggregates and mineral mixes for determination of near-solidus melts, *J. Petrol.*, *40*, 1343–1375.
- Falloon, T. J., R. F. Berry, P. Robinson, and A. J. Stolz (2006), Whole rock geochemistry of the Hili Manu peridotite, East Timor: Implications for the origin of Timor ophiolites, *Aust. J. Earth Sci.*, *53*, 637–649.
- Fouquet, Y., et al. (1991), Hydrothermal activity in the Lau back-arc basin: Sulfides and water chemistry, *Geology*, *19*, 303–306.
- German, C. R., E. T. Baker, D. P. Connelly, J. E. Lupton, J. Resing, R. D. Prien, S. L. Walker, H. N. Edmonds, and C. H. Langmuir (2006), Hydrothermal exploration of the Fonualei Rift and Spreading Center and the Northeast Lau Spreading Center, *Geochem. Geophys. Geosyst.*, *7*, Q11022, doi:10.1029/2006GC001324.
- Gill, J. B. (1984), Sr-Pb-Nd isotopic evidence that both MORB and OIB sources contribute to oceanic island arc magmas in Fiji, *Earth Planet. Sci. Lett.*, *68*, 443–458.
- Govers, R., and M. J. R. Wortel (2005), Lithosphere tearing at STEPS faults: Response to edges of subduction zones, *Earth Planet. Sci. Lett.*, *236*, 505–523.
- Haase, K. M., T. J. Worthington, P. Stoffers, D. Garbe-Schönberg, and I. Wright (2002), Mantle dynamics, element recycling, and magma genesis beneath the Kermadec Arc-Havre Trough, *Geochem. Geophys. Geosyst.*, *3*(11), 1071, doi:10.1029/2002GC000335.
- Hart, S. R., et al. (2000), Vailulu'u undersea volcano: The New Samoa, *Geochem. Geophys. Geosyst.*, *1*(12), doi:10.1029/2000GC000108.
- Hauri, E. H., and S. R. Hart (1993), Re-Os isotope systematics of HIMU and EMII oceanic island basalts from the South Pacific Ocean, *Earth Planet. Sci. Lett.*, *114*, 353–371.
- Hauri, E. H., N. Shimizu, J. J. Dieu, and S. R. Hart (1993), Evidence for hotspot-related carbonatite metasomatism in the oceanic upper mantle, *Nature*, *365*, 221–227.
- Hawkesworth, C. J., S. P. Turner, D. W. Peate, F. McDermott, and P. van Calsteren (1997a), Elemental U and Th variations in island arc rocks: Implications for U-series isotopes, *Chem. Geol.*, *139*, 207–221.
- Hawkesworth, C. J., S. P. Turner, D. W. Peate, F. McDermott, and P. van Calsteren (1997b), U-Th isotopes in arc magmas: Implications for element transfer from the subducted crust, *Nature*, *276*, 551–555.
- Hawkins, J. W. (1976), Petrology and geochemistry of basaltic rocks of the Lau Basin, *Earth Planet. Sci. Lett.*, *28*, 283–296.
- Hawkins, J. W. (1995), Evolution of the Lau Basin insights from ODP Leg 135, in *Active Margins and Marginal Basins of the Western Pacific*, *Geophys. Monogr. Ser.*, vol. 88, edited by B. Taylor and J. Natland, pp. 125–173, AGU, Washington, D. C.

- Hawkins, J. W., and J. T. Melchior (1985), Petrology of Mariana Trough and Lau Basin basalts, *J. Geophys. Res.*, *90*, 11,431–11,468.
- Hawkins, J. W., and J. H. Natland (1975), Nephelinites and basanites of the Samoan linear volcanic chain: Their possible tectonic significance, *Earth Planet. Sci. Lett.*, *24*, 427–439.
- Hergt, J. M., and C. J. Hawkesworth (1994), Pb-, Sr-, and Nd-isotopic evolution of the Lau Basin: Implications for mantle dynamics during back-arc opening, *Proc. Ocean Drill. Program Sci. Results*, *135*, 505–517.
- Honda, E., K. B. Lewis, and Shipboard Party (1985), A marine geological and geophysical survey of the Northern Tonga Ridge and adjacent Lau Basin, *Nat. Resour. Tonga Field Rep. 1*, 125 pp., Minist. of Lands, Surv. and Nat. Resour., Nuku'alofa, Kingdom of Tonga.
- Jarosewich, E. J., J. A. Nelen, and J. A. Norberg (1980), Reference samples for electron microprobe analyses, *Geostand. Newsl.*, *4*, 257–258.
- Jordahl, K. A., M. K. McNutt, and D. W. Caress (2004), Multiple episodes of volcanism in the Southern Austral Islands: Flexural constraints from bathymetry, seismic reflection, and gravity data, *J. Geophys. Res.*, *109*, B06103, doi:10.1029/2003JB002885.
- Kessel, R., M. W. Schmidt, P. Ulmer, and T. Pettke (2005), Trace element signature of subduction-zone fluids, melts and supercritical liquids at 120–180km depth, *Nature*, *437*, 724–727.
- Kimura, J.-I., and T. Yoshida (2006), Contributions of slab fluid, mantle wedge and crust to the origin of Quaternary lavas in the NE Japan Arc, *J. Petrol.*, *47*, 2185–2232, doi:10.1093/petrology/eg1041.
- Langmuir, C. H., et al. (2005), Vent discovery and petrological sampling of the Lau Back Arc Basin, *R/V Kilo Moana KM 0417 Cruise Rep.*, 82 pp., Natl. Sci. Found., Washington, D. C.
- Le Bas, M. J. (2000), IUGS reclassification of the high-Mg and picritic volcanic rocks, *J. Petrol.*, *41*, 1467–1470.
- Le Maitre, R. W., et al. (1989), *A Classification of Igneous Rocks and Glossary of Terms: Recommendations of the International Union of Geological Sciences Subcommittee on the Systematics of Igneous Rocks*, 193 pp., Blackwell Sci., Oxford, U. K.
- Loock, G., W. F. McDonough, S. L. Goldstein, and A. W. Hofmann (1990), Isotopic compositions of volcanic glasses from the Lau Basin, *Mar. Min.*, *9*, 235–245.
- Lupton, J. E., D. G. Pyle, W. J. Jenkins, R. Greene, and L. Evans (2004), Evidence for an extensive hydrothermal plume in the Tonga-Fiji region of the South Pacific, *Geochem. Geophys. Geosyst.*, *5*, Q01003, doi:10.1029/2003GC000607.
- Maas, R., M. B. Kamenetsky, A. V. Sobolev, V. S. Kamenetsky, and N. V. Sobolev (2005), Sr-Nd-Pb isotopic evidence for a mantle origin of alkali chlorides and carbonates in the Udachnaya kimberlite, Siberia, *Geology*, *35*, 549–552.
- MacLeod, C. J. (1996), Geodynamics of the Tonga subduction zone and Lau Backarc basins, *Eos Trans. AGU*, *77*(46), Fall Meet. Suppl., F325.
- Malahoff, A., and T. J. Falloon (1991), Preliminary report of the Akademik Mstislav Keldysh/Mir cruise 1990 Lau Basin leg (May 7–21), *SOPAC Cruise Rep. 137*, 27 pp., Pac. Islands Appl. Geosci. Comm., Suva, Fiji.
- McConachy, T. F., R. J. Arculus, C. J. Yeats, R. A. Binns, F. J. A. Barriga, B. I. A. McInnes, S. Sestak, B. Rakau, and T. Tevi (2005), New hydrothermal activity and alkaline volcanism in the backarc Coriolis Troughs, Vanuatu, *Geology*, *33*, 61–64.
- McKenzie, D., and R. K. O'Nions (1991), Partial melt distributions from inversion of rare earth element concentrations, *J. Petrol.*, *32*, 1021–1091.
- Millen, D. W., and M. W. Hamburger (1998), Seismological evidence for tearing of the Pacific Plate at the northern termination of the Tonga subduction zone, *Geology*, *26*, 659–662.
- Norton, I. O. (2000), Global hotspot reference frames and plate motion, in *The History and Dynamics of Global Plate Motions*, *Geophys. Monogr. Ser.*, vol. 121, edited by M. A. Richards, R. G. Gordon, and R. D. van de Hilst, pp. 339–357, AGU, Washington, D. C.
- Parson, L. M., and D. L. Tiffin (1993), Northern Lau Basin: Backarc extension at the leading edge of the Indo-Australian plate, *Geo Mar. Lett.*, *13*, 107–115.
- Pearce, J. A., M. Ernewein, S. H. Bloomer, L. M. Parson, B. J. Murton, and L. E. Johnson (1995), Geochemistry of Lau Basin volcanic rocks: Influence of ridge segmentation and arc proximity, in *Volcanism Associated With Extension at Consuming Plate Margins*, edited by J. L. Smellie, *Geol. Soc. Spec. Publ.*, *81*, 53–75.
- Pin, C., and J. F. Santos-Zaldugui (1997), Sequential separation of light rare-earth elements, thorium and uranium by miniaturized extraction chromatography: Application to isotopic analyses of silicate rocks, *Anal. Chim. Acta*, *339*, 79–89.
- Pin, C., D. Briot, C. Bassin, and F. Poitrasson (1994), Concomitant separation of strontium and samarium-neodymium for isotopic analysis in silicate samples, based on specific extraction chromatography, *Anal. Chim. Acta*, *298*, 209–217.
- Plank, T., and C. H. Langmuir (1998), The chemical composition of subducting sediment and its consequences for the crust and mantle, *Chem. Geol.*, *145*, 325–394.
- Poreda, R. (1985), Helium-3 and deuterium in backarc basin basalts: Lau Basin and Mariana Trough, *Earth Planet. Sci. Lett.*, *76*, 244–254.
- Poreda, R., and H. Craig (1993), He and Sr isotopes in the Lau Basin mantle: Depleted and primitive mantle components, *Earth Planet. Sci. Lett.*, *119*, 319–329.
- Raczek, I., K. P. Jochum, and A. W. Hofmann (2003), Neodymium and strontium isotope data for USGS reference materials BCR-1, BCR-2, BHVO-1, BHVO-2, AGV-1, AGV-2, GSP-1, GSP-2 and eight MPI-DING reference glasses, *Geostand. Newsl.*, *27*, 173–179.
- Regelous, M., K. D. Collerson, A. Ewart, and J. I. Wendt (1997), Trace element transport rates in subduction zones: Evidence from Th, Sr and Pb isotope data for Tonga-Kermadec Lavas, *Earth Planet. Sci. Lett.*, *150*, 291–302.
- Robinson, P. (2003), XRF analysis of flux-fused discs, paper presented at Geoanalysis 2003: The 5th International Conference on the Analysis of Geological and Environmental Materials, Geol. Surv. of Finland, Rovaniemi, Finland.
- Robinson, P., A. T. Townsend, Z. Yu, and C. Munker (1999), Determination of scandium, yttrium and rare earth elements in rocks by high resolution inductively coupled plasma-mass spectrometry, *Geostand. Newsl.*, *23*, 31–46.
- Rogers, N. W., C. J. MacLeod, and B. J. Murton (1989), Petrogenesis of boninitic lavas from the Limassol Forest Complex, Cyprus, in *Boninites and Related Rocks*, edited by A. J. Crawford, pp. 288–313, Unwin Hyman, London.
- Sharaskin, A. Ya., I. K. Pustchin, S. K. Zlobin, and G. M. Kolesov (1983), Two ophiolite sequences from the basement of the northern Tonga arc, *Ofioliti*, *8*, 411–430.
- Sinton, J. M., and P. Fryer (1987), Mariana Trough lavas from 18°N: Implications for the origin of back arc basin basalts, *J. Geophys. Res.*, *92*, 12,782–12,802.

- Sinton, J. M., R. C. Price, K. T. Johnson, H. Staudigel, and A. Zindler (1991), Petrology and geochemistry of submarine lavas from the Lau and North Fiji backarc basins, in *Basin Formation, Ridge Crest Processes and Metallogenesis in the North Fiji Basin, Circum-Pac. Counc. Energy Miner. Resour. Earth Sci. Ser.*, vol. 12, edited by L. W. Kroenke and J. V. Eades, pp. 155–177, Am. Assoc. Pet. Geol., Tulsa, Okla.
- Smith, G. P., D. A. Wiens, K. M. Fischer, L. M. Dorman, S. C. Webb, and J. A. Hildebrand (2001), A complex pattern of mantle flow in the Lau backarc, *Science*, *292*, 713–716.
- Smith, W. H. F., and D. T. Sandwell (1997), Global sea floor topography from satellite altimetry and ship depth soundings, *Science*, *277*, 1956–1962.
- Sobolev, A. V., and M. Chaussidon (1996), H₂O concentrations in primary melts from supra-subduction zones and mid-ocean ridges: Implications for H₂O storage and recycling in the mantle, *Earth Planet. Sci. Lett.*, *137*, 45–55.
- Sobolev, A. V., and L. V. Danyushevsky (1994), Petrology and geochemistry of boninites from the north termination of the Tonga Trench: Constraints on the generation conditions of primary high-Ca boninite magmas, *J. Petrol.*, *35*, 1183–1211.
- Sun, S. S., and W. F. McDonough (1989), Chemical and isotopic systematics of oceanic basalts: Implications for mantle composition and processes, in *Magmatism in the Ocean Basins*, edited by A. D. Saunders and M. J. Norry, *Geol. Soc. Spec. Publ.*, *42*, 313–345.
- Sunkel, G. (1990), Origin of petrological and geochemical variations of Lau Basin lavas (SW Pacific), *Mar. Min.*, *9*, 205–234.
- Tanaka, T., et al. (2000), JNd1-1: A neodymium isotopic reference in consistency with La Jolla neodymium, *Chem. Geol.*, *168*, 279–281.
- Tappin, D. R. (1994), The Tonga Frontal-arc basin, in *South Pacific Sedimentary Basins*, edited by P. F. Balance, pp. 157–176, Elsevier, Amsterdam.
- Tappin, D. R., T. R. Bruns, and E. L. Geist (1994), Rifting of the Tonga/Lau Ridge and formation of the Lau backarc basin: Evidence from site 840 on the Tonga Ridge, *Proc. Ocean Drill. Program Sci. Results*, *135*, 367–372.
- Turner, S. P., and C. J. Hawkesworth (1997), Constraints on flux rates and mantle dynamics beneath island arcs from Tonga-Kermadec lava geochemistry, *Nature*, *389*, 568–573.
- Turner, S. P., C. J. Hawkesworth, N. W. Rogers, J. Bartlett, T. J. Worthington, J. M. Hergt, J. A. Pearce, and I. E. M. Smith (1997), ²³⁸U-²³⁰Th disequilibria magma petrogenesis and flux rates beneath the depleted Tonga-Kermadec island arc, *Geochim. Cosmochim. Acta*, *61*, 4855–4884.
- Ulmer, P. (1989), Partitioning of high field strength elements among, olivine, pyroxenes, garnet and calc-alkaline picrobasalt: Experimental results and an application, in *Annual Report of the Director of the Geophysical Laboratory, Year Book Carnegie Inst. Washington*, *89*, 42–47.
- Vance, D., and M. F. Thirlwall (2002), An assessment of mass discrimination in MC-ICPMS using Nd isotopes, *Chem. Geol.*, *185*, 227–240.
- Volpe, A. M., J. D. Macdougall, and J. W. Hawkins (1988), Lau Basin basalts (LBB): Trace element and Sr-Nd isotopic evidence for heterogeneity in backarc basin mantle, *Earth Planet. Sci. Lett.*, *90*, 174–186.
- Wendt, J. I., M. Regelous, K. D. Collerson, and A. Ewart (1997), Evidence for a contribution from two mantle plumes to island-arc lavas from northern Tonga, *Geology*, *25*, 611–614.
- Woodhead, J. D. (2002), A simple method for obtaining highly accurate Pb isotope data by MC-ICP-MS, *J. Anal. At. Spectrom.*, *17*, 1–6.
- Woodhead, J. D., F. Volker, and M. T. McCulloch (1995), Routine Pb isotope determinations using a ²⁰⁷Pb-²⁰⁴Pb double spike: A long-term assessment of analytical precision and accuracy, *Analyst*, *120*, 35–39.
- Workman, R. K., S. R. Hart, M. Jackson, M. Regelous, K. A. Farley, J. Blusztajn, M. Kurz, and H. Staudigel (2004), Recycled metasomatized lithosphere as the origin of the Enriched Mantle II (EM2) end-member: Evidence from the Samoan Volcanic Chain, *Geochem. Geophys. Geosyst.*, *5*, Q04008, doi:10.1029/2003GC000623.
- Wright, D., et al. (1996), New Seabeam 2000 bathymetry and sidescan data on the Tonga Forearc and Trench: Results from Boomerang Leg 8, an ODP site survey, *Eos Trans. AGU*, *77*(46), Fall Meet. Suppl., F326.
- Wright, D. J., S. H. Bloomer, C. J. MacLeod, B. Taylor, and A. M. Goodlife (2000), Bathymetry of the Tonga Trench and Forearc: A map series, *Mar. Geophys. Res.*, *21*, 489–511.
- Yaxley, G. M., and D. H. Green (1998), Reactions between eclogite and peridotite: Mantle refertilization by subduction of oceanic crust, *Schweiz. Mineral. Petrogr. Mitt.*, *78*, 243–255.
- Yu, Z., P. Robinson, A. T. Townsend, C. Munker, and A. J. Crawford (2000), Determination of HFSE, Rb, Sr, Mo, Sb, Cs, Tl and Bi at ng g⁻¹ levels in geological reference materials by magnetic sector ICP-MS after HF/HClO₄ high pressure digestion, *Geostand. Newsl.*, *24*, 39–50.
- Zellmer, K. E., and B. Taylor (2001), A three-plate kinematic model for Lau Basin opening, *Geochem. Geophys. Geosyst.*, *2*(5), doi:10.1029/2000GC000106.
- Zlobin, S. K., G. M. Kolesov, and N. N. Kononkova (1991), Development of within-plate magmatism on the landward and offshore slopes of the Tonga Trench, *Ofioliti*, *16*, 17–35.